MEASUREMENT OF CO_2 ADSORPTION CAPACITY ON SELECTED TURKISH COALS FOR CO_2 SEQUESTRATION PURPOSES

A THESIS SUBMITTED TO
THE BOARD OF GRADUATE PROGRAMS
OF
MIDDLE EAST TECHNICAL UNIVERSITY, NORTHERN CYPRUS CAMPUS

BY

BIENVENU CHRISTIAN BUNANI KEZA

IN PARTIAL FULFILLMENT OF THE REQUIREMENTS
FOR
THE DEGREE OF MASTER OF SCIENCE
IN SUSTAINABLE ENVIRONMENT AND ENERGY SYSTEMS PROGRAM

FEBRUARY 2021

Approval of the Board of Graduate Programs

Prof. Dr. Oğuz Solyalı
Chairperson

I certify that this thesis satisfies all the requirements as a thesis for the degree of Master of Science

Asst. Prof. Dr. Ceren İnce Derogar
Program Coordinator

This is to certify that we have read this thesis and that in our opinion it is fully adequate, in scope and quality, as a thesis for the degree of Master of Science.

Asst. Prof. Dr. Doruk Alp
Co-Supervisor

Asst. Prof. Dr. Aykut Argönül
Supervisor

Examining Committee Members:

Asst. Prof. Dr. Bengü Bozkaya Schrotter
METU Northern Cyprus Campus
Chemical Engineering Program

Asst. Prof. Dr. Aykut Argönül
METU Northern Cyprus Campus
Chemical Engineering Program

Asst. Prof. Dr. Doruk Alp
METU Northern Cyprus Campus
Petroleum and Natural Gas Engineering Program

Prof. Dr. Salih Saner
Near East University
Department of Petroleum and Natural Gas Engineering

Asst. Prof. Dr. Cemal Albayrak
METU Northern Cyprus Campus
Chemistry Group

I hereby declare that all information in this document has been obtained and presented in accordance with academic rules and ethical conduct. I also declare that, as required by these rules and conduct, I have fully cited and referenced all material and results that are not original to this work.

Bunani Keza, Bienvenu Christian

Signature:

ABSTRACT

MEASUREMENT OF CO_2 ADSORPTION CAPACITY ON SELECTED TURKISH COALS FOR CO_2 SEQUESTRATION PURPOSES

Bunani Keza, Bienvenu Christian
Master of Science, Sustainable Environment and Energy Systems Program
Supervisor: Asst. Prof. Dr. Aykut Argönül
Co-Supervisor: Asst. Prof. Dr. Doruk Alp

February 2021, 112 Pages

The rapid industrialization in the nineteenth century caused an increase in energy consumption. This consumption is mainly met by burning fossil fuels which are the primary source of CO_2 emissions. Geological storage is one option that can substantially reduce CO_2 emissions in the atmosphere. In this work, the storage capacities of four different coal basins in Turkey have been estimated: Soma, Tunçbilek, Tekirdağ-Saray and Afşin-Elbistan.

First, CO_2 adsorption capacities of samples from the four coal basins were measured using the volumetric method at 40 °C and incremental pressures up to 85 bars.

Four different adsorption models were found to fit experimental data well (Langmuir modified, Langmuir modified+k, D-R modified and D-R modified +k) with an average relative error of less than ±7 %. Among these, the D-R modified model was the best fitting model.

Accordingly, maximum adsorption capacity for all coal samples (all on "daf" basis) was calculated. Moreover, the storage capacities of the four coal basins were calculated to be 62.1 Mt CO_2 for Soma, 17.73 Mt CO_2 for Tunçbilek, 4.91 Mt CO_2 for Tekirdağ-Saray and 29.89 Mt CO_2 for Afşin-Elbistan. It was estimated that Soma

coal seam could store the CO_2 emissions from a typical 100 MW coal power plant for about 102 years, Tunçbilek for about 29 years, Tekirdağ-Saray for about 8, and Afşin-Elbistan for 49 years.

Keywords: Keywords: Adsorption Isotherms, Carbon Dioxide, Volumetric Method, Carbon Sequestration, Coal Seams.

ÖZ

KARBONDİOKSİT DEPOLAMA AMACIYLA ÇEŞİTLİ TÜRK KÖMÜRLERİ İÇİN CO_2 YÜZE TUTUNMA KAPASİTESİNİN ÖLÇÜMÜ

Bunani Keza, Bienvenu Christian
Yüksek Lisans, Sürdürülebilir Çevre ve Enerji Sistemleri Programı
Tez Yöneticisi: Dr. Öğr. Üyesi. Aykut Argönül
Ortak Tez Yöneticisi: Dr. Öğr. Üyesi Doruk Alp

Şubat 2021, 112 sayfa

19. yüzyılda hızlı sanayileşme ile birlikte enerji tüketimi de ciddi boyutta artmıştır. Bu tüketim büyük oranda, karbon-dioksit (CO_2) salınımının ana kaynağı olan fosil yakıtların yakılması ile karşılanmaktadır. CO_2'in yeraltı kayaçlara basılıp saklanması, havaya salınımı büyük ölçekte azaltacak yöntemlerden biridir. Bu çalışmada, Türkiye'deki dört önemli kömür yatağının; Soma, Tunçbilek, Tekirdağ-Saray ve Afşin-Elbistan, saklama sığası (depolama kapasitesi) araştırılmıştır.

İlk olarak, bu dört yataktan gelen kömür örneklerinin CO_2 tutunma sığası (adsorpsiyon kapasitesi) volumetrik yöntem ile 40 °C'de ve 85 bar basınca kadar ölçülmüştür.

Dört farklı tutunma sığası matematik modeli (Langmuir modified, Langmuir modified+k, D-R modified and D-R modified+k) deney sonuçlarının modellenmesinde kullanılmış ve bunlar deney sonuçlarına %7'den az bir hata ile eşleşmiştir. Bu modellerin arasından D-R modified modeli en iyi (en az hata ile) eşleşen modeldir.

Bunun sonrasında, bütün kömür örnekleri için (kuru külsüz bazda) azami "adsorpsiyon sığası" değerleri hesaplanmıştır. Sonuç olarak, dört kömür yatağının toplam CO_2 saklama sığalarının şu kapasitelere denk geldiği hesaplanmıştır; Soma için 62.1 Mt, Tunçbilek için 17.73 Mt, Tekirdağ-Saray için 4.91 Mt, ve Afşin-Elbistan için 29.89 Mt. Bu değerlere göre, 100 MW'lık bir kömür santralinin yıllık CO_2 salınımı temelinde, yaklaşık olarak Soma'da 102 yıl, Tunçbilek'de 29 yıl, Tekirdağ-Saray 'da 8 yıl ve Afşin-Elbistan'da 49 yıla eşdeğer CO_2 salınımı saklanabileceği öngörülmektedir.

Anahtar Kelimeler: Adsorpsiyon İzotermi, Karbondioksit, Volumetrik Yöntem, Karbon Depolama, Kömür Yatakları

This thesis is dedicated to my Lovely Mum, Musanganire Mukarushema Asnath, and my siblings, Ihorere Jules, Binezero Gilbert, Nzibonera Gilbert, Mahinyuza Jean-Paul, Muramire Gilberte

I love you all so much

ACKNOWLEDGMENTS

I would like to express my sincere thanks to my supervisor, Dr.-Ing. Aykut Argönül, for his patience, efforts, enthusiasm, criticism and time. You have shaped me into a better engineer, and for that, I will always be grateful. Thank you for many lunches we had together, talks and discussions beyond my thesis; I felt cared for and loved. I am truly thankful for everything you did for me for the past three years.

To my co-advisor, Dr Doruk Alp, thank you for encouragements, friendship, and many friendly talks we had once in a while. When I was almost giving up, you were there to let me know I was doing okay, which kept me going. Thank you for the patience and guidance throughout this work.

My deep appreciation goes to the laboratory manager Abdullah Önal, Hasan Okaygun, Kaya Hoca, and all other lab technicians, they showed me love, and they helped me in all possible ways they could; without them, this thesis would not have been completed. Thank you very much.

Many Thanks to Prof. Dr Salih Saner and Dr Emre Artun, they helped me so much at the beginning of my thesis, and I am forever grateful.

Thank you to all the friends and students, especially in the bible club. You have made my time in METU much more fun and have made me feel special.

Finally, a huge thanks to my mum. I am where I am in life because of your sacrifice and love.

"Trust in the Lord with all your heart and lean not on your own understanding; in all your ways, acknowledge him, and he will make your paths straight."

Proverbs 3:5-6.

TABLE OF CONTENTS

LIST OF TABLES

TABLES

LIST OF FIGURES

FIGURES

LIST OF ABBREVIATIONS

ABBREVIATIONS

BET	Brunauer, Emmett, and Teller Equation
BP	British Petroleum
CBM	Coalbed Methane
CCS	Carbon Capture and Storage
CO_2CRC	The Cooperative Research Centre for Greenhouse Gas
D-A	Dubinin and Astakhov
D-R	Dubinin and Radushkevich
E.U	European Union
ECBM	Enhanced Coalbed Methane Recovery
ELI	Ege Linyitleri İşletmesi
EOS	Equation of State
GFZ	German Research Centre for Geosciences
IEA	International Energy Agency
IUPAC	International Union of Pure and Applied Chemistry
MTA	General Directorate of Mineral Research and Exploration
ppm	parts per million
PTRC	Petroleum Technology Research Centre
SECARB	The Southeast Regional Carbon Sequestration Partnership
SEM	Scanning Electron Microscopy
TKI	General Directorate of Turkish Coal Enterprises
UNFCCC	United Nations Framework Convention on Climate Change
daf	dry, ash free basis

LIST OF SYMBOLS

SYMBOLS

P_{sc}	The pressure at standard condition	bars
P	The pressure at reservoir condition	bars
P_o	Saturation vapor pressure of the adsorbate	bars
T_{sc}	The temperature at standard condition	Kelvin (K)
T	Reservoir temperature	Kelvin (K)
Z_{sc}	The compressibility of gas at standard condition	
V_{coal}	The volume of the coal seam	m^3
V_{ske}	The volume of the coal sample	cc
V_a	The volume of the adsorbed phase	cc
V_{sa}	The volume of the sample cell	cc
V_{void}	Free volume (void volume) in the sample cell	cc
V_m	Langmuir monolayer capacity (in Equation 5.2)	
Z	Compressibility factor for gas	
n_{inject}	Total moles of gas transferred into the sample cell	mmol
n_{ex}	Gibbs (experimentally measured) excess adsorption	mmol/g
n_{abs}	Absolute adsorbed amount	mmol/g
n_{max}	Maximum adsorption capacity	mmol/g
Γ	Total amount of gas per unit area	mol/m^2
Eo	Characteristic heat of adsorption	kJ/mole
$\emptyset$	Cleat porosity	fraction
ρ_a	The density of the adsorbed phase	mol/cc,
ρ	The density of the free gas phase	mol/cc
ρ_{coal}	The density of the coal	g/cc,
ρ_o	Organic fraction density	g/cc,
ρ_w	Water density	g/cc
ρ_{as}	Ash density	g/cc
$V_{L.}$	The Langmuir volume	cc/g
β	The affinity coefficient	
B_g	Formation volume factor for the gas phase	-
$ScCO_2$	Supercritical carbon dioxide	
R	The universal gas constant	$m^3 \cdot atm \cdot K^{-1} \cdot mol^{-1}$

CHAPTER 1

INTRODUCTION

1.1 Climate change and global response

The presence of greenhouse gases or active radiative gases (water vapour, carbon dioxide (CO_2), methane (CH_4), nitrous oxide (N_2O), chlorofluorocarbons (CFC_s) and ozone (O_3)) in the atmosphere is what makes our life on earth possible. They do this by keeping our planet warm enough to support life as we know it [1], [2]. For the past few decades, this process known as "greenhouse effect" has been viewed as threatening due to the increase in global mean temperature and climate change. This is due to the rapid rise in the concentration of anthropogenic greenhouse gases in the atmosphere. CO_2 is the most dominant of them, accounting for 76 % of the total emissions, with an average lifetime in the atmosphere of hundreds of years [2], [3].

The rapid growth of industrialization in the nineteenth century caused the increase in energy consumption, mainly from burning fossil fuels which are the primary source of CO_2 emissions. The atmospheric concentration of CO_2 was stable throughout Human evolution at approximately 280 ppm. However, it significantly increased from 280 ppm pre-industrial period to 410 ppm in 2018 with an annual rate increase of 2.2 ppm [2], [4], [5] as shown in Figure 1.1. Fossil fuel share in the energy portfolio remains at more than 80 %, and studies show that global consumption of fossil fuels will continue to be the primary source of energy, at least for the next few decades [6]–[10].

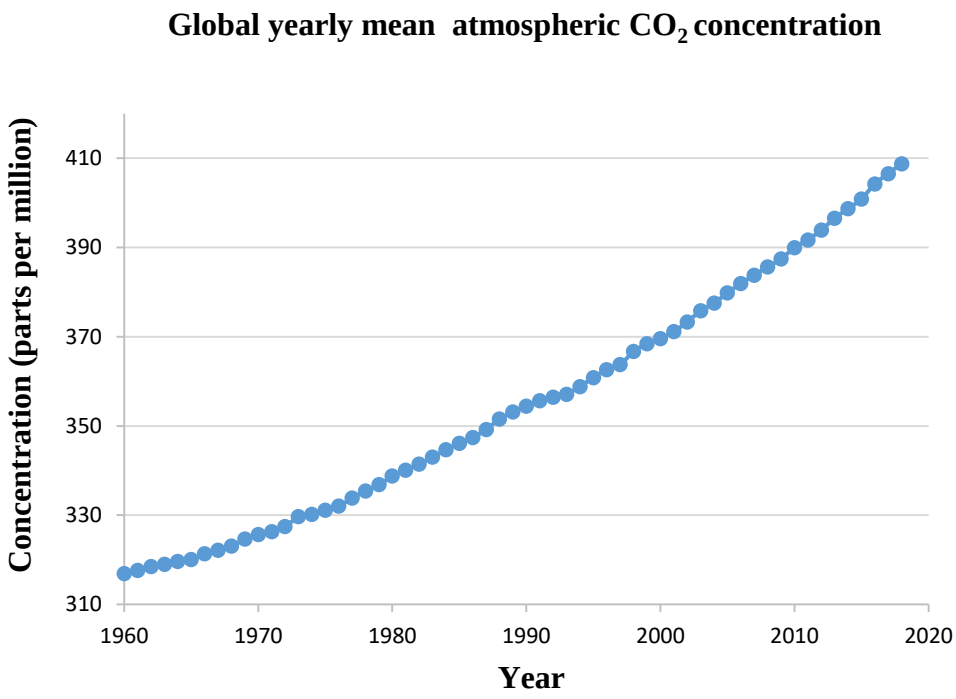

Figure 1.1. Global yearly mean CO_2 concentration from 1960 to 2018 [11]

According to the IEA (International Energy Agency), carbon dioxide emissions have already reached two-thirds of the point-of-no-return threshold (450 ppm of CO_2), which will result in a 2 °C increase in the current global temperature [12]–[14].

To tackle climate change, caused mainly by the combustion of fossils fuels, the United Nations Framework Convention on Climate Change (UNFCCC) convened in 2015 in Paris. As a result, an agreement was reached. It required all parties to sign and submit commitments and targets to be achieved to address this issue of global warming. Although this accord leaves individual governments to determine the terms to address the climate change issues in their context, the Paris agreement creates robust international transparency. It requires that the successive policies be more substantial than previously taken [15]–[17].

The Paris agreement is widely known for restraining global temperature below two °C above the pre-industrial level. Moreover, this implies that the global emissions of CO_2, which happens to account for over 80% of the global warming, be limited to 42 and 22 billion tons in 2030 and 2050 [18]. If nothing is done to mitigate the increase of anthropogenic CO_2, its concentration will reach 450 ppm in just three decades, increasing the average global temperature by 2°C-3°C [2]. Different studies [17], [19]–[21] show that this increase will have catastrophic consequences. To mention a few, It will cause polar region ice to melt, causing the sea levels to rise, destruction of biodiversity, human health risks, impact on wildlife and ecosystems, pressure on food security, changing weather patterns and various extreme weather events [18].

Scientists have been exploring different approaches to reduce carbon dioxide emissions, as shown in Figure 1.2. These are, 1) mitigation through geo-engineering, 2) removal through ocean fertilization, biological sequestration, or 3) reducing the emissions of CO_2 in the atmosphere through improved efficiency, fuel switching, and Carbon capture and storage (CCS) [22]–[24].

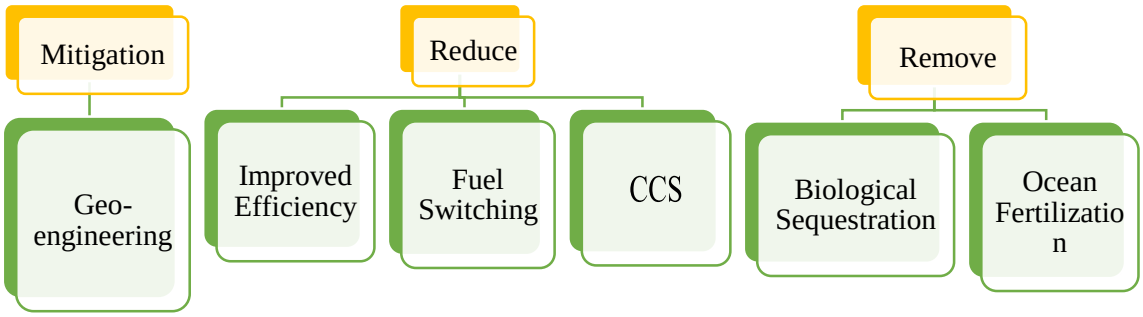

Figure 1.2. CO_2 mitigation options to reduce climate change-related issues

Of all these alternatives, the only technology that can substantially reduce CO_2 emissions from the energy industry is carbon capture and storage (CCS) in deep saline formations, drained oil and gas fields, oceans, or non-minable coalbeds [6], [9], [25].

CHAPTER 2

GEOLOGICAL CO_2 STORAGE

The term CO_2 capture and storage (CCS) refers to the method of collecting, transporting, and safely disposing of carbon dioxide from the air or other pollution sources to the storage site and its final stage in underground reservoirs (coal seams, depleted oil and gas reservoirs, methane hydrate reservoirs, shales or underground saline aquifers) [23], [26], [27].

2.1 Worldwide CO_2 storage projects

The continued reliance on fossils fuels requires developing technologies to facilitate the Carbon Capture and Storage (CCS) if one wants to reduce the accumulation of CO_2 in the atmosphere. The geological storage projects worldwide have been mainly focused on saline aquifers and depleted oil and gas reservoirs, as shown in Table 2.1. This section intends to inform the readers of several CCS projects worldwide.

For the past few years, the US Department of Energy has invested in CCS projects development programs known as the carbonSAFE projects [28]. These projects focus on developing geological storage for 50+ megatons (Mt) of carbon dioxide from industrial sources across the US.

To this date, 13 pre-feasibility and six complex feasibility projects are underway, and more details can be found in [28], [29].

Several other major projects have been carried out in the past. Table 2.1 gives details on some of the current and past major CO_2 storage projects worldwide.

Table 2.1. Worldwide CO_2 storage projects.

Name of the project & Company	**Country**	**Date of operation**	**Depth (m)**	**Reference**
In-salah (BP, Statoil, Sonatrach)	Algeria	2004-2011	Depleted gas reservoir /1900m	[30]–[34]
Ketzin Project (GFZ. and Ketzin partners)	Germany	2008-2013	Sandstone reservoir / 630m	[35]–[37]
Sleipner project (Statoil)	North Sea, Norway	1996-	A deep saline reservoir 800-1000m	[27], [38], [39]
Weyburn-Midale (Cenovus Energy, Apache Canada, PTRC)	Canada	2000-	EOR. in 2 carbonate fields, 1500m	[40]–[43]
Snøhvit project (Statoil ASA., Petoro AS, Total E&P, Norge AS)	Norway	2008-	Saline Tubasan sandstone formation 2600m below the seabed	[33], [44]–[46]
Otway Basin project CO_2CRC (Cooperative Research Centre)	Australia	2008-2011	Depleted gas reservoir (2000m)	[47]–[49]
Cranfield project (SECARB)	The USA.	2009-2015	Saline reservoir, Cranfield oil field	[33], [50]–[52]

2.2 CO_2 storage in coal-seams

Coalbeds are both the source and reservoir rock for a significant amount of methane gas, known as coalbed methane (CBM). This gas, which has been generated during the coalification process, is stored in coals through different mechanisms:

- ✓ Adsorbed gas molecules within micropores
- ✓ Free gas (in cleats or fractures)
- ✓ And as a gas dissolved in groundwater within coal fractures.

Like the primary porosity in conventional oil and gas reservoirs, the micropores in coal are the coal's primary gas storage. Gas molecules are generally adsorbed within these micropores, and these micropores are responsible for more than 90 % of the gas storage in coalbeds [53]. The hydrostatic pressure retains the adsorbed gas through geologic time. If the pressure is reduced by erosion or other factors, the adsorbed gas is desorbed, leaving little or no gas behind.

CO_2 sequestration in coal seams is the process of storing the captured CO_2 in deep unminable coal seams. Unminable seams are either too thin, too deep, high in sulfur or too low in calorific value are considered non-minable because they are not economically feasible [26], [54].

The use of coal seams as a reservoir rock for CO_2 storage has gained attention for the past few decades, and many studies have been published, and others are still unfolding [23], [27], [29], [55]–[68]. There are significant amounts of water and methane gas in the cleats and pores of a coal-seam. This methane gas was generated due to the microbial, thermal and catalytic decomposition of the organic material found in coal seams [69]. A portion of this methane gas is produced by pumping out the water existing in the cleats. Once CO_2 is injected into the coal beds, it gets adsorbed on the coal pore matrix replacing the remaining methane gas, and the adsorbed CO_2 permanently remains adsorbed in the coal. It has been experimentally shown in different studies that molecules of CO_2 are more preferentially adsorbed in the coal matrix than methane molecules [23], [70]–[74]. Generally, in coalbeds, molecules of CO_2 or CH_4 are physically adsorbed; this means that they can easily be desorbed by reducing pressure or by heating; see chapter 5 for more details.

Several studies have estimated the worldwide storage capacity of coal seams to be between 3Gt-200Gt [7], [23], [61], [67], [75]. These estimates are in most studies based on the assumption that two molecules of CO_2 are adsorbed for every CH_4 molecule in coal [67].

CHAPTER 3

COAL DEPOSITS OF TURKEY

3.1 Lignite resources of Turkey: geology and reserves

Lignite (a type of coal with low heat content) deposits in Turkey cover 110 000 km^2, approximately 15 % of the entire land. According to their age, 2 % is Eocene, 6 % is Oligocene, 41 % is Miocene, and 51 % is Pliocene in age. They are widely distributed throughout the country, as shown in Figure 3.1 and were formed under variable tectonic regimes during geological times, explaining the differences in genetic and quality variations [76]. There are four main basins in Turkey: Central Anatolia, covering 558.9 $km^{2,}$ around 50 % of the total area; Aegean basin covers 345.3 km^2; Thrace basins 219.8 km^2, and East Anatolia 184.9 km^2 [77].

The lignite reserves estimation in Turkey started as early as a century ago, in 1940, and were reported to be around 1.13 gigatons (Gt) [77]. The reserves estimation improved throughout the years as more fields kept being discovered. Table 3.1 lists years in which assessment had been done, the body which published the data, the reference, and the reserve estimation. Over the years, the values have discrepancies mainly due to the confusion on the difference between possible, probable, proved reserves. Nevertheless, they show how much progress has been made both in exploration and research.

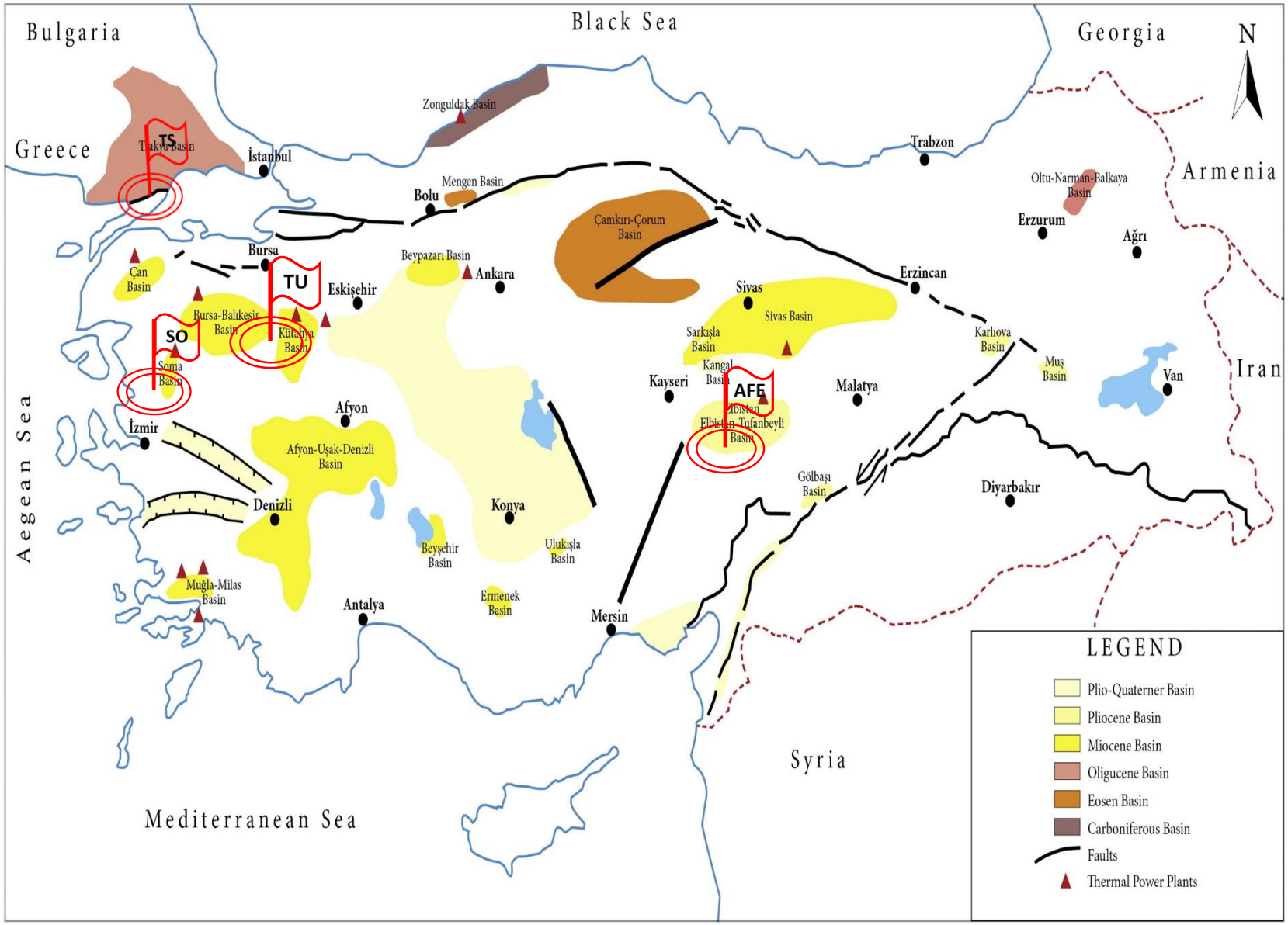

Figure 3.1. Coal basins of Turkey and their coal age classification [77]

Table 3.1. Turkey's lignite reserves estimation from 1940-2011 [77]

Publisher of the information	**Year**	**Total reserve estimated (gigatons, Gt)**
Electrical Power Resources Survey & Development Administration	1940	Possible: 1.13
		Probable:0.143
General Directorate of Mineral Research and Exploration (MTA)	1945	0.201
	1959	0.231
General Directorate of Turkish Coal Enterprises (TKI)	1973	8.337
World Energy Council Turkish National Committee	1986	7.84
	2002	8.074
	2008	11.4
TKİ (2012) & MTA (2010)	2011	12.6

As of 2018, the lignite reserves are about 17.46 Gt, whereas hard coal reserves amount to 1.3 Gt [78].

3.2 Geological setting of the basins studied

This study used coal samples obtained from Tunçbilek (TU), Afşin-Elbistan (AFE), Soma (SO), and Tekirdağ-Saray (TS) basin as shown on Figure 3.1.

3.2.1 Soma basin

Soma coal basin is located in the Aegean region in western Turkey, about 90 km away from Manisa city. It is one of the first reserves explored in Turkey after the establishment of MTA in 1935. It contains a total reserve of around 861.45 Mt of coal [79]. The total tons extracted from the open pit per year adds up to 10.4 Mt. 7.7

Mt of the produced coal is used by six units' coal-fired power plants in Manisa, with a capacity of 990 MW, while 2.7 Mt is used for domestic and industrial purposes [80], [81]. This basin which belongs to the Miocene epoch is divided into three coal seams, (lower-seam), (middle-seam) and (upper-seam) [82]. In thickness, the Soma coal formation is around 325 m. It primarily consists of (1) conglomerate and sandstone-dominated layers with an average thickness of approximately 100 m. (2) Lower lignite seam, with an average thickness of approximately 15 m. (3) layers of limestone and sandstone, which consist of the middle lignite seam, is approximately 50-60 m thick [83], [84]. Figure 3.2 show a stratigraphic columnar section of the Soma lignite deposit. The lower lignite seam is the thickest, with around 15-22 m, and it lies between the marlstone unit and claystone units.

3.2.2 Tunçbilek basin

The Tunçbilek district is located in the Western part of Turkey and is about 60 km away from Kutahya city. The Miocene aged Tunçbilek-Domanic basin is located in western Anatolia-Turkey, and it includes two series of Neogene sediments [85]. The lower one is called the Tunçbilek series and is the one that contains approximately 317.73 Mt of lignite potential [79]. The upper one is called the Domanic series, and it lies on the Tunçbilek series, and an unconformity separates these formations. Figure 3.3 shows that the coal basins of Tunçbilek also contain non-coal layers and are found comparatively less in the upper and lower parts of the coal seam while they are more widespread in the middle parts [84].

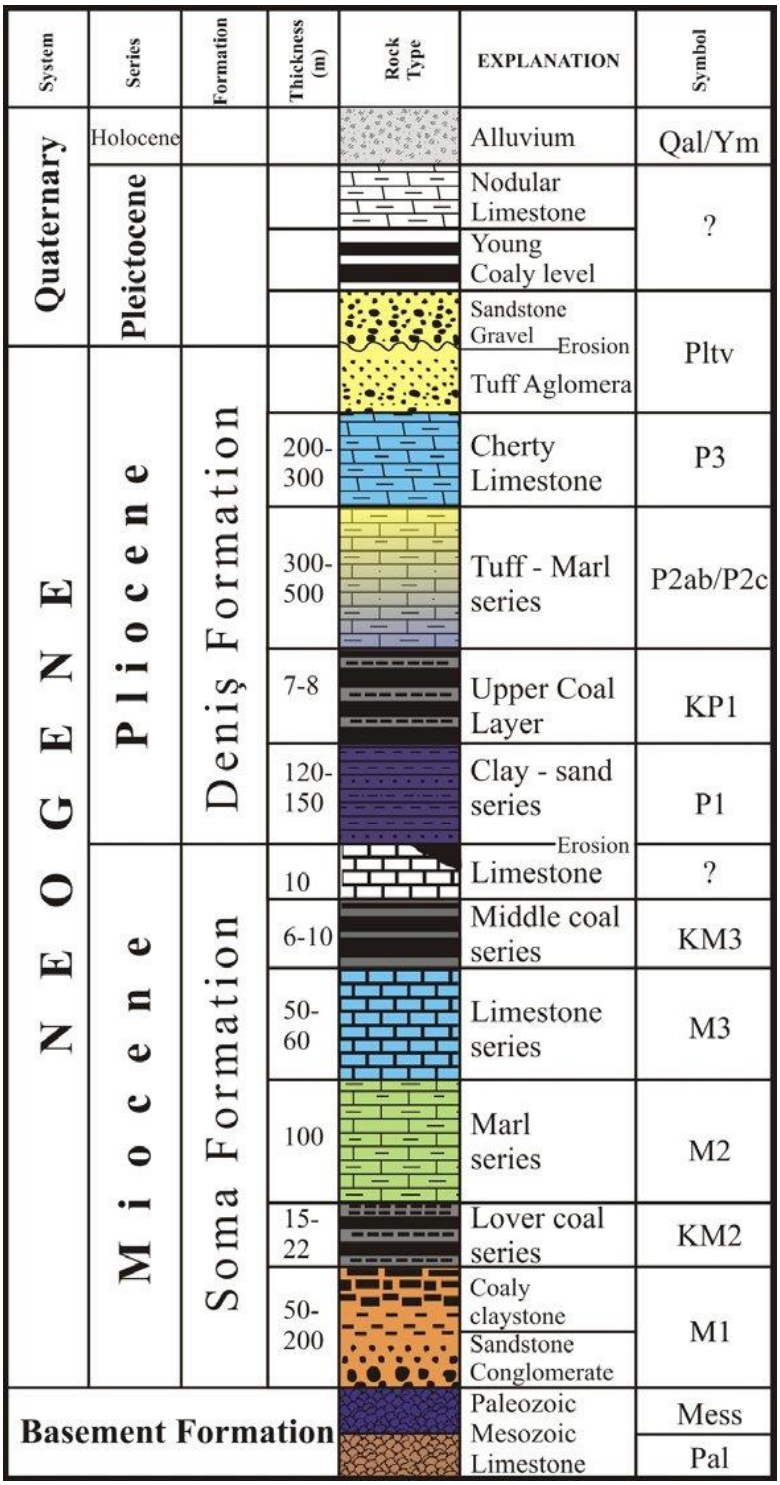

Figure 3.2.The stratigraphic columnar section of the Soma coal basin [86].

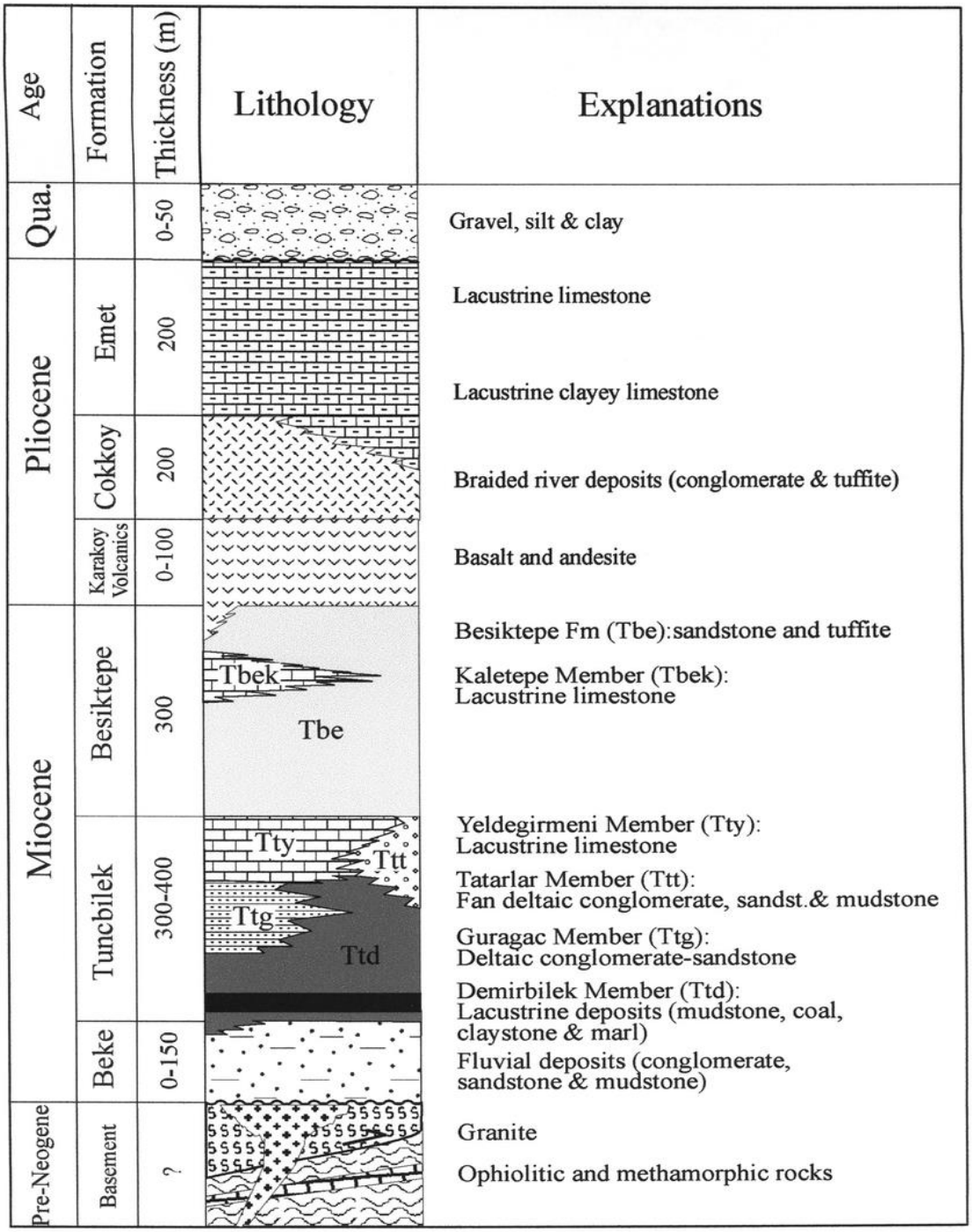

Figure 3.3.The stratigraphic columnar section of the Tunçbilek coal basin [87].

3.2.3 Tekirdağ-Saray basin

This basin consists of three sectors: Edirkoy, Kucukyoncali and Safaalancali, all situated in the Thrace region. This district contains 141.17 Mt of coal with a calorific value of less than 2000 kcal/kg, indicating a low-grade quality coal [79], [88].

Lignite formations are seen in two separate seams, which have economic value. The thickness of the coal-bearing series increases from the north to the south. The average thickness of the coal-bearing series in the field is nearly 110 meters. The coal is overlain by Pliocene aged clay, sand, sandstone, conglomerate and limestone, as shown on the columnar section of the basin in Figure 3.4 [89].

3.2.4 Afşin-Elbistan basin

Afşin-Elbistan is situated in the South-East of Turkey, in the Kahramanmaraş province, within the Afşin and Elbistan districts. Majorly, it is a Pliocene basin covering a total area of 900 km sq. [90]. The basin possesses a reserve of approximately 4.642 billion tons (Gt) and is the largest basin and one of the most important Turkish basins, especially for electricity generation [79]. It is a set multi-layered lignite sequence consisting of many seams interfacing with humic[1] and coal limnic sediments such as clay and gyttja[2] deposits see Figure 3.5.

---

[1] *Humus are organic compounds found in soil or peat material*
[2] Gyttja refers to "*a formation that is of sapropelic, black or brown mud with organic matter and has many gastropod shells"*

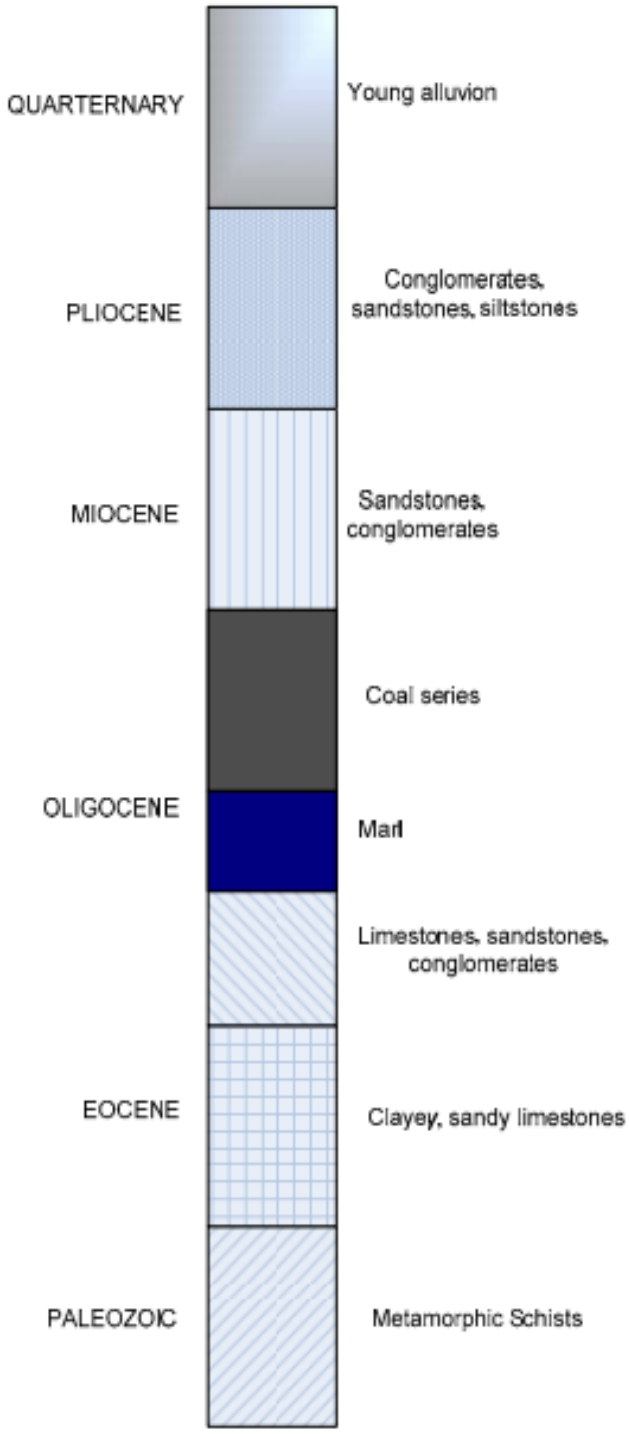

Figure 3.4:The stratigraphic columnar section of the Tekirdağ-Saray coal basin [89].

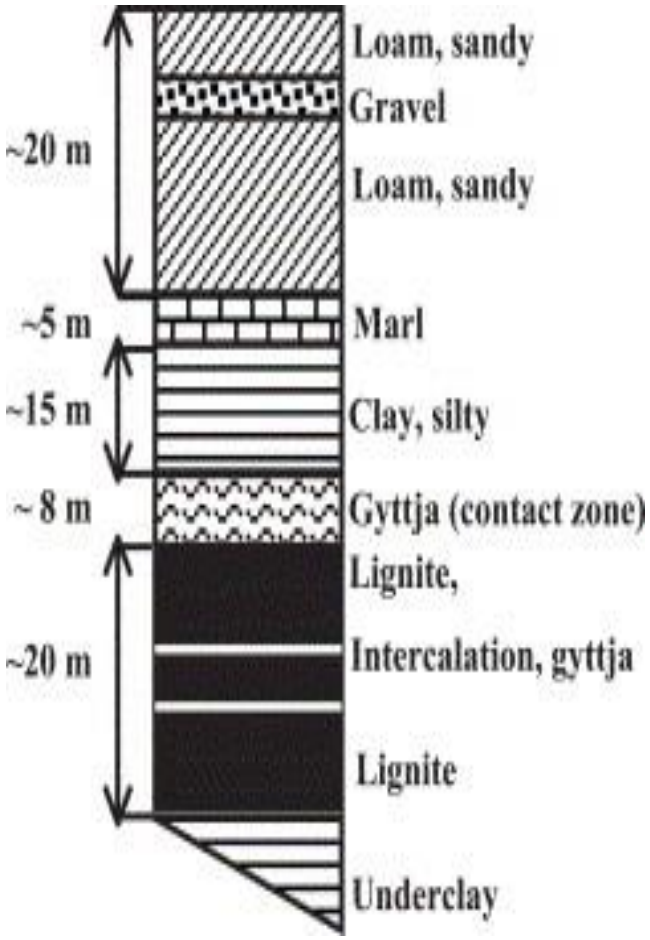

Figure 3.5.The stratigraphic columnar section of the Afşin-Elbistan coal basin. [91].

3.3 CO_2 storage in coal seams in Turkey

CO_2 storage activities in coal seams in Turkey have been mostly focused in the district of Zonguldak. This region is preferred for storage because it contains deeper seams, difficult and expensive to mine [92]. The Zonguldak coal basin is the only Turkish hard coal region, with coal seams suitable for coalbed methane (CBM) production [93]. In 2009, Sinayuc and Gumrah [66] used a simulation program to predict the basin's capacity for enhanced coalbed methane recovery (ECBM). However, in their study, they found that a CO_2 injection rate of nearly 5192 t/y would

only represent 0.3% of the annual CO_2 emission from the Zonguldak Catalagzi power plant. Therefore, they concluded that the project aiming at enhanced coalbed methane (ECBM) recovery would be much more feasible and successful than carbon dioxide storage. In 2012, Kok and Vural [94] drafted a clean coal technology roadmap for Turkey. They identified major CO_2 emitters such as coal-fired power plants, cement and iron-steel factories, and oil refineries and matched them with the nearest storage location. Their study's conclusion is summarized in Table 3.2**.** Until now, there is no CO_2 storage reported in coalbeds in Turkey [12]. However, through the European Union (EU) seventh framework research program, a project was recently carried out to estimate Turkey's coal mines' storage capacities. The estimated storage capacities were found to be between 3.7-13 Mt and 5.6-32 Mt CO_2 for the Soma and Zonguldak fields, respectively [95].

Table 3.2. Potential CO_2 capture and storage locations in Turkey [94].

Storage location	**CO_2 sources (Coal Power Plants, Iron-Steel, Cement and Oil Refineries: they will be all referred to Power Plants in this table)**
Manisa Soma lignite	Power plants, in Izmir, Manisa and Aydin
Kutahya Tavsanhi lignite	Power plants around Kutahya
Bursa lignite	Power plants, in Bursa and Kocaeli
Çayirhan and Kirsehir lignite	Power plants in Ankara and Kirsehir
Mugla-Yatagan lignite	Power plants in Mugla
Zonguldak hard coal	Power plants in Zonguldak
Oil/gas fields in Thrace	Plants around Kirklareli
Kahraman Maras-Elbistan lignite reserve	Power plants in Kahraman Maras, Osmaniye and Hatay

CHAPTER 4

STRUCTURE OF COAL

4.1 Origin and formation of coal

Coal is a combustible rock primarily formed from ancient plants accumulated in fens, bogs, salt marshes and some swampy anaerobic environment near the surface where the complete decay of the materials was prevented [96], [97].

Once the terrestrial plants (leaf, stem) in swampy areas die and fall off, they get covered with water, silt, sand, and other sediments. Under normal conditions, these materials would decay. However, the sediments and water prevent the plants material from reacting with oxygen and decomposing to carbon dioxide and water [98]. This mixture of plants and sediments is then attacked by anaerobic bacteria and converted into simpler forms, mainly pure carbon and simple carbon and hydrogen [99], [100]. The initial stage of the decay of this woody and soft material is known as **peat**.

Over several millions of years, this peat material accumulates. As the new sediments are deposited, it gets buried deep, with pressure, time, and temperature peat undergoes chemical and physical changes that, over time, progress through different ranks of coal [97]. This process is known as "**coalification**", and it is the geochemical process that transforms peat to lignite, lignite to sub-bituminous, sub-bituminous to bituminous coal and finally to anthracite. Once peat is compressed to a point where the inherent water content is less than 75%, it is referred to as coal [101]. In many parts of the world, this peat material is used as fuel after being dried up. It is considered low-quality fuel and environmentally damaging because it burns poorly with a lot of smoke [96], [102]. Figure 4.1 illustrates the stages of coal maturation from plants' deposition until the anthracite coal formation. It shows the process involved and describes the main chemical reactions involved at every stage.

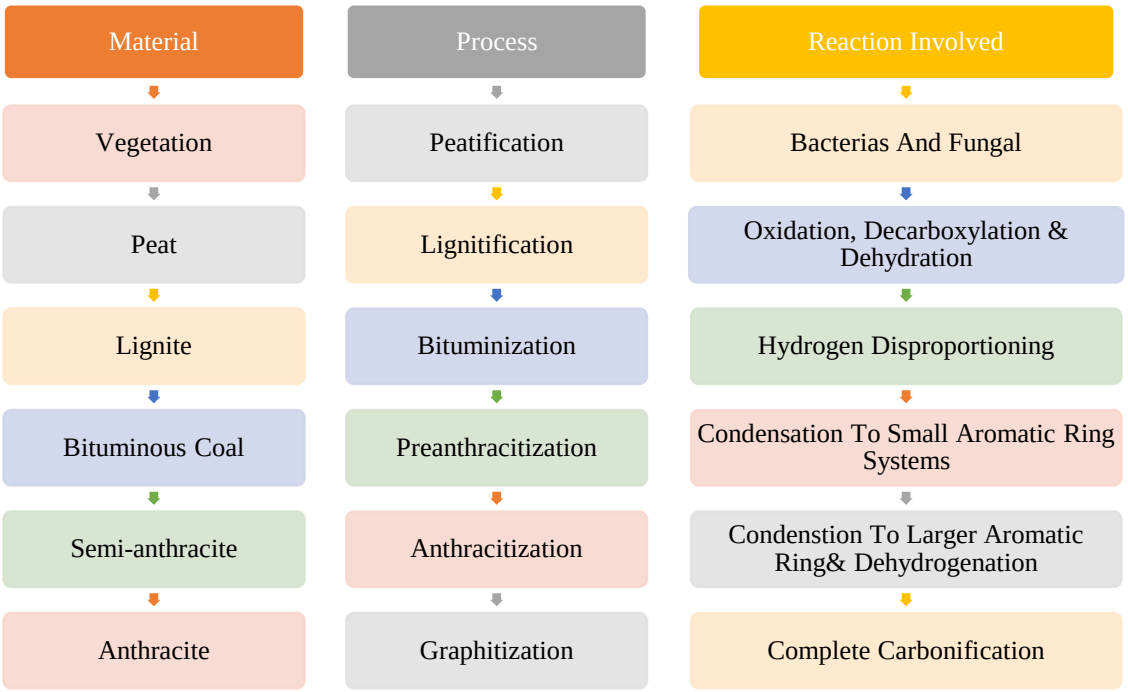

Figure 4.1. The coalification process. (Figure is modified from Miller [103])

4.2 Coal composition

Coal is composed mainly of organic material (**macerals**), mineral matter and water. The organic component maceral is responsible for the combustion energy and is the source of methane gas. Maceral is also the provider of the internal surface on which gases are adsorbed and stored.

The macerals are the (optical) microscopically identifiable components in coal with different physical and chemical properties such as color, shape, morphology, and degree of preservation of cell structure, reflectance level, and fluorescence intensity [104]. They originate from the dead plant tissues that have been compacted with other sediments at the time of deposition and have been chemically altered through the coalification process.

Macerals are classified into three groups (**vitrinite, liptinite, inertinite**) according to the degree of their reflectance.

Vitrinite macerals are produced from humic substances formed due to lignin and cellulose modification products (e.g., stems, trunks, roots, and branches) [105]. The maceral group of **inertinite** originates from the same material as the vitrinite group but has a higher aromatization and condensation degree. Compared to the vitrinite group, their reflectance is considerably higher, notably in low and medium-rank coals. They have higher carbon and lower hydrogen and oxygen contents compared to vitrinite group macerals at the same rank because they were degraded through carbonization, oxidization, or subjected to chemical or bacterial attacks prior to coalification, usually in the peat stage [100], [104], [105]. The **liptinite** group consists of macerals derived from hydrogen-rich plants such as pollen, spores, cuticles, waxes, resins and algae. This group is chemically more resistant to physical and chemical degradation than other macerals [100], [101].

4.2.1 Coal rank

The rank of coal indicates the stage reached by coal during the coalification process. Although coal is described in singular, it differs from type to type. The difference depends on the degree of metamorphism to which the peat material has been exposed for millions of years. Table 4.1 describes different types of coal and shows the properties and compositions of these coals. It shows that lignite is classified as low-rank coal or the immature one, whereas anthracite is ranked as the most mature coal type with more than 95 % carbon content [63], [99].

Table 4.1. Coal rank classification and uses [105]

Low-Rank Coals		**High-Rank Coals**	
Lignite	Sub-bituminous	Bituminous	Anthracite
17 % of total world coal resource	30 % of total world coal resource	52 % of the total world coal resource	1 % of total world coal resource
Used mainly in power generation	Power generation, cement manufacture	Manufacture of iron and steel	Domestic/industrial

Carbon and the heating values increase ⇨

⇦ **Moisture and ash content increase**

For their industry uses, high-rank coal is more desirable since it burns more cleanly, with high heating value, and it leaves fewer ashes. Vitrinite macerals are the most abundant of many coals, and they change continuously through the coalification process. It is often used to determine coal's rank since its characteristics are relatively easy to distinguish under the microscope [106].

4.2.2 Pore size distribution in coal

It is commonly accepted that void space in coals is a dual system of **pores and cleats**, as shown in Figure 4.2. Like in many other porous rocks, coals' porosity refers to the coal matrix's void volume. Total void volume is the sum of matrix pore space and the cleat/fracture system volume in the coalbed. In coal, there are mainly two types of cleats. **Face cleats,** which are dominant, are mostly continuous throughout the coal seam, and their surfaces are widely spaced. The **butt cleats,** on the other hand, are not continuous, and in many cases, they end at the intersection with face cleats [107], [108].

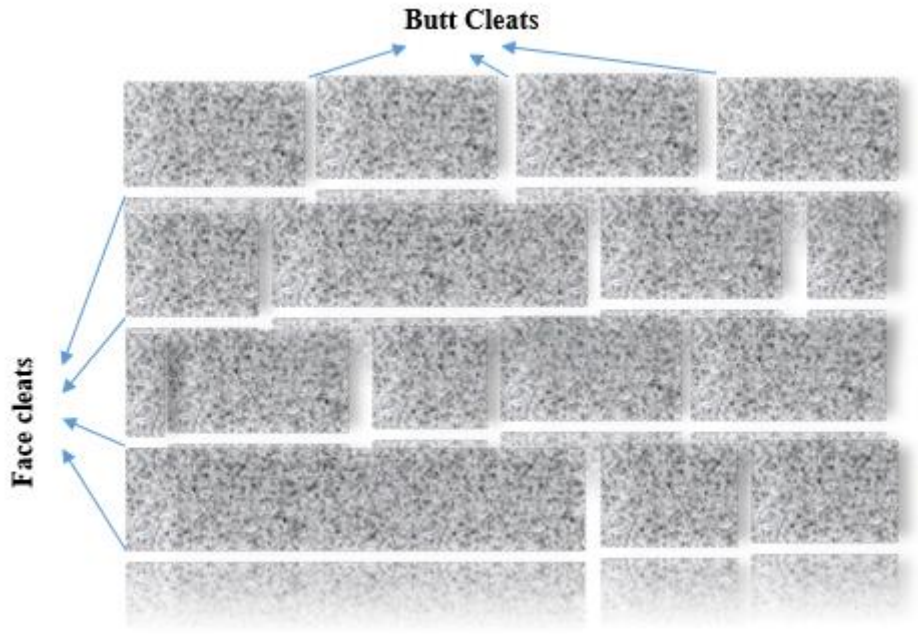

Figure 4.2. Cleat system in coal.

There are pores of different sizes in the coal matrix, and they are divided into four categories [23]. Tiny pores (sub-micropores) of diameters less than 0.8 nanometers, small pores (micropores) with diameter between 0.8 and 2 nanometers, medium pores (mesopores) with pore diameter between 2 and 50 nanometers and bigger pores (macropores) with pore diameter greater than 50 nanometers.

The cleats or fractures system are usually filled with water, whereas pores existing in the matrix contain the adsorbed gas (e.g. methane) [63]. Smaller pores have higher surface area compared to bigger pores; therefore, the adsorbed amount will be proportional to the pore sizes in the particle [109].

In the laboratory, several techniques are commonly used to analyze the size and distribution of pores. Some of these techniques are mercury intrusion, thin section analysis, image analysis, and gas adsorption [110]. Different methods are used to measure porosity in coals, such as scattering methods using X-rays/electron scattering, fluid probe methods, and microscopic methods such as optical/scanning electron microscopy (SEM) [23].

The most commonly used in laboratories is the fluid probe method. In this method, the common fluids used are helium, CO_2, nitrogen and methane. These fluids are preferred due to their small molecular size, as shown in Table 4.2 below. However, in coalbeds and shale reservoirs, with micropores less than 2 nm, helium is preferable because of its size and inertness. Helium has the smallest molecular size among other gases, and it is expected to permeate the entire coal structure and produce a more precise measurement of the void volume [111].

Table 4.2. The molecular diameter of gases used in porosity measurements

Gas	**Molecular diameter (nm) at $25°C$** [112]	**Kinetic diameters (nm)** [113]
Helium (He)	0.216	0.260
Nitrogen (N_2)	0.370	0.364
Methane (CH_4)	0.406	0.38
Carbon dioxide (CO_2)	0.454	0.33

CHAPTER 5

THEORY OF ADSORPTION

Adsorption is essentially an exothermic process at the interface of two phases in which molecules of a compound in gas or liquid states accumulate at an **adsorbent** surface [114].

The adsorbents' surfaces are unsaturated and therefore have active sites ready and waiting to interact with other molecules. When the intermolecular forces between solid-gas overpower those existing in gas molecules themselves, gas molecules will start accumulating on the solid's surface, and this process is what we refer to as **adsorption** of a gas on a solid [115]. The term **desorption** refers to the ejection of the previously adsorbed molecules from the solid surface. The term **absorption** or "imbibition", on the other hand, refers to the diffusion or penetration of molecules inside the bulk volume of the other material (i.e. absorbent) [116]. Therefore, the adsorption process is a surface phenomenon at the surface, whereas, in absorption, molecules permeate or dissolve inside a liquid or solid [117]. The adsorption process can take place in two ways: physical adsorption and chemical adsorption.

5.1 Physical adsorption

Physical adsorption, which is also referred to as physisorption or Van der Waals adsorption, occurs when the forces involved are intermolecular Van der Waals forces between the **adsorbate** and **adsorbent**. Physical adsorption usually consists of the formation of thick, multiple layers on the adsorbent surface. This process is reversible by heating or decreasing pressure, and molecules can easily desorb from the surface due to the weak force [118], [119].

5.2 Chemical adsorption

Chemical adsorption, sometimes referred to as chemisorption, occurs due to chemical bonding between adsorbate and adsorbent. These covalent, hydrogen or ionic bonds are much stronger than van der walls forces. Thus, this process is considered to be “almost” irreversible [120]. Chemical adsorption occurs as a monolayer structure and stops when the active or available sites are full (occupied).

5.3 Adsorption isotherms

The number of moles adsorbed by a solid is dependent on the temperature and pressure. Moreover, it depends on both the solid (adsorbent) properties and the adsorbing gas [98]. The plot of change in the adsorbed amount against pressure at constant temperature is called the adsorption isotherm. According to the IUPAC classification, there are six types of adsorption isotherms (see Figure 5.1).

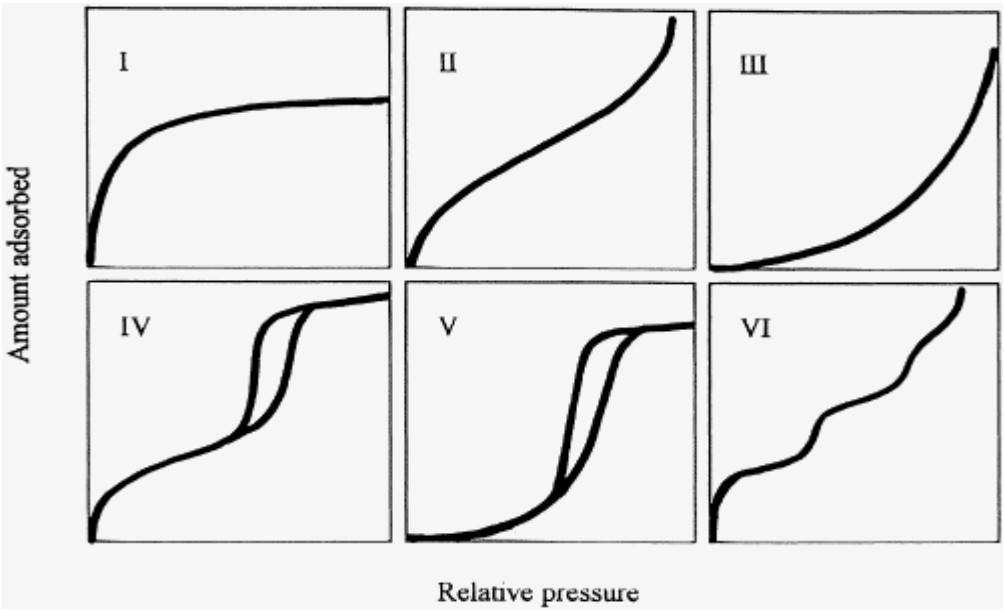

Figure 5.1. Adsorption isotherms according to the IUPAC classification [121]

Type 1 isotherms represent the adsorption of gas molecules to the solid having micropores. This type reaches an equilibrium point, indicating the monolayer’s

completion or the complete filling of the accessible pores by the gas molecules. [122]. **Type II Isotherms** are found typically in non-porous or macroporous adsorbents. The saturation point is not attained, and therefore the adsorption occurs in successive layers [120]. **Type III isotherms** are usual for non-porous or macroporous adsorbent with weak adsorbent-adsorbate interactions. **Type IV isotherms** are typical in mesoporous adsorbents, and they are characterized by a hysteresis loop, which indicates the filling of mesopores by capillary condensation [123]. **Type V isotherms** are typical for macroporous adsorbents and are also characterized by the hysteresis loop. The stepwise formation of multilayer on non-porous adsorbent surfaces is classified as **Type VI** in IUPAC classification, but it is rare [121].

5.4 Adsorption equilibrium equations

Various adsorption models are used in the literature to describe adsorption processes [124], [125]. Some of the most commonly used for CO_2 adsorption in coals are given in details in the following sections.

5.4.1 Langmuir isotherm

Irving Langmuir proposed a model in 1918 [126]. This model is which is used to describe a type I isotherm see Figure 5.2, has been widely used in literature to measure CH_4 and CO_2 adsorption on solids [117], [127]–[133]. In this model, several assumptions are made [120]: (1) the adsorption is localized, this means molecules remain at the site of adsorption until desorbed, (2) the heat of adsorption is taken as constant (thus, all sites are energetically the same, and there are no interactions between adsorbate molecules), (3) each site can hold only one adsorbate molecule, (4) the surface of the adsorbent is covered only by a monolayer of adsorbed molecules.

Langmuir adsorption model is expressed as follows [121]:

$$n_{ads} = \frac{n_{max} \cdot P}{P_L + P} \qquad 5.1$$

where n_{ads} : moles adsorbed, (mol/g), P: the pressure of adsorbate, (bars), n_{max} : maximum adsorption capacity (mol/g), P_L: Langmuir pressure that corresponds to a half of n_{max} (bars) see Figure 5.2.

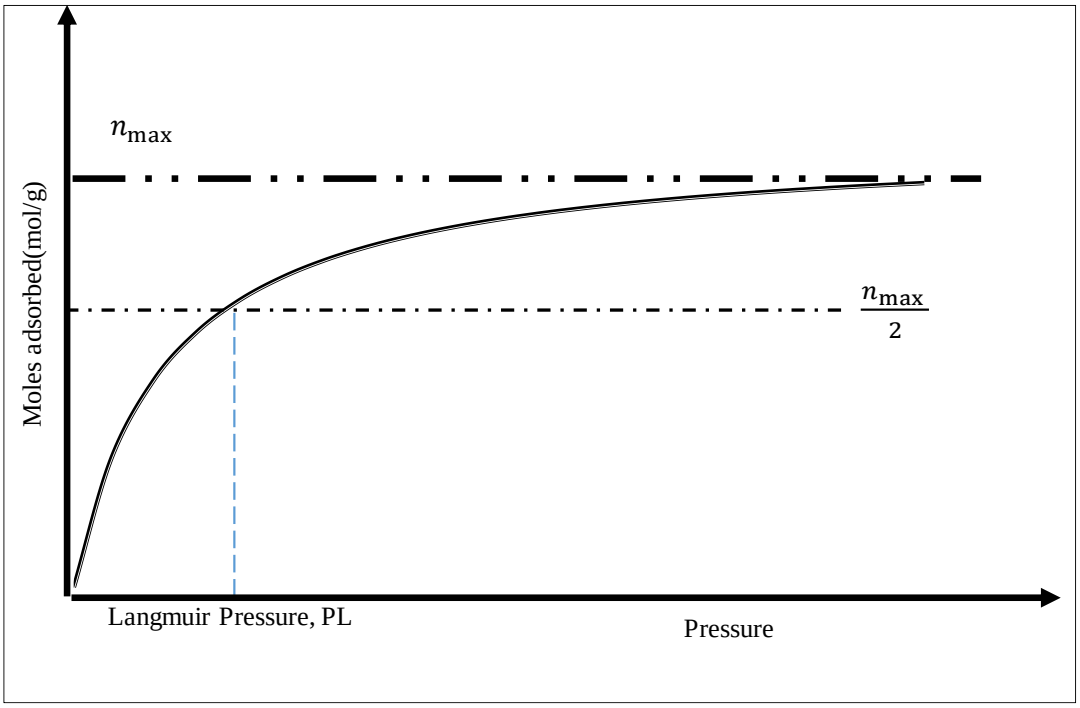

Figure 5.2. Langmuir isotherm.

Modified Langmuir model

Equation 5.1 can also be expressed:

$$n_{ads} = n_{max} \cdot \frac{\rho_g}{\rho_L + \rho_g}$$

where n_{max} is the maximum adsorption capacity and ρ_L is the density at which the half of n_{max} is adsorbed.

A modified version of the Langmuir model [134] includes a correction factor that enables it to be used with excess adsorption.

The modified equation is expressed as:

$$n_{ex} = n_{max} \cdot \left(1 - \frac{\rho_g}{\rho_a}\right) \frac{\rho_g}{\rho_L + \rho_g} \qquad 5.2$$

where ρ_a and ρ_g are adsorbed phase density and free gas density, respectively.

Another form which is widely used is the Langmuir modified +k model [134]–[136]

$$n_{ex} = n_{max} \cdot \left(1 - \frac{\rho_g}{\rho_a}\right) \frac{\rho_g}{\rho_L + \rho_g} + k \cdot \rho_g \qquad 5.3$$

This k-term is added to account for volume changes due to compression and swelling in coal and errors in void volume calculations [135].

5.4.2 The Brunauer-Emmett-Teller (BET) equation

The Langmuir isotherm is not valid in many cases, especially for non-porous or macroporous solids where the adsorption does not reach a saturation point. The surface area's determination also presents a significant challenge, which the monolayer theory could not address. If the adsorption capacity were limited to a monolayer, the determination of adsorption equilibrium from experimental data with a known gas molecular size would be enough for the surface area's estimation. However, the main issue is that, in chemisorption, the adsorption sites are widely spaced, and therefore, many sites are left unoccupied [137].

Multilayer formation begins at pressures far below the amount needed for the completion of the monolayer. Hence it is not possible to determine the monolayer capacity from experimental data. In 1938 Stephen Brunauer, Paul Emmett and

Edward Teller [138] addressed this issue by developing a model to account for multilayer adsorption and extract information on monolayer capacity.

This model was based on several assumptions (i) there is no interaction between neighboring adsorbed molecules, (ii) the heats of adsorption evolved to fill the second layer, and subsequent layers of molecules are equal to the heat of condensation/liquefaction of adsorbate molecules (iii) at saturated vapor pressure, adsorbate liquefies (condenses to liquid) on the surface of the solid, leading to infinite layers [120], [139]–[141]. The BET isotherm model is valid in the range between relative pressure values of ($0.05 < P/Po < 0.35 - 0.40$) [137].

The linearized form of the BET equation is expressed as:

$$\frac{P}{V \cdot (P_o - P)} = \frac{1}{V_m . C} + \frac{(C-1) \cdot P}{V_m \cdot C \cdot P_o} \qquad 5.4$$

V: volume of adsorbed vapor at STP.
Vm: monolayer capacity at STP.
P: partial pressure of the adsorbate
Po: saturation vapor pressure of the adsorbate

C: is a constant

$$C = e^{\frac{|\Delta H_1| - |\Delta_{v \to L} H|}{R \cdot T}}$$

In this expression, ΔH_1 is the enthalpy of adsorption of the first layer of gas, and $\Delta_{v \to L} H$ is the enthalpy of liquefaction of the gas.

5.4.3 Polanyi's potential theory

In 1914, Polanyi [142] assumed lines of the same potential energy around the adsorbent (solid) into which the adsorbing gas molecules fell.

The region between each set of equipotential lines corresponds to a particular adsorbed volume. As shown in Figure 5.3, Polanyi ascribed a volume εi to the space between the ith equipotential lines.

The potential energy of equipotential lines W is assumed to be independent of the temperature so that the expression 5.5 will essentially be an isotherm equation [143]. The characteristic adsorption curve expression:

$$W = f(\varepsilon) \qquad 5.5$$

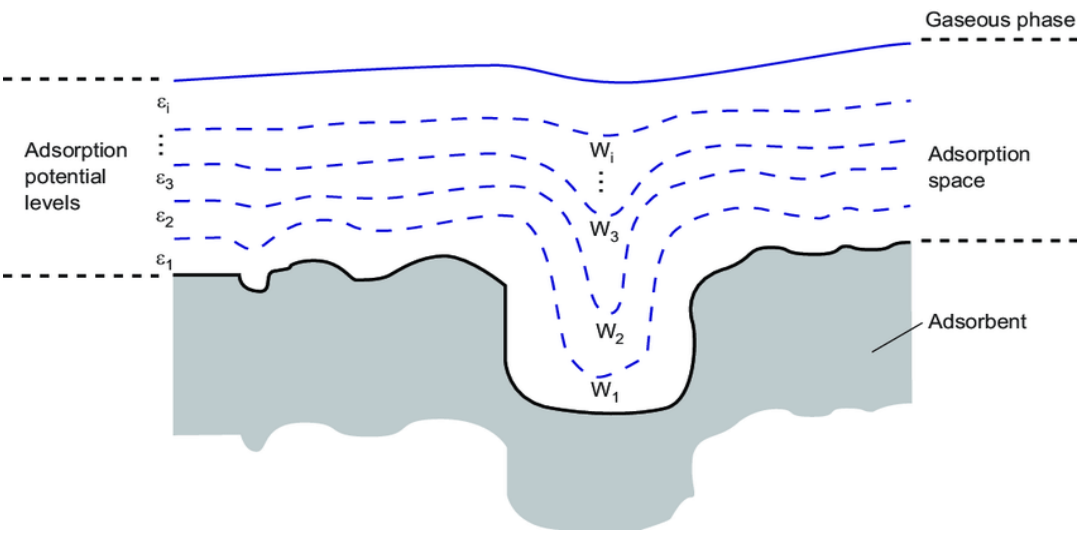

Figure 5.3. The schematic representation of Polanyi's potential theory [144].

The adsorption potential is defined as the energy required to compress the gas from a certain pressure P to the saturation pressure Po. Thus, considering one mole of a perfect gas of volume v, the adsorption potential is:

$$\varepsilon = \Delta F = \int_{P}^{Po} VdP = R \cdot T \cdot ln(\frac{P_o}{P}) \qquad 5.6$$

where ΔF is the free energy change and P_o is the saturated vapor pressure. The volume adsorbed, according to Polanyi's Theory, is:

$$W = n \cdot V_m \qquad 5.7$$

where *n*: number of moles adsorbed per unit mass of sorbent, *Vm*: molar volume

The characteristic curve is plotted by using these two equations (5.6 & 5.7). That is by plotting $n \cdot V_m \; vs \; R \cdot T \cdot ln\left(\frac{P_o}{P}\right)$.

In 1967, based on Polanyi's theory [145], Dubinin proposed an adsorption model known as the theory of micropores filling [146]. This theory states that the adsorbate fills the pore volume in microporous solids and does not form distinct layers in the pores see Figure 5.4. Coal is one of the microporous adsorbents, which means that the adsorption process is not limited only to the surface but also to the volume filling.

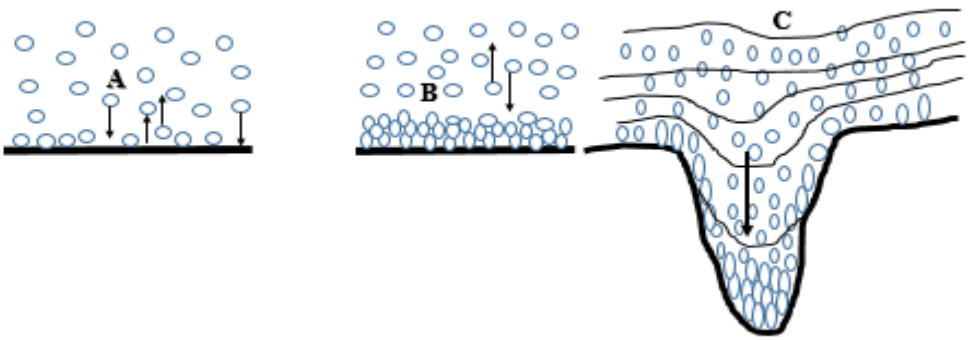

Figure 5.4. A schematic representation of adsorption mechanisms, (A) Langmuir model, (B) B.E.T model and (C) Dubinin model. (Figure is modified from R.M. Flores [99])

Later on, Dubinin and Astakhov (D-A) [147] proposed a model derived by energy balance where gas is filled in the micropores of adsorbent

The model can be expressed as:

$$n_{ads} = n_{max} \cdot e^{-\left(\left(\frac{R \cdot T}{\beta \cdot E_o}\right)^n\right) \cdot \left(\ln\left(\frac{P_o}{P}\right)\right)^n} \qquad 5.8$$

where n_{ads} is the amount adsorbed, n_{max} is the adsorption capacity in micropores (micropores volume). R is the gas constant, T is the temperature, β is the affinity coefficient, E_0 is the heat of adsorption, P_o is the saturated vapor pressure, and n is the heterogeneity parameter ranging from 1 to 4, indicating the degree of heterogeneity in the material.

Dubinin and Radushkevich (D-R) restricted n = 2 for some. Thus the D-R model is expressed as:

$$n_{ads} = n_{max} \cdot e^{-\left(\left(\frac{R \cdot T}{\beta \cdot Eo}\right)^n\right) \cdot \left(\ln\left(\frac{P_o}{P}\right)\right)^2} \qquad 5.9$$

In a simpler form, it can be written as:

$$n_{ads} = n_{max} \cdot e^{-D\left(\ln\left(\frac{\rho_a}{\rho_g}\right)\right)^2} \qquad 5.10$$

where the parameter $D = \left(\frac{R \cdot T}{\beta \cdot Eo}\right)^2$ is related to coal affinity for CO_2. β Is the affinity coefficient between CO_2 and the coal, (β = 0.35 for CO_2) and E_o is the characteristic heat of adsorption.

For the adsorption of CO_2 in coal, the original D-R model can be modified to include a correction factor that enables it to be used with excess adsorption

$$n_{ex} = n_{max} \cdot \left(1 - \frac{\rho_g}{\rho_a}\right) \cdot e^{-D\left(\ln\left(\frac{\rho_a}{\rho_g}\right)\right)^2} \qquad 5.11$$

To account for volumetric changes in coal samples, the additional k-term was added to the model, and the resulting expression is:

$$n_{ex} = n_{max} \cdot \left(1 - \frac{\rho_g}{\rho_a}\right) \cdot e^{-D\left(\ln\left(\frac{\rho_a}{\rho_g}\right)\right)^2} + k \cdot \rho_g \qquad 5.12$$

Ozdemir and his colleagues adjusted the D-A model to account for volumetric effects such as coal swelling by [148] :

D-A model by Ozdemir and co-workers

$$n_{ex} = n_{max} \cdot \left(1 - \frac{\rho_g}{\rho_a}\right) \cdot e^{-\left(\left(\frac{R \cdot T}{\beta \cdot Eo}\right)^n\right) \cdot \left(ln\left(\frac{Po}{P}\right)\right)^n} + \rho_g \cdot \Delta V \qquad 5.13$$

Other studies [134], [135] proposed a new D-R modified model that can describe gas adsorption at supercritical conditions. A proportionality term *k* was added to describe different effects, including Henry's law dissolution of gas, errors of cell volume and helium density, penetration of various gases, rock swelling and shrinkage effects [135].

The D-R modified +*k* model is given by:

$$n_{ex} = n_{max} \cdot \left(1 - \frac{\rho_g}{\rho_a}\right) \cdot e^{-\left(\left(\frac{RT}{\beta Eo}\right)^2\right) \cdot \left(ln\left(\frac{\rho_a}{\rho_g}\right)\right)^2} + k \cdot \rho_g \qquad 5.14$$

where ρ_a, ρ_g are the adsorbate density and free gas density, respectively, *k* is the proportionality constant.

5.5 Excess adsorption concept

The actual adsorbed amount cannot be measured by the volumetric methods. This is because volumetric methods do not account for the volume occupied by the adsorbed phase, as shown in Figure 5.5. Gibbs [149] defines the excess adsorbed amount n_{ex} as the amount of gas calculated to have adsorbed if the volume of adsorbed phase, V_a is ignored.

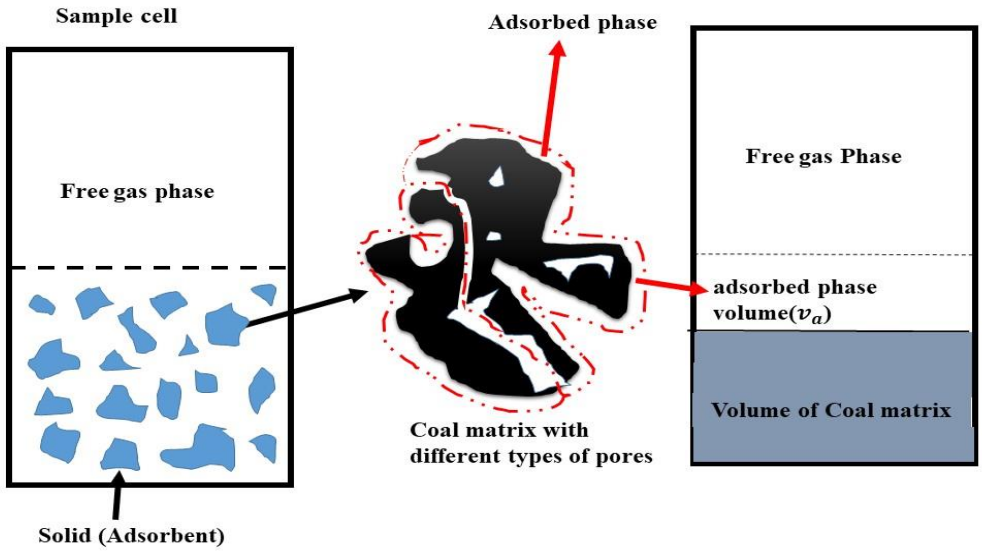

Figure 5.5. The schematic description of gas adsorption on coal matrix.

There are two forces involved in adsorption systems, between molecules themselves and between adsorbent and molecules. When these two forces come in equilibrium, they form an imaginary invisible layer at some distance x (see Figure 5.6) from the adsorbent surface. Any gas molecules between the adsorbent surface and the layer are held by the adsorbent force. In general, as molecules of the free gas phase approach the adsorbent surface, their density will change as a function of distance. Area A symbolizes molecules with a density greater than the free gas density. Area B symbolizes the hypothetical case in which the density of free gas does not change as molecules approach the surface of the solid. As a result, the excess adsorption is

represented by area A. the absolute adsorption is the area A+B, which represent all gas molecules held in the adsorption field by the adsorbent forces [50], [150], [151].

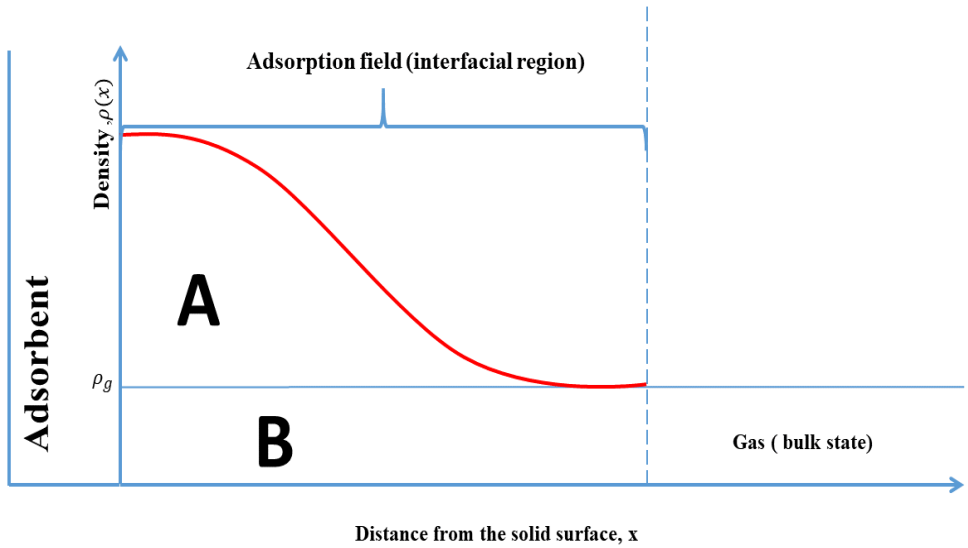

Figure 5.6. The Gibbs model's interpretation with a density profile against distance from the adsorbent surface. (Figure is modified from Gumma and Talu [152])

Mathematically absolute adsorption can be written as:

$$\Gamma_{abs} = \int_{0}^{\infty} \left(\rho(x)\right) dx \qquad 5.15$$

However, this integral diverges. Therefore, this prompted Gibbs to introduce the adsorption excess theory [152]. He assumed that at a certain distance x from the adsorbent's surface, the adsorption field created by the solid becomes negligible, and the density of the adsorbed molecules becomes equal to the density of the free gas phase [153]. Therefore, he defined the excess adsorption as:

$$\Gamma_{ex} = \int_{lower\ limt}^{x} \left(\rho(x) - \rho_g\right) dx$$

The lower limit is assumed to be zero, which corresponds to the surface of the solid. By making *x* large enough, the density function will eventually be reduced to the free gas phase. Hence the value of *x*, in this case, will be infinity,

The following expression is Excess adsorption:

$$\Gamma_{ex} = \int_{0}^{\infty} \left(\rho(x) - \rho_g\right) dx \qquad 5.16$$

For rigid solids,

$n_{abs} = n_t - \rho V_{void}$

where ρ is the molar density of the gas in the free space, n_t the total moles of gas transferred into the sample cell, and V_{void} *is* the void volume in the sample cell.
Gibbs excess adsorption equation models [134]:

$n_{ex} = n_{abs} - \rho_g Va$

where v_a is the volume of the adsorbed phase.

$$n_{ex} = n_{abs} + \rho_g \left(-\frac{n_{abs}}{\rho_a}\right) \qquad 5.17$$

where ρ_a is the density of the adsorbed phase.

The shape of the density function shown in Figure 5.6 is not necessarily correct; some studies have shown that in the interfacial region, the density may be higher or even lower than the free gas density [149], [151]–[155].

There is not yet any rigorous ways to determine the adsorbed density. In this study, the tentative density was determined from the graphical method, as explained in Appendix C. This method is based on equation 5.17; the excess number of moles will become zero when the free gas density increases and reach the adsorbed phase density. Therefore, by plotting the density versus the excess number of moles adsorbed, we can determine the adsorbed phase density by looking at the intercept

of the linear part of the density profile where excess moles become zero [150]. This density is then used as the initial point for the adsorption modelling optimizations.

5.6 Effects of coal rank and moisture on adsorption

Bustin and Clarkson [156], performed an adsorption study on a series of Australian coals; the objective of their study was to quantify the effects of coal composition, coal rank and gas content on methane adsorption; they found a good correlation between coal vitrinite content and the micropore capacity. Chikatamarla and Crosdale [157], performed experiments on dry coals from various coal ranks, from high volatile bituminous coal to anthracite. They found that mineral matter content decreases the adsorption capacity. Moreover, in high bituminous coal, the adsorption capacity increases with the vitrinite content, whereas in low bituminous coal, there was no clear correlation observed. Yalcin and Gurdal [158], investigated the correlation between coal properties and gas adsorption capacity. They performed experiments on 81 coal ranging from medium to high bituminous coals. However, there was no consistent trend in methane adsorption capacity with coal composition or ranks. Busch et al. [159] studied the adsorption behaviour of various coal from the argonne premium coal program with vitrinite reflectance ranging from 0.25 to 1.68 %. They observed that at low pressures, the adsorption increases with coal rank, especially for wet coals. This is because higher-ranking coals have more surface area than low ranking coals. Gareth et al. [160] found that rank is critical in the adsorption process of coal. In the bituminous and anthracite coals, the highest methane adsorption was observed on the highest ranking coals. However, there was no positive correlation between sub-bituminous coal and methane adsorption capacity. Hildenbrand et al. [161], using a computational method to study the methane sorption capacity of central European coals they found that sorption storage capacity increases with coal rank for moist coal, agreeing with previous studies

In another study, Day et al. [162] investigated the relationship between coal properties and Supercritical CO_2 sorption capacity. They experimented 30 different

coals, mainly from Australia, the USA and Poland, at 16 MPa and 53 °C in a gravimetric apparatus. They found a weak correlation between CO_2 adsorption and coal compositions. They concluded that CO_2 sorption capacity could not reliably be determined based on the coal rank. Ozdemir and Schroeder [163] studied the influence of moisture on coal. They found that the adsorption on dried coal gives a U shape relationship when plotted with coal rank, but for the moist or wet coal samples, there was an almost linear relationship between coal rank and adsorption. Zhang et al. [55], also found the U-shaped relationship between adsorption capacity and coal rank on four dry coal samples from China. Yves and Busch [74] presented a conceptual model to describe the competitive adsorption between CO_2 and CH_4 behavior on wet coals of different coal ranks. Concerning the coal rank, they found that sorption on dry coals increases up to a point and decreases with increasing the rank, displaying a parabolic-shaped behavior. The study also showed that the gas sorption on moist coals increases linearly with the rank.

Nie et al. [164], studied the sorption properties of four dry coals with different ranks. They found that the maximum adsorption capacity on dry coal samples displays a U-shaped curve when plotted against the coal rank. The same dry coals were placed under constant humidity to adsorb moisture on an equal basis. They observed that the adsorption for wet coals decreased compared to the dry coals. In addition, they also confirmed a positive linear relationship with coal ranks. Deyond and Xiaojie [130] tested 11 coals with various ranks, and their study was to find factors that influence gas adsorption capacity. They found that the volume adsorbed increased with vitrinite reflectance. In addition to this, Debadutta et al. [165] also tested several coals from Raniganj coalfield, and they found that the vitrinite reflectance had a strong relation ($R^2 = 0.7$) with the Langmuir volume. The reason for such a positive correlation is that higher-ranking coals have more surface area than low ranking coal. As the coalification process continues, the reduction of water and cracking of the clog up oils reopens the micropores systems and increases the adsorption sites

In 1997, Levy et al. [166] studied the Bowen coals' methane adsorption capacity and the influence of coal properties on adsorption. Concerning the moisture effects, they

observed that as the coals' moisture content increased from 0.9-3.7 percentage of weight, the adsorption decreased linearly at approximately five ml/g at every 1 % increase in moisture. Ozdemir and Schroeder [163] studied the effects of moisture content on adsorption isotherms on Argonne premium coals. They found the adsorption on wet coals samples are much less than in dry coals. They attribute this behavior to the filling or blocking of the pore space by water molecules that would otherwise be available for CO_2 molecules. Guo et al. [167] performed experiments on low-rank coals from Shenbei and Tiefa coalfields in China. They studied the effects of moisture content on adsorptions. Their study's key finding was that: The more the moisture content, the fewer adsorption sites available for the adsorbing gas. Water preferentially adsorb on oxygen and nitrogen functional groups in coal, resulting in decreased adsorption sites available for CO_2. Water could also adsorb CO_2, forming what is known as "water clusters". These clusters would reduce the adsorption potential of CO_2 as well. However, they also found that as the moisture content increases and reach a particular value, its effects on adsorption are not clear and may no longer be the primary factor affecting the adsorption.

CHAPTER 6

EXPERIMENTAL METHODOLOGY

In this study, the volumetric (manometry) method was used to measure adsorption. This method is commonly used because it is inexpensive and easy to implement compared to other approaches. The setup consists of a reference cell and a sample cell. The gas is injected into the reference cell, and then it is expanded into the sample cell containing the sample. The number of adsorbed moles are calculated by measuring the pressure drop and using real gas state equations.

6.1 Experimental setup

The experimental design schematic and the actual photo of the setup are given in & Figure 6.2. The description of each component is also provided in Table 6.1. The setup consists of a high-pressure sample cell and a Reference cell of 75 cc and 71 cc, respectively. These cells are made from brass and can handle high pressure up to 280 bars.

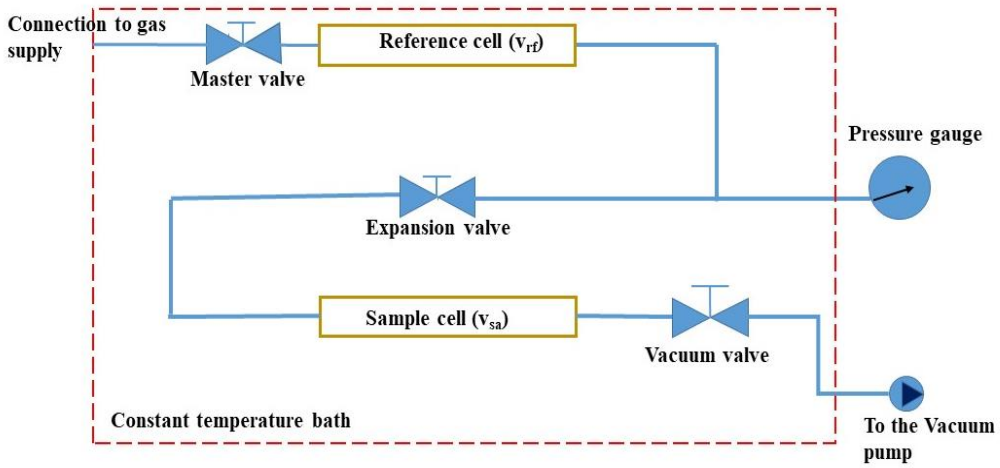

Figure 6.1. Volumetric adsorption experiment diagram.

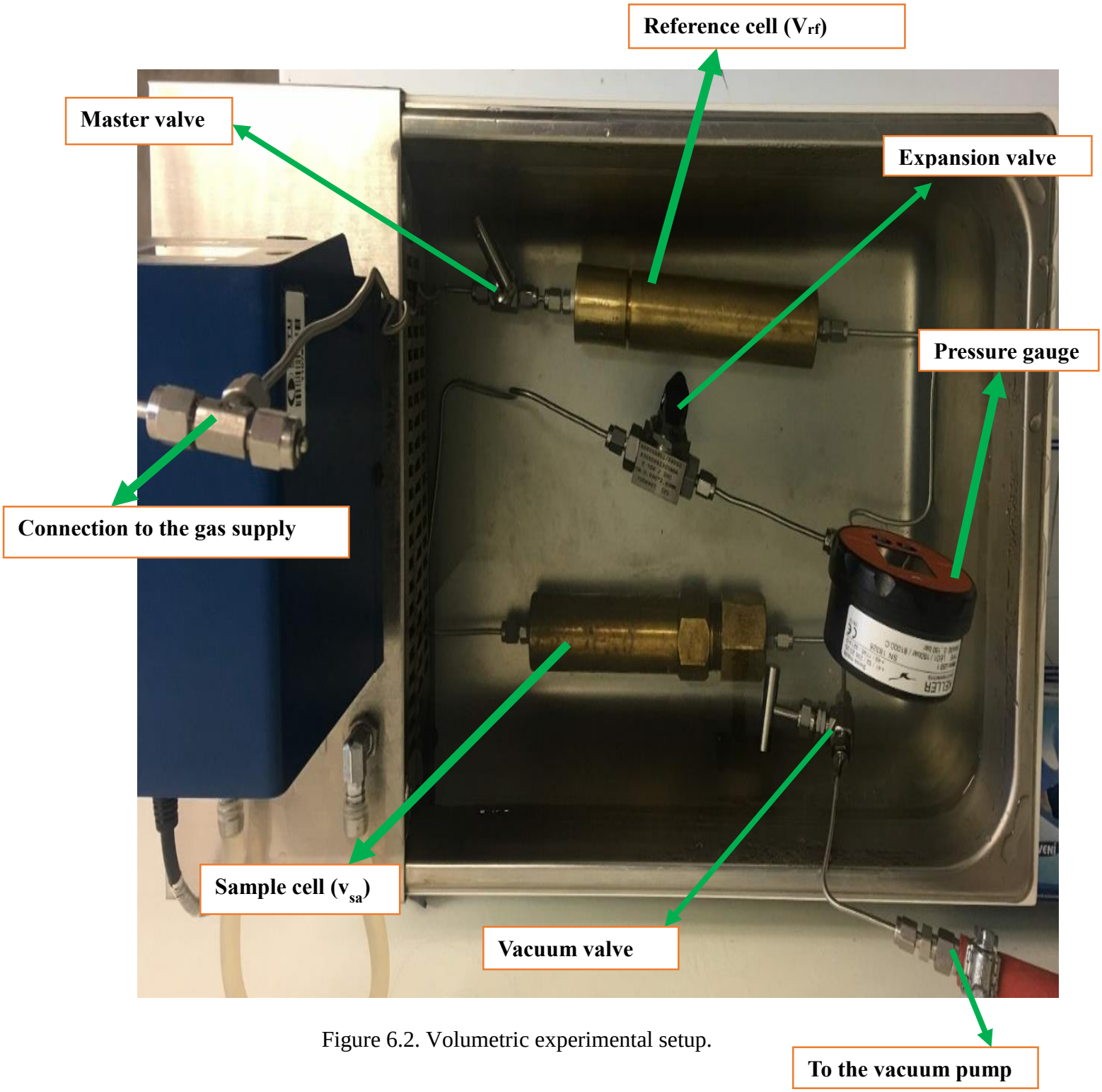

Figure 6.2. Volumetric experimental setup.

Table 6.1. Components of the volumetric method used in this study

Components	Description
Gas Cylinders	Two gas cylinders, He of purity of 99.5-100 %, from Praxair, Inc. CO_2 from Linde plc of purity of 99.9 %,
Tubing and Fittings	stainless steel (SS) 1/8" and a 1/16" tubing, purchased from Swagelok
Valves	Two types of Valves were both purchased from the Hamlet company. A two-way H-6800-SS-L-1/8-RCSS type and a two-way H-99.
Reference and Sample Cells	These cells were self-fabricated from brass material. They could handle pressure up to 280 bars.
Pressure Gauge	LEO1 Digital Manometer. Range -1 to 150 Bar with an accuracy of less than 0.2 % FS and peak reading mode at 5kHz was purchased from Keller AG company. Operating temperature 0 to 50 °C, 3 V internal battery of type CR 2430 for up to 1,000 hours operation (150 hours in peak mode) and IP65 Protection.
Water Bath	The constant temperature water bath was purchased from DAIHAN Scientific Co.Ltd, model WiseCircu WCB-22, temp. range & accuracy: ambient＋5℃~ 100℃, ±0.1℃ accuracy
Vacuum Pump	A vacuum pump, E5zA2B-053/Busch SV 1005 D, was purchased from Hanning Elektro-Werke.
Filter Papers	Filter papers were purchased from the fann instrument company. Their sizes were 3.5 inches or 9 cm in diameter

6.2 Coal sample preparation

As shown in Figure 6.3 — Figure 6.6, the four coal samples from Soma, Tunçbilek, Tekirdağ-Saray and Afşin-Elbistan basin, were used in this study. Before the experiments, the samples were first hand-crushed to have the same particle size. The crushed sample instead of a whole coal lump or bigger particles is important because it minimizes diffusion time for adsorption [168]. First, each coal sample was crushed in a mortar and pestle, shown in Figure 6.7. The sample was screened using different meshes of different sizes (see Figure 6.8). The sizes of meshes are as follows: No: 10 (2 mm), 18 (1 mm), 35 (0.5 mm), 60 (0.250mm), 120 (0.125 mm), 230 (0.063 mm). A sieve shaker (Figure 6.9) was used to shake coal particles for 20 minutes to obtain coal powders with the expected coal particle size. A certain mass (as shown in Appendix A) of (0.250 mm) coal powder was made for each sample's adsorption experiment.

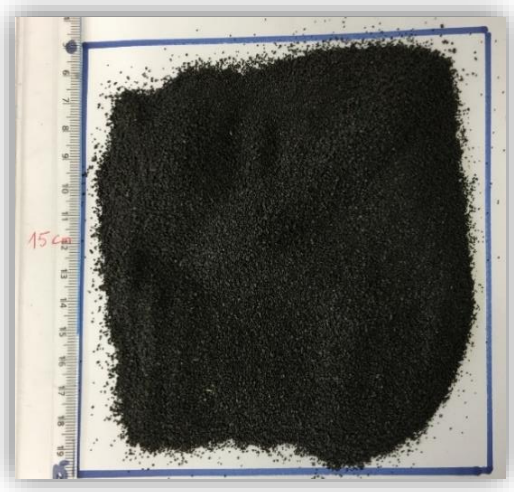

Figure 6.3. Soma coal sample

Figure 6.4. Tunçbilek coal sample

Figure 6.5. Tekirdağ-Saray coal Sample

Figure 6.6. Afşin-Elbistan coal sample

After sieving, samples were placed in the oven, as shown in Figure 6.10**,** to remove surface and inherent moisture**.** They were heated up to 110 °C for 36 hours before being loaded into the sample cell. Samples must be prevented from accumulating any moisture before they can be loaded into the sample cells because adsorption is greatly affected by moisture content.

Figure 6.7. The mortar and pestle

Figure 6.8. The sieves

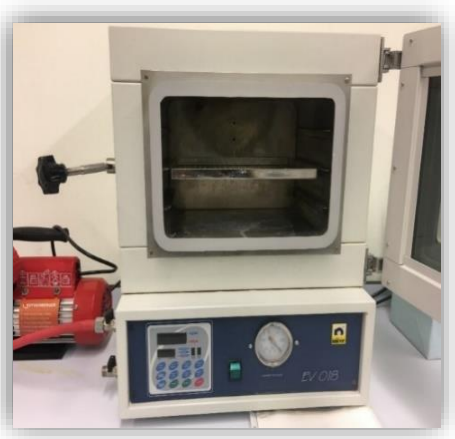

Figure 6.9. The sieve shaker. Figure 6.10. The drying oven

The proximate and ultimate analysis of the four coal samples was conducted by ELI (Ege Linyit Isletmeleri) laboratory, according to TS 4744 and TS 5122 standards. Both analyses are presented in Table 6.2 & Table 6.3. In the table, the letters mean *C:* Carbon, *H*: Hydrogen, *N*: Nitrogen, *O*: Oxygen, *FC*: Fixed Carbon *NCV*: Net Calorific Value, *M*: Moisture Content and *VM*: Volatile Matter. All the data presented here are evaluated on a dry basis**.**

Table 6.2. Proximate analyses and vitrinite reflectance values of the coal samples

COAL SEAM	**Vitrinite reflectance (%) Ro**	**Ash* (%)**	**VM* (%)**	**NCV* (kcal/kg)**	**FC (%)***
Soma	0.35-0.48 [169]	8.53	41.41	6346	50.06
Tunçbilek	0.42 -0.51 [87]	24.44	34.16	5725	41.4
Tekirdağ-Saray	0.24–0.37 [170]	19.09	43.87	5099	37.04
Afşin-Elbistan	0.21 to 0.28 [171]	41.86	51.22	1916	6.92

*Determined by ELI laboratories according to TS 4744 and TS 5122

*All values on a dry basis

Table 6.3. Ultimate analyses of coal samples

COAL SEAM	C (%)*	H (%)*	O (%)*	S (%)*	N (%)*
Soma	68.88	4.65	15.10	1.57	1.27
Tunçbilek	59.55	4.20	7.27	1.94	2.60
Tekirdağ-Saray	56.51	4.14	15.75	3.24	1.27
Afşin-Elbistan	29.59	1.97	24.15	1.97	0.46

*Determined by ELI laboratories according to TS 4744 AND TS 5122

*All values on a dry basis

6.3 Volumetric experimental procedure

After the sample was transferred into the sample cell and connections between the sample cell and the reference cell have been made, the whole setup is then put into the constant temperature water bath at 40 °C. Before measuring adsorption isotherms, the system was checked for pressure leaks using helium. When no leak was detected for about 5-8 hours, then we proceeded with the experiment.

Before starting the experiment, the system was first evacuated from any gas that may be trapped inside. The vacuum pump was used to remove any gas trapped inside. The procedure shown in Figure 6.11 are explained in details as follows:

STEP 1

- All valves in the system (as seen in Figure 6.11) are closed, and pressure in the reference cell is equal to the sample cell's pressure.
- A certain amount of gas is allowed into the reference cell by opening the master valve until the desired pressure is reached and the master valve is closed.
- Few minutes are allowed for pressure and temperature equilibration in the reference cell.

STEP 2

- The expansion valve is then opened, allowing the gas to flow from the reference cell to the sample cell.

STEP 3

- The adsorption starts and the pressure values are recorded every 5 minutes.

STEP 4

- When pressure remains constant for about 20 minutes, the pressure is recorded as the equilibrium pressure.

For the second injection

Once the equilibrium pressure is recorded, the expansion valve is closed.

1) The master valve is opened to increase pressure in the reference cell.
2) The experiment is repeated from step 1 to step 4.

By measuring pressure values before and after expansion, both in the sample cell and the reference cell, the amount of gas adsorbed at each pressure level is calculated. The adsorption isotherm is constructed by repeating these procedures until the highest desired gas pressure measurement is achieved.

Closing procedure for all the experiments

1) Once the experiment finishes, gas in the system and connections is vented out
2) Gas cylinders are closed, and the temperature bath is turned off.
3) After the sample was removed from the cell, both sample and reference cells were dried in the drying oven at 110 °C for about 30 minutes.
4) The new sample is then loaded in the sample cell, and the same procedure from step 1 to step 4 is repeated.

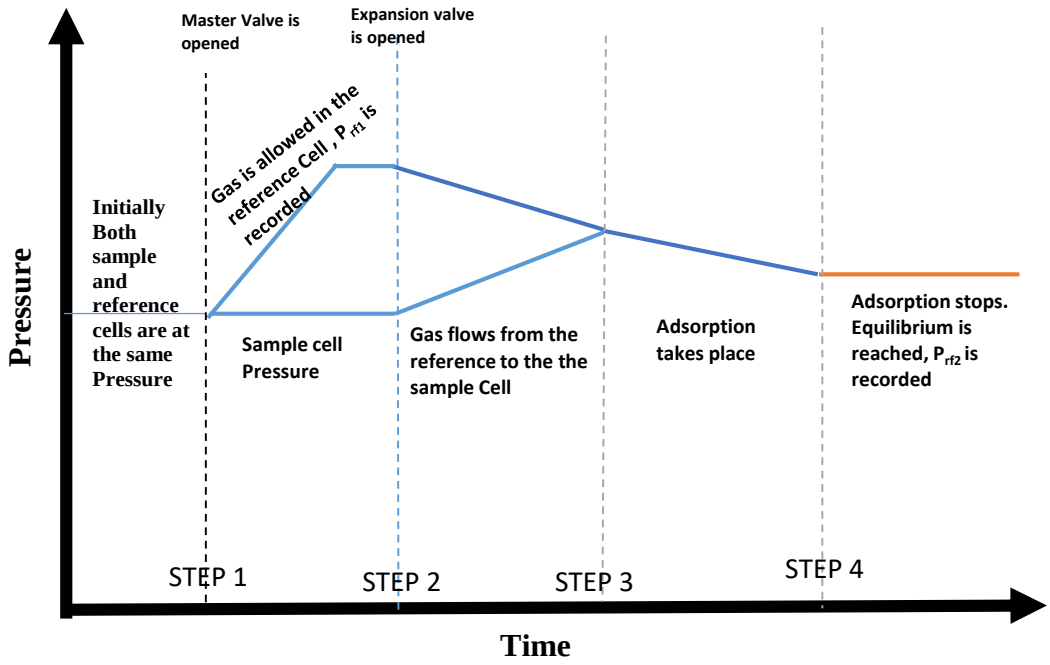

Figure 6.11. Procedure for gas adsorption using a volumetric method.

6.3.1 Void volume estimation

The void volume includes the pipe volume, reference cell volume, sample cell volume unoccupied by the sample, and matrix pore volume. Generally, helium is widely used for the determination of the void volume. The reason is that helium has a relatively small molecular size which allows penetrating small pores that would otherwise not be reached by bigger molecules. In addition to this, helium is generally considered non-adsorbing gas on coals [133].

The empty volume of sample and reference cells were estimated using the helium expansion method. Similarly, after the sample is loaded in the sample cell, the void volume is estimated using equation 6.1 (the derivation of this equation is found in Appendix A):

$$V_{void}(n) = \frac{\frac{P_n}{Z_n} - \frac{P_{eqn}}{Z_{eq2n}}}{\frac{P_{eqn}}{Z_{eqn}} - \frac{P_{eq(n-1)}}{Z_{eq(n-1)}}} \cdot V_{rf} \qquad 6.1$$

where P_n is the pressure in the reference cell, bars, and Z_n is the compressibility constant at pressure P_n, $P_{eq(n-1)}$ is the Equilibrium pressure of the previous step and $Z_{eq(n-1)}$ is compressibility constant at pressure $P_{eq(n-1)}$.

The estimation of the void volume was carried out using helium injection, and the interval of pressure was between 10 and 100 bars. Equation 6.1 was then re-written as $V_{void} = \left(\frac{a}{b}\right) \cdot V_{rf}$, by plotting *a* against *b*, the slope was obtained. Therefore by multiplying slope with the reference volume V_{rf} the void volume is found. The compressibility constant for helium at any temperature was estimated by using the Sudibandrio equation 6.2 [172]

$$Z_{He} = 1 + \frac{1471 \cdot 10^{-6} - 4779 \cdot 10^{-9} \cdot T + 4\,92 \cdot 10^{-11} \cdot T^2}{P} \qquad 6.2$$

where *T* is the temperature in Kelvin, *P* is the pressure in bars.

6.3.2 Adsorption capacity estimation

The adsorption capacity was also measured in the same way as the void volume. The gas law expression was used to estimate the void volume. This expression is universal, and by calculating the value of *Z* at every pressure injection, it can be applied to supercritical conditions.

$$P \cdot V = Z \cdot n \cdot R \cdot T \qquad 6.3$$

where *P* is the pressure in the closed system, *V* is the volume in this closed system, *Z* is the compressibility factor, *n* is the number of moles of free gas in this closed system, *R* and *T* are both the gas universal constant and temperature in this closed system respectively.

Initially, for the first injection, the reference cell was filled by CO_2, and the gas law in the reference cell is expressed:

$$P_1 \cdot V_{rf} = Z_1 \cdot n_{inject} \cdot R \cdot T \qquad 6.4$$

where P_1 is the pressure in reference cell, V_{rf} is the volume of the reference cell, Z_1 is the gas compressibility factor at the pressure P_1, n_{inject} is the moles of gas injected in the reference cell.

When we open the expansion valve, the gas is expanded to the sample cell, and this continues until the equilibrium is reached. The gas law in equilibrium condition is:

$$P_{eq1} \cdot \left(V_{rf} + V_{void}\right) = Z_{eq1} \cdot n_{free} \cdot R \cdot T \qquad 6.5$$

The mass balance for the first injection is:

$$n_{inject} = n_{free} + n_{adsorbed} \qquad 6.6$$

Where n_{inject} are the moles of gas injected in the reference cell, n_{free} are the moles of free gas in both cells at the equilibrium condition, $n_{adsobred}$ are the moles of gas adsorbed in the coal matrix in the equilibrium condition.

$$P_{eq1} \cdot \left(V_{rf} + V_{void}\right) = Z_{eq1} \cdot n_{free} \cdot R \cdot T$$

$$P_1 \cdot V_{rf} = Z_1 \cdot n_{inject} \cdot R \cdot T$$

$$n_{adsorbed} = n_{inject} - n_{free}$$

Therefore, moles adsorbed for the first injection are given by

$$n_{adsorbed} = \frac{V_{rf}}{RT} \cdot \left(\frac{P_1}{Z_1} - \frac{P_{eq1}}{Z_{eq1}}\right) - \left(\frac{P_{eq1}}{Z_{eq1}}\right) \cdot \frac{V_{void}}{RT} \qquad 6.7$$

For the second injection step,

$$n_{inject} + n_{residual} = n_{free} + n_{adsorbed}$$

where $n_{residual}$ denotes the number of moles existing in the sample before the second injection.

For the second injection, we will have P_2 & Z_2 are the new pressure injection and compressibility constant on the second step. P_{eq2} & Z_{eq2} are the equilibrium pressure and gas compressibility of the second step.

Similarly, for the second step, we will have:

$$P_2 \cdot V_{rf} = Z_2 \cdot n_{inject} \cdot R \cdot T$$

$$P_{eq2} \cdot \left(V_{rf} + V_{void}\right) = Z_{eq2} \cdot n_{free} \cdot R \cdot T$$

$$P_{eq1} \cdot (V_{void}) = Z_{eq1} \cdot n_{residual} \cdot R \cdot T$$

Rearranging equations to give the number of moles adsorbed

$$n_{inject} + n_{residual} - n_{free} = n_{adsorbed}$$

Calculation of moles adsorbed from the second step

$$n_{adsorbed} = \frac{V_{rf}}{R \cdot T} \cdot \left(\frac{P_2}{Z_2} - \frac{P_{eq2}}{Z_{eq2}}\right) - \left(\frac{P_{eq2}}{Z_{eq2}} - \frac{P_{eq1}}{Z_{eq1}}\right) \cdot \frac{V_{void}}{R \cdot T} \qquad 6.8$$

The total moles adsorbed at the second pressure injection is Step 1+ Step 2:

$$n_{adsorbed} =$$

$$\frac{V_{rf}}{RT} \cdot \left(\frac{P_1}{Z_1} - \frac{P_{eq1}}{Z_{eq1}}\right) - \left(\frac{P_{eq1}}{Z_{eq1}}\right) \cdot \frac{V_{void}}{RT}$$

$$+$$

$$\frac{V_{rf}}{R \cdot T} \cdot \left(\frac{P_2}{Z_2} - \frac{P_{eq2}}{Z_{eq2}}\right) - \left(\frac{P_{eq2}}{Z_{eq2}} - \frac{P_{eq1}}{Z_{eq1}}\right) \cdot \frac{V_{void}}{R \cdot T}$$

The total moles adsorbed at the third pressure injection, Step 1+ Step 2+ Step 3

$$n_{adsorbed} =$$

$$\frac{V_{rf}}{RT} \cdot \left(\frac{P_1}{Z_1} - \frac{P_{eq1}}{Z_{eq1}}\right) - \left(\frac{P_{eq1}}{Z_{eq1}}\right) \cdot \frac{V_{void}}{RT}$$

+

$$\frac{V_{rf}}{R \cdot T} \cdot \left(\frac{P_2}{Z_2} - \frac{P_{eq2}}{Z_{eq2}}\right) - \left(\frac{P_{eq2}}{Z_{eq2}} - \frac{P_{eq1}}{Z_{eq1}}\right) \cdot \frac{V_{void}}{R \cdot T}$$

+

$$\frac{V_{rf}}{R \cdot T} \cdot \left(\frac{P_3}{Z_3} - \frac{P_{eq3}}{Z_{eq3}}\right) - \left(\frac{P_{eq3}}{Z_{eq3}} - \frac{P_{eq2}}{Z_{eq2}}\right) \cdot \frac{V_{void}}{R \cdot T}$$

The number of moles adsorbed at any pressure is given by:

$$n_{adsorbed(n)} = \left(\sum_{i=1}^{n} \left(\frac{P_i}{Z_i} - \frac{P_{eqi}}{Z_{eqi}}\right)\right) \cdot \frac{V_{rf}}{R \cdot T} - \left(\frac{V_{void}}{R \cdot T} \cdot \frac{P_{eqn}}{Z_{eqn}}\right) \qquad 6.9$$

CHAPTER 7

RESULTS AND DISCUSSION

7.1 Excess adsorption capacity

The experimentally measured amounts of CO_2 were plotted against the equilibrium pressure. These isotherms represent the excess number of moles (n_{ex}). The excess number of moles, as explained in section 5.5, is the amount of gas calculated to have adsorbed if the volume of adsorbed phase, V_a is ignored [173]. Figure 7.1 shows excess adsorption isotherms of the Soma (SO), Tunçbilek (TU), Tekirdağ-Saray (TS) and Afşin-Elbistan (AFE) samples.

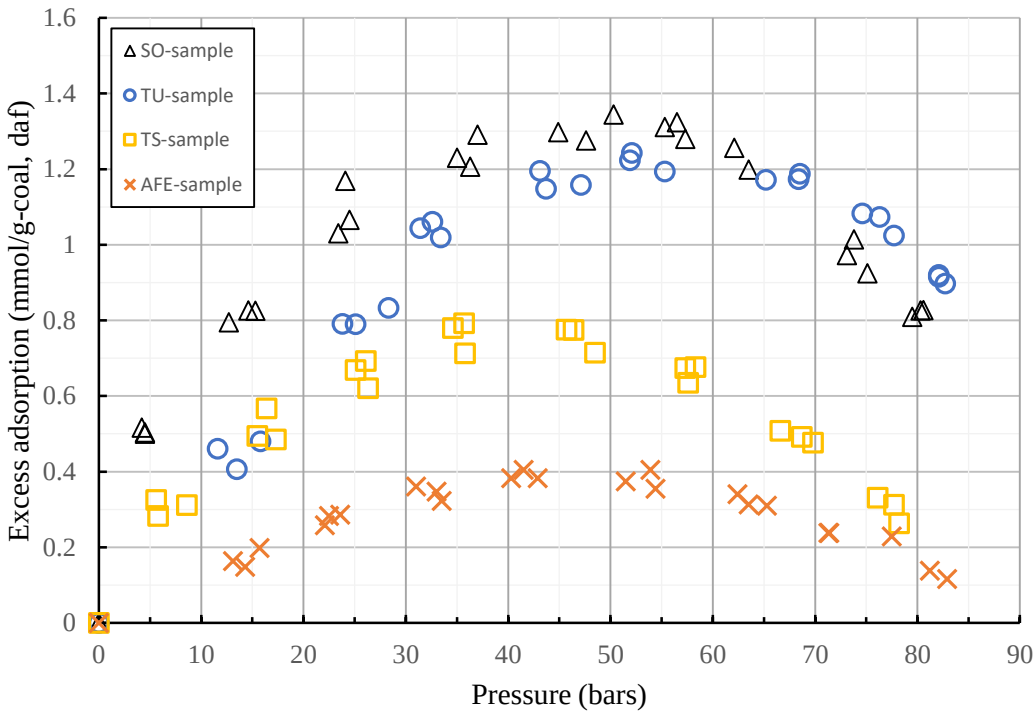

Figure 7.1. Excess adsorption isotherms of the four coal samples.

As expected, with increasing pressure, the amount adsorbed (excess adsorption) increases, goes through a maximum and then decreases (see Figure 7.1). The reason for this behavior is that in volumetric experiments, the adsorbed phase volume is not accounted for in the calculation.

In the experiment, the sample cell's equilibrium pressures were measured, and the number of moles in the sample cell is calculated by multiplying pressure with the void volume (see equation 6.9). This equation assumes that the void volume is constant, but the adsorbed phase occupies part of the initial void volume in reality. This causes an error in the estimation of the number of moles in the free gas phase.

Therefore, in reality, the number of moles in the free gas phase is over-estimated, and the number of moles in the adsorbed phase is under-estimated. This underestimation is proportional to the difference between the adsorbed phase density and free gas density. Once the adsorbed phase's density is determined, this under-estimation is corrected, and consequently, the absolute adsorption isotherms are obtained (see Figure 7.6).

Initially, the densities of both the adsorbed phase and free gas molecules increase with pressure. However, the adsorbed phase's density tends to increase faster towards a maximum value [174]. At some point, the difference between both densities reaches a maximum, which corresponds to the maximum point in the excess adsorption isotherm.

7.2 Adsorption modelling

In this study, the Langmuir and D-R models were selected based on their success in many studies done, particularly on coal [132], [134], [136], [145], [175]–[180]. In order to fit these models to the experimental data, one needs to introduce an error function. There are many error functions used in the literature [181], [182]. In this study, the Average Relative Error (ARE) was used to determine the best fit model.

The expression is given by:

$$\text{ARE} = \frac{100}{N}\sum_{i=1}^{N}\left(\frac{\left|n_{exp} - n_{model}\right|}{n_{\text{exp}}}\right)_i \qquad 7.1$$

where N, is the number of experiments, n_{exp} the experimental data and n_{model} is the number of moles estimated by the model. The Microsoft (MS) Excel solver tool was employed to minimize the sum of errors between the model and the experimental data. The model that gives the minimum sum indicates the best fit.

Among all the models, the D-R–modified model was found to be the best fitting model; it showed the minimum deviation from the experimental data. All the fitted parameters for all the models are given in appendix G, and the parameters for the D-R modified model are presented in Table 7.1.

Table 7.1. Fitted parameters for D-R–modified model

	n_{max} (mmol/g)	D (coal affinity to CO_2)	ρ_a (mol/cc)	ARE (%)
Soma	1.95	0.776	0.0113	4.92
Tunçbilek	1.90	0.897	0.0126	3.74
Tekirdağ-Saray	1.22	0.117	0.0075	5.92
Afşin-Elbistan	0.63	0.127	0.0072	5.06

It should be noted that the parameter *k*, which accounts for the volumetric changes in coal (i.e. swelling, contraction) and possible errors in estimating the void volume and the cell volume [135], was found to be zero for all cases. This indicates that those errors or changes have no significant effect on experimental results under this study's conditions. Sakurov et al. studied CO_2 adsorption in coals up to 200 bars and indicated that the *k*-term for the D-R–modified+*k* model is significant for high pressures [135].

Other researchers (e.g., [136], [145], [162], [178], [179]) who worked with high pressure up to around 200 bars, also reported a non-zero value for the k-term. On the other hand, the incremental pressure of about 85 bars, which is the maximum pressure used in this study's experiments, is not high enough to experience the effects of these volumetric changes.

7.2.1 Model fitting procedure

The initial guesses provided for fitting by MS Excel were obtained as follows:

1) At every pressure experiment repeated, the density of the bulk gas versus excess adsorbed moles was plotted.

2) From the density profile, the initial guess for adsorbed phase density ($\rho_{a,i}$) is estimated (see appendix C).

4) By inserting $\rho_{a,i}$ into equation 5.17, the n_{abs} values can be estimated.

5) The maximum value of n_{abs} is used as the initial guess value for n_{max}

6) For Langmuir models, the initial guess for ρ_L was estimated as the density corresponding to half of n_{max}.

7.3 The excess adsorption isotherms

The excess adsorption isotherms of coal samples are displayed in Figure 7.2—Figure 7.5.

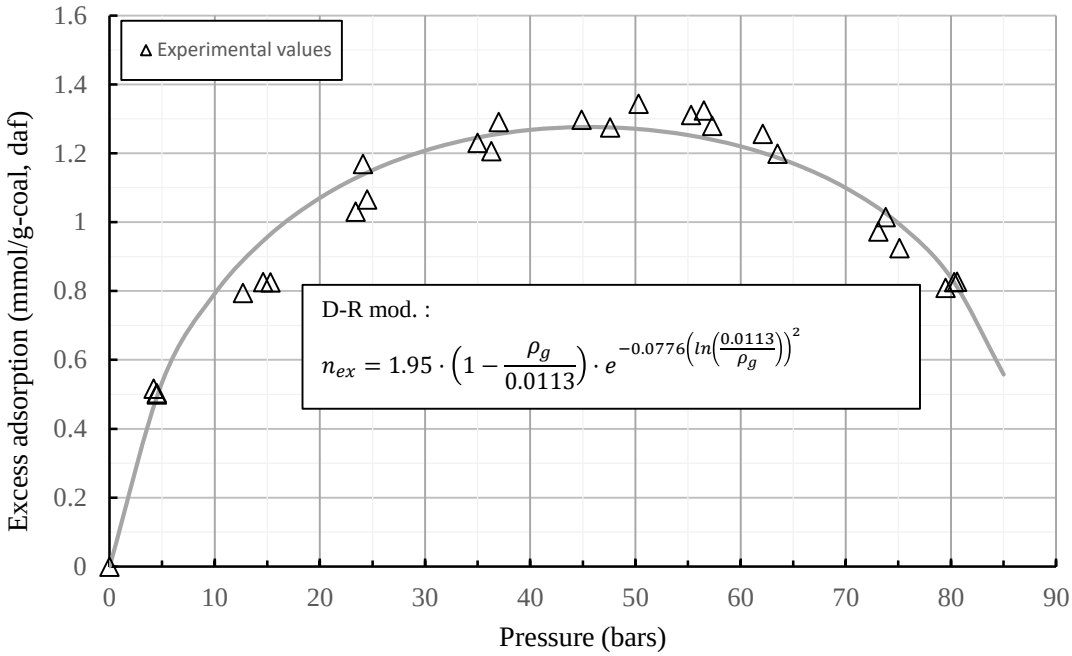

Figure 7.2. Excess adsorption modelling for Soma coal sample

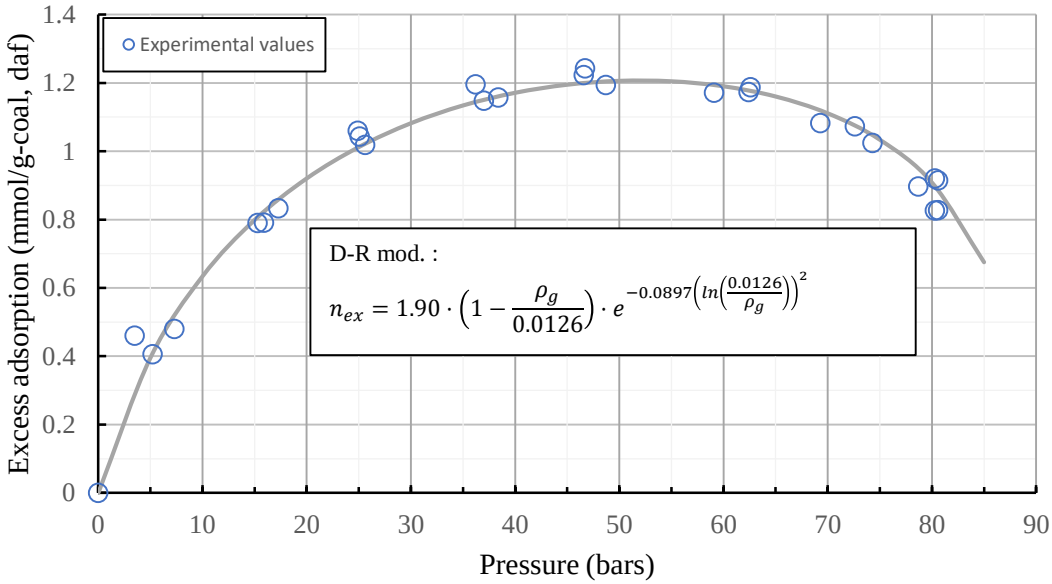

Figure 7.3. Excess adsorption modelling for Tunçbilek coal sample.

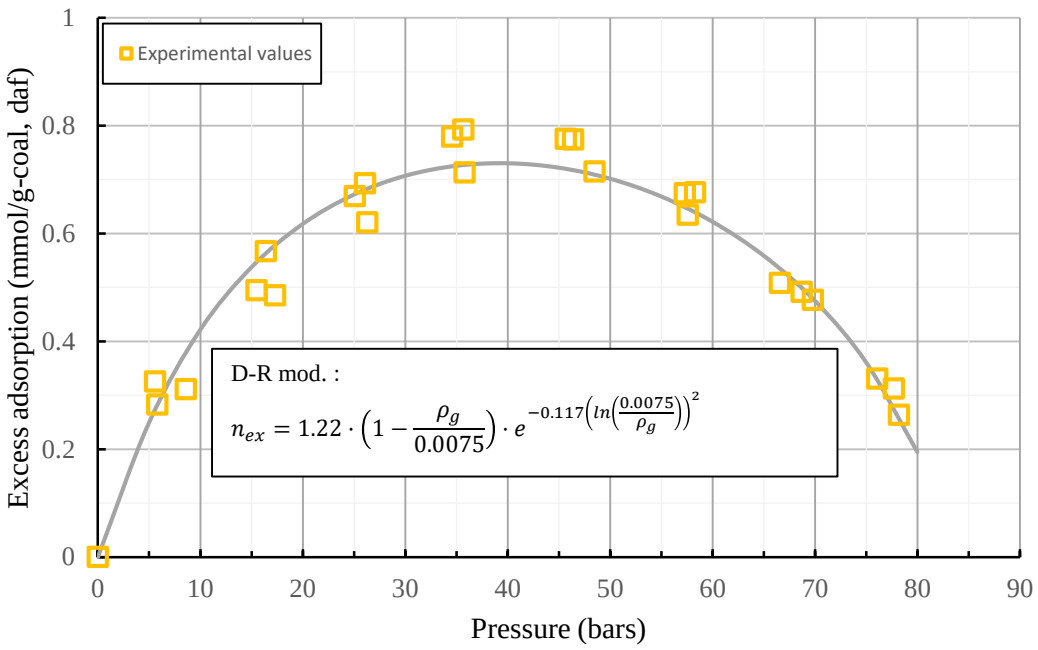

Figure 7.4. Excess adsorption modelling for Tekirdağ-Saray coal sample

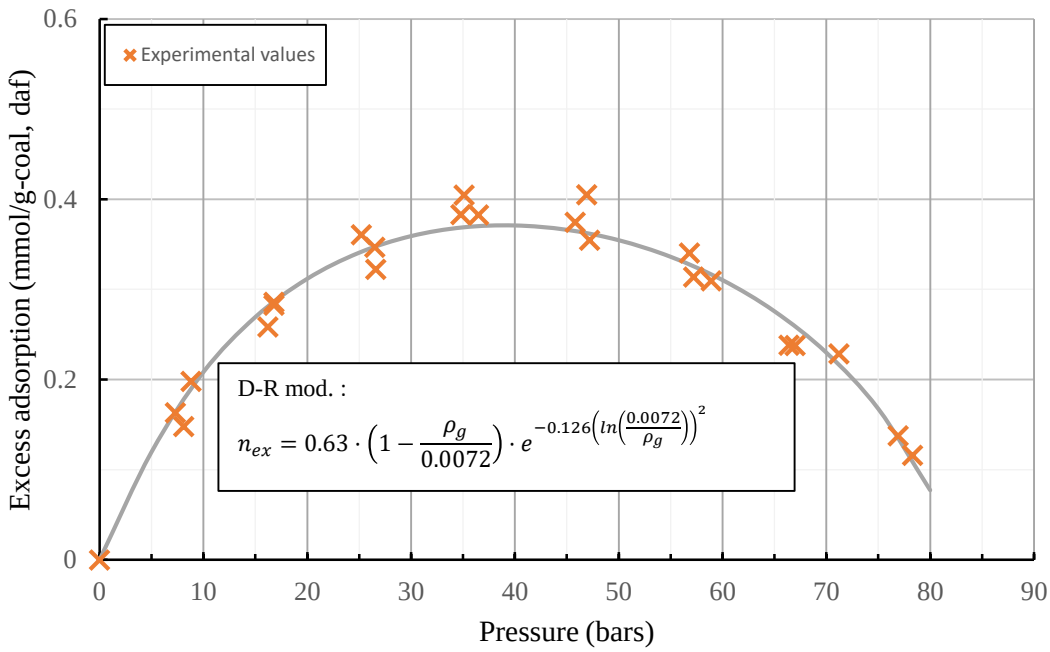

Figure 7.5. Excess adsorption modelling for Afşin-Elbistan coal sample

Figure 7.6 shows that Soma and Tunçbilek coals show the highest adsorption capacity for CO_2, whereas Afşın-Elbistan coal has the least. It can also be seen that AFE coal has already reached its maximum capacity at around 50 bars.

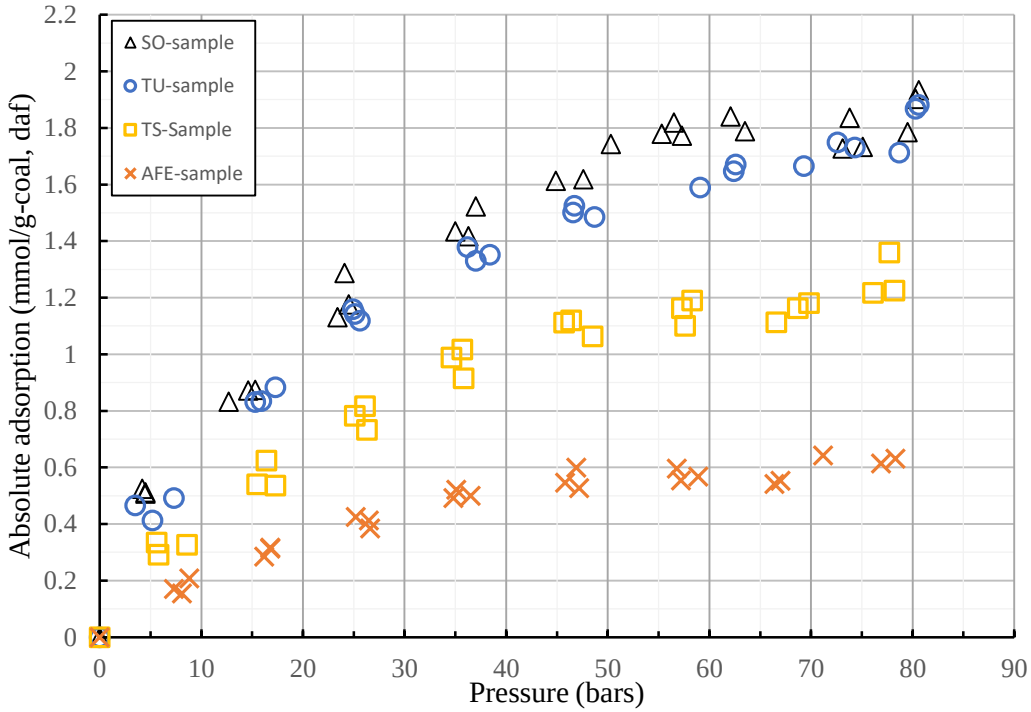

Figure 7.6. Absolute adsorption isotherms for all coal samples

Table 7.2. Comparison of CO_2 adsorption capacity and vitrinite reflectance

Coal samples	n_{max} **(mmol/g-coal)***	**Vitrinite Reflectance % Ro**	**FC (%)***
Soma	1.78	0.35—0.48	50.06
Tunçbilek	1.43	0.42 —0.51	41.4
Tekirdağ-Saray	0.987	0.24—0.37	37.04
Afşın-Elbistan	0.366	0.21—0.28	6.92

*measured on a dry basis (not ash-free)

Fixed carbon is the organic part in coal that provides the surface area for molecules to adsorb; it is known that the higher the fixed carbon content, the higher the

adsorption capacity [183]. This behavior can also be observed in Table 7.2. The coals with a higher percentage of fixed carbon have higher adsorption capacity.

The n_{max} appears to increase with the vitrinite reflectance. Vitrinite macerals are the indicators of maturity in a particular type of coal. As the coal undergoes coalification, these shiny macerals change their reflectance properties. By looking at their reflectance values, Tunçbilek and Soma coal samples are almost similar in maturity, while the Afşin-Elbistan sample remains the most immature (low quality) of them all. Accordingly, one can conclude that there is a positive correlation with n_{max} and vitrinite reflectance.

7.4 Coal-seam storage capacity estimation

Different studies have been done to estimate the storage capacity of coal seams [29], [184], [185]. In this study, the following expression has been used:

$$Storage\ capacity = free\ gas\ + adsorbed\ gas \qquad 7.2$$

$$Storage\ capacity = V_{coal} \cdot \emptyset \cdot \frac{S_g}{B_g} + V_{coal} \cdot \rho_{coal} \cdot (1 - \emptyset) \cdot n_{max} \cdot (1 - a - m)$$

where V_{coal} is the volume of the coal seam (m^3), S_g is the gas saturation, B_g is the gas formation factor, ρ_{coal} is the density of coal (g/cc), n_{max} the maximum storage capacity of coal estimated from the models (mmol/g) $\emptyset$ is the cleat porosity, and a & m are ash content and moisture content, respectively.

The cleat porosity of coal is assumed to be less than 1 % [63], [186]. Generally, for minable coal, the density values range between 1.25 g/cc to 1.70 g/cc, increasing with the rank of coal.

Seidle [63] gives a method of estimating coal density in the absence of laboratory measurements.

$$\rho_{coal} = \frac{1}{\frac{1-a-w}{\rho_o} + \frac{a}{\rho_{as}} + \frac{w}{\rho_w}}$$

where:

ρ_{coal} = coal bulk density, g/cc,

ρ_o = organic fraction density, g/cc,

ρ_{as} = ash density, g/cc,

ρ_w = water density, g/cc, assumed to be 1 g/ cc

$a =$ ash content, %

$w =$ moisture content, %

Seidle [63] suggests that the organic and ash densities for reservoir engineering purposes can be assumed to be 1.25 and 2.55 g/cc, respectively.

Arnold [98] suggests that the free gas saturation in the cleats can be taken as 10 %. The gas formation volume factor (B_g) can be calculated as follows [187]:

$$B_g = \frac{V}{V_{SC}} = \frac{P_{sc}}{P} \cdot \frac{T}{T_{sc}} \cdot \frac{Z}{Z_{sc}}$$

where:

P_{sc} : Pressure at standard condition (1.013 bars)

P : Pressure at Reservoir condition (bars)

T_{sc} : Standard temperature (293.15 K)

Z_{sc}: The compressibility of gas at standard condition

T: Reservoir temperature, (313.15 K)

These storage capacity estimates are significant in reducing the impact of CO_2 emissions in Turkey. To see their impact, we selected a 100 MW coal power plant and calculated CO_2 emissions. In literature, the average CO_2 emissions from coal power plants range between 0.58-1.5 kg/kWh [188]. The value of 1 kg/kWh for coal power plants was used as suggested by Sinayuc [66].

For 100 MW power plant, assuming the availability of 70 %, it will produce

$$\text{Energy (kWh/year)} = 100 \cdot 1000 \cdot 365 \cdot 24 \cdot 0.7$$

Energy $=6.15 \cdot 10^8$ kWh/year,

By using the emission factor of 1 $kgCO_2$/kWh, we get 0.613 megatons of CO_2 produced annually; Table 7.3 shows the total estimated reserves of each coal basins and the amount of CO_2 which can be stored in each basin (see also Figure 7.7).

Based on the estimated storage capacity values, the Soma basin can store all the CO_2 emissions from this power plant for about 102 years, Tunçbilek for 29 years, Afşin Elbistan basin for 49 Tekirdağ-Saray for about eight years.

Table 7.3. Estimated CO_2 storage potential for the basins studied

Coal basin	**Estimated reserves (Mt)** [79]	**Specific Storage ($ktCO_2$/Mt-coal)**	**Estimated Storage (Mt CO_2)**	**Storage potential (years)**
Soma	861.45	72.1	62.11	102
Tunçbilek	317.73	55.8	17.72	29
Tekirdağ-Saray	141.18	34.8	4.92	8
Afşin-Elbistan	4642	6.44	29.89	49

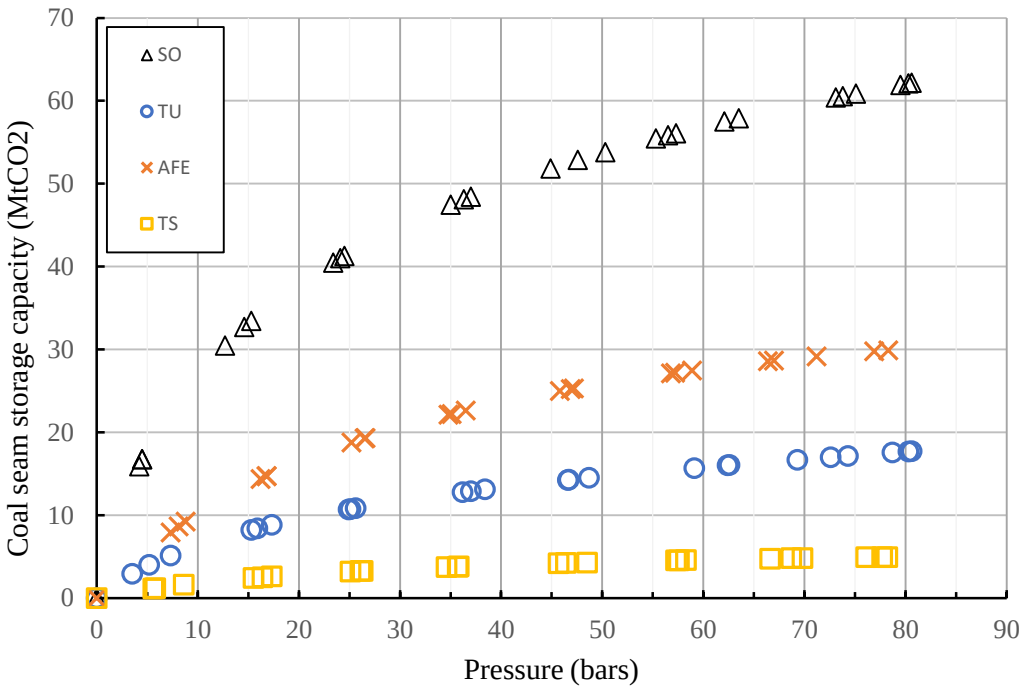

Figure 7.7. The storage capacity of the four selected coal-basins in Turkey, based on their reported reserves

Figure 7.7 show coal seam storage with respect to the pressure. This storage estimation is based on the basin reserves between 2005-2019, as reported in Table 7.3. Afşin-Elbistan has the biggest reserves, about five times Soma and more than ten times that of Tunçbılek; however, one can see that it has a low storage capacity compared to Soma. By comparing the fixed carbon and storage capacities, there is a positive relationship between the samples. Therefore, it can be concluded that the storage capacity is a function of organic components in coal. On the other hand, it is essential to note that the values reported represent both minable and possibly non-minable, considering that minable reserves would be too close to the surface, rightly with no confining strata, they are not valid candidates for CCS. Thus, for CCS purposes, it is more accurate to use only non-minable coal reserves volumes for estimating the storage capacity.

CHAPTER 8

SUMMARY AND CONCLUSIONS

In this study, CO_2 adsorption experiments were conducted on samples from four different coal (lignite) seams of Turkey, namely Soma, Tunçbilek, Tekirdağ–Saray and Afşin–Elbistan. Based on the results of volumetric adsorption experiments performed at 40 ^{o}C and incremental pressure of around 85 bars, the following is concluded:

- Four different adsorption models (Langmuir modified, Langmuir Modified+k, D-R modified and D-R modified +k) were found to fit the experimental data well, with an average relative error (ARE) of less than ±7 %.
- The D-R modified model was the best fit for all coals.
- Effects of compression & swelling of coal and calculation errors on void volume are lumped into the k-terms of the corresponding models. These k-terms turned out to be zero per the curve-fit analysis in this study. Therefore, it is not possible to conclude if there were any swelling effect under the investigated conditions.
- Based on the D-R-modified model fit parameters, the maximum adsorption capacity (n_{max}) of CO_2 was found to be 1.95 mmol/g for Soma, 1.9 mmol/g for Tunçbilek, 1.22 mmol/g for Tekirdağ-Saray and 0.63 mmol/g for Afşin-Elbistan samples (all on "daf" basis).
- Per Table 7.2 a positive correlation is observed between n_{max} and both fixed carbon (FC) and vitrinite reflectance.
- Maximum storage capacities of four basins were estimated to be: for Soma basin 62.1 Mt CO_2, for Tunçbilek 17.73 Mt CO_2, for Tekirdağ-Saray 4.91 Mt CO_2, and for Afşin-Elbistan 29.89 Mt CO_2. These capacities would correspond to 102, 29, 8 and 49 years of emissions storage for a hypothetical 100 MW coal power plant, for Soma, Tunçbilek, Tekirdağ-Saray and Afşin-Elbistan basins, respectively.

CHAPTER 9

RECOMMENDATIONS

In this study, the maximum incremental pressure reached was about 85 bars, which is not necessarily very high, considering the whole range of probable CO_2 sequestration pressures. Therefore, a piston pump or compressor capable of achieving high-pressures could be used in order to replicate sequestration conditions for deeper coal seams. Moreover, using sensitive pressure transducers would increase the accuracy of the measurements. Furthermore, a data acquisition computer would allow smoother data collection.

In this study, the samples were crushed to reduce the time for the diffusion of CO_2 into the coal matrix. However, using larger chunks of coal would be a better representation of the actual physical structure of the subsurface rock. Albeit, such experiments might take longer for CO_2 to diffuse thoroughly into the coal matrix.

It is known that some coals swell in the presence of an adsorbing gas, such as CO_2. Even though such effects were not detected in this study, future work with other coal samples might point to such mechanism. Therefore, quantifying coal's volumetric changes as pressure increases and how such changes can be minimized should not be overlooked. The literature reviewed did not suggest any practical and direct method to measure coal swelling. One method to explore would be using the Archimedes principle and measuring the amount of water displaced before and after the experiments.

In field storage projects, CO_2 injection follows the preliminary production of in-situ water and CH_4. In the pore space, injected CO_2 replaces CH_4 gas, which exists naturally in a coal-seam. Hence, it is of interest to investigate the competitive adsorption of CH_4 and CO_2 in coals.

In addition, herein storage capacities of the coal basins were estimated based on the original total amount of coal reserves. Considering that minable reserves would be too close to the surface, possibly with no confining strata, they are not valid candidates for CCS. Thus, it would be more accurate to use only non-minable coal reserves volumes for estimating storage capacity.

Finally, cap-rock (confining layer) integrity and long-term interaction of CO_2 with coal would ensure storage project safety and should be investigated.

REFERENCES

[1] J. Mitchell, “The ‘Greenhouse’ effect and climate change,” *Rev. Geophys.*, vol. 27, no. 1, p. 115, Feb. 1989.

[2] S. K. Kaliyavaradhan and T. C. Ling, “Potential of CO2 sequestration through construction and demolition (C&D) waste - An overview,” *Journal of CO2 Utilization*, vol. 20. Elsevier Ltd, pp. 234–242, 01-Jul-2017.

[3] M. N. Anwar *et al.*, “CO2 utilization: Turning greenhouse gas into fuels and valuable products,” *J. Environ. Manage.*, vol. 260, p. 110059, Apr. 2020.

[4] L. Jiang, Z. Chen, and S. M. Farouq Ali, “Feasibility of carbon dioxide storage in post-burn underground coal gasification cavities,” *Appl. Energy*, vol. 252, p. 113479, Oct. 2019.

[5] I. Loladze, J. M. Nolan, L. H. Ziska, and A. R. Knobbe, “Rising Atmospheric CO_2 Lowers Concentrations of Plant Carotenoids Essential to Human Health: A Meta-Analysis,” *Mol. Nutr. Food Res.*, vol. 63, no. 15, p. 1801047, Aug. 2019.

[6] M. Davarazar *et al.*, “Underground carbon dioxide sequestration for climate change mitigation - A scientometric study,” *J. CO2 Util.*, vol. 33, pp. 179–188, Oct. 2019.

[7] M. Jafari, S. C. Cao, and J. Jung, “Geological CO2 sequestration in saline aquifers: Implication on potential solutions of China’s power sector,” *Resour. Conserv. Recycl.*, vol. 121, pp. 137–155, Jun. 2017.

[8] R. B. Jackson, P. Friedlingstein, R. M. Andrew, J. G. Canadell, C. Le Quéré, and G. P. Peters, “Persistent fossil fuel growth threatens the Paris Agreement and planetary health,” *Environmental Research Letters*, vol. 14, no. 12. Institute of Physics Publishing, p. 121001, 04-Dec-2019.

[9] M. L. Szulczewski, C. W. MacMinn, H. J. Herzog, and R. Juanes, “Lifetime

of carbon capture and storage as a climate-change mitigation technology," *Proc. Natl. Acad. Sci. U. S. A.*, vol. 109, no. 14, pp. 5185–5189, Apr. 2012.

[10] V. Ediger, "An integrated review and analysis of multi-energy transition from fossil fuels to renewables," in *Energy Procedia*, 2019, vol. 156, pp. 2–6.

[11] C. Le Quéré *et al.*, "Global Carbon Budget 2017," *Earth Syst. Sci. Data*, vol. 10, pp. 405–448, 2018.

[12] Ü. Şahin, A. A. Aşıcı, S. Acar, P. Gedikkaya-Bal, A. O. Karababa, and L. Kurnaz, "Coal report: Turkey's coal policies related to climate change, economy and health," Istanbul, 2016.

[13] D. J. Wuebbles and A. K. Jain, "Concerns about climate change and the role of fossil fuel use," *Fuel Process. Technol.*, vol. 71, no. 1–3, pp. 99–119, Jun. 2001.

[14] M. den Elzen and M. Meinshausen, "Meeting the EU 2°C climate target: Global and regional emission implications," *Clim. Policy*, vol. 6, no. 5, pp. 545–564, 2006.

[15] R. S. Dimitrov, "The Paris Agreement on Climate Change: Behind Closed Doors," *Glob. Environ. Polit.*, vol. 16, no. 3, pp. 1–11, Jul. 2016.

[16] M. Hulme, "1.5 °C and climate research after the Paris Agreement," *Nat. Clim. Chang.*, vol. 6, p. 222, Feb. 2016.

[17] J. Rogelj *et al.*, "Paris Agreement climate proposals need a boost to keep warming well below 2 °C," *Nature*, vol. 534, no. 7609, pp. 631–639, Jun. 2016.

[18] United Nations Environment Programme, "The Emissions Gap Report 2012," Nairobi, 2014.

[19] C. Donnelly *et al.*, "Impacts of climate change on European hydrology at

1.5, 2 and 3 degrees mean global warming above preindustrial level," *Clim. Change*, vol. 143, no. 1–2, pp. 13–26, Jul. 2017.

[20] R. e. al. Henderson, "Climate change in 2018: Implication for Business," *Harvard Business School Publishing*, 2018. [Online]. Available: www.hbsp.harvard.edu. [Accessed: 18-Jun-2019].

[21] D. H. Reed, "Impact of Climate Change on Biodiversity," in *Handbook of Climate Change Mitigation*, New York, NY: Springer US, 2012, pp. 505–530.

[22] D. Leung, G. Caramanna, and M. M. Maroto-Valer, "An overview of current status of carbon dioxide capture and storage technologies," *Renew. Sustain. Energy Rev.*, vol. 39, pp. 426–443, Nov. 2014.

[23] * Curt M. White *et al.*, "Sequestration of Carbon Dioxide in Coal with Enhanced Coalbed Methane RecoveryA Review," *Energy & Fuels*, vol. 19, no. 3, pp. 659–724, May 2005.

[24] M. M. Mohanty and B. K. Pal, "Sorption behavior of coal for implication in coal bed methane an overview," *Int. J. Min. Sci. Technol.*, vol. 27, no. 2, pp. 307–314, Mar. 2017.

[25] M. Procesi, B. Cantucci, M. Buttinelli, G. Armezzani, F. Quattrocchi, and E. Boschi, "Strategic use of the underground in an energy mix plan: Synergies among CO2, CH4 geological storage and geothermal energy. Latium Region case study (Central Italy)," *Appl. Energy*, vol. 110, pp. 104–131, Oct. 2013.

[26] M. D. Corum, K. B. Jones, and P. D. Warwick, "CO2 Sequestration Potential of Unmineable Coal—State of Knowledge," *Energy Procedia*, vol. 37, pp. 5134–5140, Jan. 2013.

[27] C. Hermanrud *et al.*, "Storage of CO2 in saline aquifers–Lessons learned from 10 years of injection into the Utsira Formation in the Sleipner area," *Energy Procedia*, vol. 1, no. 1, pp. 1997–2004, Feb. 2009.

[28] M. Sullivan, T. Rodosta, K. Mahajan, and D. Damiani, “An overview of the Department of Energy’s CarbonSAFE Initiative: Moving CCUS toward commercialization,” *AIChE J.*, Nov. 2019.

[29] M. D. Aminu, S. A. Nabavi, C. A. Rochelle, and V. Manovic, “A review of developments in carbon dioxide storage,” *Applied Energy*, vol. 208. Elsevier Ltd, pp. 1389–1419, 15-Dec-2017.

[30] P. S. Ringrose *et al.*, “The in salah CO2 storage project: Lessons learned and knowledge transfer,” in *Energy Procedia*, 2013, vol. 37, pp. 6226–6236.

[31] A. Mathieson, J. Midgely, I. Wright, N. Saoula, and P. Ringrose, “In Salah CO2 storage JIP: CO2 sequestration monitoring and verification technologies applied at Krechba, Algeria,” in *Energy Procedia*, 2011, vol. 4, pp. 3596–3603.

[32] J. Rutqvist, D. W. Vasco, and L. Myer, “Coupled reservoir-geomechanical analysis of CO2 injection and ground deformations at In Salah, Algeria,” *Int. J. Greenh. Gas Control*, vol. 4, no. 2, pp. 225–230, Mar. 2010.

[33] M. Dahiru, “Carbon Dioxide Storage in The UK Southern North Sea: Experimental and Numerical Analysis,” Cranfield University, cranfield, 2015.

[34] Y. Pamukcu, S. Hurter, L. Jammes, D. Vu-Hoang, and L. Pekot, “Characterizing and predicting short term performance for the in Salah Krechba field CCS joint industry project,” in *Energy Procedia*, 2011, vol. 4, pp. 3371–3378.

[35] A. Szizybalski, T. Kollersberger, F. Möller, S. Martens, A. Liebscher, and M. Kühn, “Communication supporting the research on CO2 storage at the Ketzin pilot site, Germany-a status report after ten years of public outreach,” in *Energy Procedia*, 2014, vol. 51, pp. 274–280.

[36] M. Streibel, R. J. Finley, S. Martens, S. Greenberg, F. Möller, and A.

Liebscher, “From pilot to demo scale - Comparing Ketzin results with the Illinois basin-decatur project,” in *Energy Procedia*, 2014, vol. 63, pp. 6323–6334.

[37] H. Würdemann *et al.*, “CO2SINK-From site characterisation and risk assessment to monitoring and verification: One year of operational experience with the field laboratory for CO2 storage at Ketzin, Germany,” *Int. J. Greenh. Gas Control*, vol. 4, no. 6, pp. 938–951, Dec. 2010.

[38] B. Dupuy, V. Torres, A. Ghaderi, E. Querendez, and M. Mezyk, “Constrained AVO for CO2 Storage Monitoring at Sleipner,” in *Energy Procedia*, 2017, vol. 114, pp. 3927–3936.

[39] A. K. Furre, O. Eiken, H. Alnes, J. N. Vevatne, and A. F. Kiær, “20 Years of Monitoring CO2-injection at Sleipner,” in *Energy Procedia*, 2017, vol. 114, pp. 3916–3926.

[40] K. Brown, S. Whittaker, M. Wilson, W. Srisang, H. Smithson, and P. Tontiwachwuthikul, “The history and development of the IEA GHG Weyburn-Midale CO2 Monitoring and Storage Project in Saskatchewan, Canada (the world largest CO2 for EOR and CCS program),” *Petroleum*, vol. 3, no. 1. KeAi Communications Co., pp. 3–9, 01-Mar-2017.

[41] D. White, “Monitoring CO2 storage during EOR at the weyburn-midale field,” in *The Leading Edge*, 2009, vol. 28, no. 7, pp. 838–842.

[42] C. D. Sandau, M. Prokipchuk, K. R. Dominato, and S. O. C. Mundle, “Soil gas investigation of an alleged gas migration issue on a residential farm located above the Weyburn-Midale CO2 enhanced oil recovery project,” *Int. J. Greenh. Gas Control*, vol. 81, pp. 11–20, Feb. 2019.

[43] S. Whittakera *et al.*, “A decade of CO2 injection into depleting oil fields: Monitoring and research activities of the IEA GHG Weyburn-Midale CO2 monitoring and storage project,” in *Energy Procedia*, 2011, vol. 4, pp. 6069–6076.

[44] A. Estublier and A. S. Lackner, “Long-term simulation of the Snøhvit CO2 storage,” in *Energy Procedia*, 2009, vol. 1, no. 1, pp. 3221–3228.

[45] T. Maldal and I. M. Tappel, “CO2 underground storage for Snøhvit gas field development,” *Energy*, vol. 29, no. 9–10, pp. 1403–1411, Jul. 2004.

[46] L. Chiaramonte, J. A. White, and W. Trainor-Guitton, “Probabilistic geomechanical analysis of compartmentalization at the Snøhvit CO2 sequestration project,” *J. Geophys. Res. Solid Earth*, vol. 120, no. 2, pp. 1195–1209, Feb. 2015.

[47] S. Sharma, P. Cook, T. Berly, and C. Anderson, “Australia’s First Geo-sequestration Demonstration Project—The CO2CRC Otway Basin Pilot Project,” *APPEA J.*, vol. 47, no. 1, p. 259, 2007.

[48] K. Dodds, T. Daley, B. Freifeld, U. Milovan, A. Kepic, and S. Sharma, “Developing a monitoring and verification plan with reference to the Australian Otway CO2 pilot project,” in *The Leading Edge*, 2009, vol. 28, no. 7, pp. 812–818.

[49] M. Urosevic, R. Pevzner, V. Shulakova, A. Kepic, E. Caspari, and S. Sharma, “Seismic monitoring of CO2 injection into a depleted gas reservoir - Otway Basin Pilot Project, Australia,” in *Energy Procedia*, 2011, vol. 4, pp. 3550–3557.

[50] C. Yang, K. Romanak, S. Hovorka, R. M. Holt, J. Lindner, and R. Trevino, “Near-surface monitoring of large-volume CO2 injection at Cranfield: Early field test of SECARB phase III,” *SPE J.*, vol. 18, no. 3, pp. 486–494, Jan. 2013.

[51] S. D. Hovorka, T. A. Meckel, and R. H. Treviño, “Monitoring a large-volume injection at Cranfield, Mississippi-Project design and recommendations,” *Int. J. Greenh. Gas Control*, vol. 18, pp. 345–360, Oct. 2013.

[52] T. A. Meckel, M. Zeidouni, S. D. Hovorka, and S. A. Hosseini, “Assessing sensitivity to well leakage from three years of continuous reservoir pressure monitoring during CO2 injection at Cranfield, MS, USA,” *Int. J. Greenh. Gas Control*, vol. 18, pp. 439–448, Oct. 2013.

[53] I. Gray, “Reservoir Engineering in Coal Seams: Part 1-The Physical Process of Gas Storage and Movement in Coal Seams,” *SPE Reserv. Eng.*, vol. 2, no. 01, pp. 28–34, 1987.

[54] N. Zhao, T. Xu, K. Wang, H. Tian, and F. Wang, “Experimental study of physical-chemical properties modification of coal after CO_2 sequestration in deep unmineable coal seams,” *Greenh. Gases Sci. Technol.*, vol. 8, no. 3, pp. 510–528, Jun. 2018.

[55] D. Zhang, Y. Cui, B. Liu, S. Li, W. Song, and W. Lin, “Supercritical Pure Methane and CO 2 Adsorption on Various Rank Coals of China: Experiments and Modeling,” vol. 25, pp. 1891–1899, 2011.

[56] W. Nah, “CO2 -Ecbm Optimisation Strategies and CO2 Storage Capacity Assessment of a European Coalfield,” 2010.

[57] G. Wang *et al.*, “Reservoir Permeability Evolution during the Process of CO2-Enhanced Coalbed Methane Recovery,” *Energies*, vol. 11, no. 11, p. 2996, Nov. 2018.

[58] M. Hadi Mosleh, M. Sedighi, M. Babaei, and M. Turner, “Geological sequestration of carbon dioxide,” *Manag. Glob. Warm.*, pp. 487–500, Jan. 2019.

[59] S. Liu, S. Sang, T. Wang, Y. Du, J. Jia, and H. Fang, “The effects of CO 2 on organic groups in bituminous coal and high-rank coal via Fourier transform infrared spectroscopy,” *Energy Explor. Exploit.*, vol. 36, no. 6, pp. 1566–1592, 2018.

[60] Martin Blunt, “Carbon dioxide storage,” *Grantham Institute for Climate-*

Imperial college Change, 2010. [Online]. Available: https://www.imperial.ac.uk/media/imperial-college/grantham-institute/public/publications/briefing-papers/Carbon-dioxide-storage----Grantham-BP-4.pdf. [Accessed: 22-Jul-2019].

[61] X. Li and Z. ming Fang, "Current status and technical challenges of CO2 storage in coal seams and enhanced coalbed methane recovery: an overview," *Int. J. Coal Sci. Technol.*, vol. 1, no. 1, pp. 93–102, 2014.

[62] M. Mazzotti, R. Pini, G. Storti, and L. Burlini, "Carbon dioxide (CO2) sequestration in unmineable coal seams and use for enhanced coalbed methane recovery (ECBM)," *Dev. Innov. Carbon Dioxide (Co*, vol. 2, pp. 127–165, Jan. 2010.

[63] J. Seidle, *Fundamentals of Coalbed Methane Reservoir Engineering*. Tulsa, Oklahoma 74112-6600 USA: PennWell Corporation, 2011.

[64] S. R. Reeves, "Geological Sequestration of CO2 in Deep, Unmineable Coalbeds: An Integrated Research and Commerical-Scale Field Demonstration Project," in *SPE Annual Technical Conference and Exhibition*, 2001, p. 10.

[65] P. Thakur, "Coalbed Methane Production from Deep Coal Reservoirs," in *Advanced Reservoir and Production Engineering for Coal Bed Methane*, Cambridge, MA 02139, United State: Elsevier, 2017.

[66] C. Sinayuc, "Modeling of Enhanced Coalbed Methane Recovery from Amasra Coalbed in Zonguldak Coal Basin," Middle East Technical University, 2007.

[67] J. Q. Shi and S. Durucan, "CO 2 Storage in Deep Unminable Coal Seams," *Oil Gas Sci. Technol. IFP*, vol. 60, no. 3, pp. 547–558, 2005.

[68] S. Wong, W. D. Gunter, and M. J. Mavor, "Economics of CO2 sequestration in coalbed methane reservoirs," *Soc. Pet. Eng. - SPE/CERI Gas Technol.*

Symp. 2000, GTS 2000, 2000.

[69] L. Gao, M. Mastalerz, and A. Schimmelmann, “Chapter 2 - The Origin of Coalbed Methane,” in *Coal Bed Methane: From Prospect to Pipeline*, P. Thakur, S. Schatzel, and K. Aminian, Eds. Oxford: Elsevier, 2014, pp. 7–29.

[70] S. Ottiger, R. Pini, G. Storti, and M. Mazzotti, “Competitive adsorption equilibria of CO2 and CH4 on a dry coal,” *Adsorption*, vol. 14, no. 4–5, pp. 539–556, Oct. 2008.

[71] A. Pajdak, M. Kudasik, N. Skoczylas, M. Wierzbicki, and L. Teixeira Palla Braga, “Studies on the competitive sorption of CO2 and CH4 on hard coal,” *Int. J. Greenh. Gas Control*, vol. 90, p. 102789, Nov. 2019.

[72] W. Zhou, H. Wang, Z. Zhang, H. Chen, and X. Liu, “Molecular simulation of CO2 /CH4 /H2O competitive adsorption and diffusion in brown coal,” *RSC Adv.*, vol. 9, no. 6, pp. 3004–3011, 2019.

[73] F. E. Hall, Z. Chunhe, K. A. M. Gasem, R. L. Jr., and Y. Dan, “Adsorption of Pure Methane, Nitrogen, and Carbon Dioxide and Their Mixtures on San Juan Basin Coal,” Stillwater, Oklahoma, 2002.

[74] Y. Gensterblum, A. Busch, and B. M. Krooss, “Molecular concept and experimental evidence of competitive adsorption of H2O, CO2 and CH4 on organic material,” *Fuel*, vol. 115, pp. 581–588, Jan. 2014.

[75] B. Durand, “Carbon dioxide capture and storage,” *Int. At. Energy Agency*, vol. 43, no. 7, pp. 1–32, Jan. 2005.

[76] R. Oskay, K. Christanis, A. Karayigit, and H. Inaner, “Coal deposits of Turkey: properties and importance on energy demand,” *Bull. Geol. Soc. Greece*, vol. 47, no. 4, pp. 2111–2120, 2016.

[77] V. S. Ediger, I. Berk, and A. Kösebalaban, “Lignite resources of Turkey: Geology, reserves, and exploration history,” *Int. J. Coal Geol.*, vol. 132, pp. 13–22, Oct. 2014.

[78] M. Ersoy, “Turkish Coal Mining Sector: Current state, strategy for the Future,” in *Workshop on Best Practices in Coal Mine Methane Capture and Utilisation*, 2019, no. June, p. 21.

[79] MTA, “Coal Exploration Research,” *General Directorate of the Mineral Research & Exploration of Turkey*, 2021. [Online]. Available: https://www.mta.gov.tr/v3.0/arastirmalar/komur-arama-arastirmalari.

[80] A. İ. Karayiğit, R. Littke, X. Querol, T. Jones, R. G. Oskay, and K. Christanis, “The Miocene coal seams in the Soma Basin (W. Turkey): Insights from coal petrography, mineralogy and geochemistry,” *Int. J. Coal Geol.*, vol. 173, pp. 110–128, Mar. 2017.

[81] O. Esen, S. C. Ozer, A. Soylu, A. R. Rend, and A. Fisne, “Investigation of the Coal Seam Gas Content and Compositon in Soma Coal Basin, Turkey Coal Basin, Turkey,” in *Proceedings of the 2018 Coal Operators’ Conference, Mining Engineering,, University of Wollongong, 18-20 February 2019*, 2019.

[82] U. Inci, “Lignite and carbonate deposition in Middle Lignite succession of the Soma Formation, Soma coalfield, western Turkey,” *Int. J. Coal Geol.*, vol. 37, no. 3–4, pp. 287–313, Oct. 1998.

[83] R. Brinkmann, “Mesozoic troughs and crustal structure in Anatolia,” *Bull. Geol. Soc. Am.*, vol. 83, no. 3, pp. 819–826, Mar. 1972.

[84] J. Zhao *et al.*, *Rock Mechanics in Civil and Environmental Engineering*, 1st ed., vol. 1. London: CRC Press, 2010.

[85] M. S. Akkiraz *et al.*, “Palaeoflora and climate of lignite-bearing lower-middle miocene sediments in the seyitömer and tunçbilek sub-basins, kütahya province, Northwest Turkey,” *Turkish J. Earth Sci.*, vol. 21, no. 2, pp. 213–235, 2012.

[86] S. Toprak, “Petrographic properties of major coal seams in Turkey and their

formation," *Int. J. Coal Geol.*, vol. 78, no. 4, pp. 263–275, Jun. 2009.

[87] A. I. Karayigit and Y. Celik, "Mineral matter and trace elements in miocene coals of the Tuncbilek-Domanic basin, Kutahya, Turkey," *Energy Sources*, vol. 25, no. 4, pp. 339–355, 2010.

[88] Z. Dogan, G. Onal, and O. Unver, "The Effects of Mining Methods and Coal Quality On Power Generation Cost in Turkey," in *Chemistry, Energy and the Environment*, Elsevier, 1998, pp. 343–349.

[89] H. Kose, C. Pamukcu, and E. Yalcin, "Project design of an open pit colliery in Terkidag, Turkey," *Acta Montan. Slovaca*, vol. 15, no. 2, pp. 109–120, 2010.

[90] S. Ural and F. Yuksel, "Geotechnical characterization of lignite-bearing horizons in the Afsin-Elbistan lignite basin, SE Turkey," *Eng. Geol.*, vol. 75, no. 2, pp. 129–146, Oct. 2004.

[91] S. Ural, "Comparison of fly ash properties from Afsin-Elbistan coal basin, Turkey," *J. Hazard. Mater.*, vol. 119, no. 1–3, pp. 85–92, Mar. 2005.

[92] U. Serpen, E. N. Alpkaya, and E. Ozkan, "Preliminary Investigation of Coalbed Methane Potential of the Zonguldak Basin in Turkey," *SPE Gas Technology Symposium*. Society of Petroleum Engineers, Calgary, Alberta, Canada, p. 9, 1998.

[93] L. L. Sloss, "Potential for enhanced coalbed methane recovery," London, United Kingdom, 2015.

[94] M. V. Kok and A. Vural, "The Clean Coal and Carbon Capture and Storage Technology of Turkey," *Energy Sources, Part A Recover. Util. Environ. Eff.*, vol. 34, no. 6, pp. 531–539, Jan. 2012.

[95] H. Rütters and CGS Europe Partners, "State of play on CO 2 geological storage in 28 European countries," 2013.

[96] B. J. Arnold, “Coal formation,” *Coal Handb. Towar. Clean. Prod.*, pp. 31–52, Jan. 2013.

[97] G. B. Stracher, A. Prakash, and G. Rein, “Peat: Its Origins, Characteristics, and Geological Transformations,” in *Coal and Peat Fires: a Global Perspective*, 4th ed., G. B. Stracher, A. Prakash, and G. Rein, Eds. Elsevier, 2015, pp. 13–38.

[98] E. Ozdemir, “Chemistry of the Adsorption of Carbon dioxide by Argonne Premium Coals and a Model to Simulate CO2 Sequestration in Coal Seams,” University of Pittsburgh, 2004.

[99] R. M. Flores, “Chapter 4 - Coalification, Gasification, and Gas Storage,” in *Coal and Coalbed Gas -Fueling the future*, Boston: Elsevier, 2014, pp. 167–233.

[100] S. N. Chaudhuri, “Coalification BT - Encyclopedia of Mineral and Energy Policy,” in *Encyclopedia of Mineral and Energy Policy*, no. Liess 1958, G. Tiess, T. Majumder, and P. Cameron, Eds. Berlin, Heidelberg: Springer Berlin Heidelberg, 2016, pp. 1–2.

[101] R. M. Flores, “Coal Composition and Reservoir Characterization,” in *Coal and Coalbed Gas*, 1st ed., Bruce G. Miller, Ed. Burlington, MA 01803, USA: Elsevier, 2014, pp. 235–299.

[102] A. J. Schilstra, “How sustainable is the use of peat for commercial energy production?,” *Ecol. Econ.*, vol. 39, no. 2, pp. 285–293, Nov. 2001.

[103] B. G. Miller, “The Chemical and Physical Characteristics of Coal,” *Clean Coal Eng. Technol.*, pp. 53–68, Jan. 2011.

[104] K. Xie, “Physical Characteristics of Coal,” in *Structure and Reactivity of Coal*, Berlin, Heidelberg: Springer Berlin Heidelberg, 2015, pp. 29–65.

[105] J. G. Speight, *The chemistry and technology of coal.*, 3rd ed., vol. 36, no. 3. The Taylor & Francis Group, 2013.

[106] D. R. Datta and S. N. Chaudhuri, “Encyclopedia of Mineral and Energy Policy,” in *Encyclopedia of Mineral and Energy Policy*, no. Liess 1958, 2019, pp. 3–4.

[107] S. . Laubach, R. . Marrett, J. . Olson, and A. . Scott, “Characteristics and origins of coal cleat: A review,” *Int. J. Coal Geol.*, vol. 35, no. 1–4, pp. 175–207, Feb. 1998.

[108] C. F. Rodrigues, C. Laiginhas, M. Fernandes, M. J. Lemos de Sousa, and M. A. P. Dinis, “The coal cleat system: A new approach to its study,” *J. Rock Mech. Geotech. Eng.*, vol. 6, no. 3, pp. 208–218, Jun. 2014.

[109] U. Kuila and M. Prasad, “Specific surface area and pore-size distribution in clays and shales,” *Geophys. Prospect.*, vol. 61, pp. 341–362, 2013.

[110] N. T. Burdine, L. S. Gournay, and P. P. Reichertz, “Pore Size Distribution of Petroleum Reservoir Rocks,” *J. Pet. Technol.*, vol. 2, no. 07, pp. 195–204, 2012.

[111] C. . Rodrigues and M. . Lemos de Sousa, “The measurement of coal porosity with different gases,” *Int. J. Coal Geol.*, vol. 48, no. 3–4, pp. 245–251, Jan. 2002.

[112] L. Mordfin, *Handbook of Reference Data for Nondestructive Testing*. Pennsylvania: ASTM International, 2002.

[113] N. N. Li, A. Fane, W. S. W. Ho, and T. Matsuura, “Gas Separations,” in *Advanced Membrane Technology and Applications*, New Jersey: John Wiley & Sons, Ltd, 2008, pp. 643–644.

[114] J. H. De Boer, “50 Endothermic Chemisorption and Catalysis,” *Adv. Catal.*, vol. 9, no. C, pp. 472–480, Jan. 1957.

[115] J. R. H. Ross, “Surfaces and Adsorption,” in *Contemporary Catalysis*, Elsevier, 2019, pp. 39–68.

[116] Ş. Merey, “Experimental Analysis of Adsorption Capacities and Behaviors of Shale Samples,” Middle East Technical University, 2013.

[117] R. Kecili and C. M. Hussain, “Mechanism of Adsorption on Nanomaterials,” in *Nanomaterials in Chromatography*, Elsevier Inc., 2018, pp. 89–115.

[118] A. Dąbrowski, “Adsorption - From theory to practice,” *Advances in Colloid and Interface Science*, vol. 93, no. 1–3. Elsevier, pp. 135–224, 08-Oct-2001.

[119] W. Steele, “Molecular Interactions for Physical Adsorption,” *Chem. Rev.*, vol. 93, no. 7, pp. 2355–2378, 1993.

[120] W. J. Thomas and B. Crittenden, “Fundamentals of adsorption equilibria,” in *Adsorption Technology & Design*, Elsevier, 1998, pp. 31–65.

[121] S. Gregg, K. Sing, S. J. Gregg, and K. S. W. Sing, *Adsorption, Surface Area and Porosity*, 2nd ed., vol. 63, no. 1_4. London, United Kingdom: Academic Press, 1982.

[122] M. D. Donohue and G. L. Aranovich, “Classification of Gibbs adsorption isotherms,” *Adv. Colloid Interface Sci.*, vol. 76–77, pp. 137–152, Jul. 1998.

[123] M. Muttakin, S. Mitra, K. Thu, K. Ito, and B. B. Saha, “Theoretical framework to evaluate minimum desorption temperature for IUPAC classified adsorption isotherms,” *Int. J. Heat Mass Transf.*, vol. 122, pp. 795–805, Jul. 2018.

[124] N. Ayawei, A. N. Ebelegi, and D. Wankasi, “Modelling and Interpretation of Adsorption Isotherms,” *J. Chem.*, vol. 2017, 2017.

[125] K. Y. Foo and B. H. Hameed, “Insights into the modeling of adsorption isotherm systems,” *Chemical Engineering Journal*, vol. 156, no. 1. Elsevier, pp. 2–10, 01-Jan-2010.

[126] I. Langmuir, “The adsorption of gases on plane surfaces of glass, mica and platinum,” *J. Am. Chem. Soc.*, vol. 40, no. 9, 1918.

[127] B. Adiraju, “Adsorption of CO2 on Indian coals,” National Institute of Technology Rourkela, 2010.

[128] C. Guan, S. Liu, C. Li, Y. Wang, and Y. Zhao, “The temperature effect on the methane and CO2 adsorption capacities of Illinois coal,” *Fuel*, vol. 211, pp. 241–250, Jan. 2018.

[129] J. Ekundayo and R. Rezaee, “Volumetric Measurements of Methane-Coal Adsorption and Desorption Isotherms — Effects of Equations of State and Implication for Initial Gas Reserves,” *Energies*, vol. 12, no. 2022, 2019.

[130] D. Guo and X. Guo, “The influence factors for gas adsorption with different ranks of coals,” *Adsorpt. Sci. Technol.*, vol. 36, no. 3, p. 2017, 2018.

[131] Z. Liu, Z. Zhang, X. Liu, T. Wu, and X. Du, “Pore Structure , and Adsorption Capacity Alterations,” *Energies*, vol. 12, no. 3294, p. 14, 2019.

[132] P. Bénard and R. Chahine, “Modeling of high-pressure adsorption isotherms above the critical temperature on microporous adsorbents: Application to methane,” *Langmuir*, vol. 13, no. 4, pp. 808–812, Feb. 1997.

[133] P. Dutta, S. Harpalani, and B. Prusty, “Modeling of CO2 sorption on coal,” *Fuel*, vol. 87, no. 10–11, pp. 2023–2036, Aug. 2008.

[134] M. Meng, Z. Qiu, R. Zhong, Z. Liu, Y. Liu, and P. Chen, “Adsorption characteristics of supercritical CO2/CH4 on different types of coal and a machine learning approach,” *Chem. Eng. J.*, vol. 368, pp. 847–864, Jul. 2019.

[135] R. Sakurovs, S. Day, S. Weir, and G. Duffy, “Application of a Modified Dubinin-Radushkevich Equation to Adsorption of Gases by Coals under Supercritical Conditions,” 2007.

[136] E. Ozdemir, “Dynamic nature of supercritical CO2 adsorption on coals,” *Adsorption*, vol. 23, no. 1, pp. 25–36, 2017.

[137] E. O. Timmermann, “A B.E.T.-like three sorption stage isotherm,” *J. Chem. Soc. Faraday Trans. 1 Phys. Chem. Condens. Phases*, vol. 85, no. 7, pp. 1631–1645, 1989.

[138] S. Brunauer, P. H. Emmett, and E. Teller, “Adsorption of Gases in Multimolecular Layers,” *J. Am. Chem. Soc.*, vol. 60, no. 2, pp. 309–319, 1938.

[139] D. M. Ruthven, *Principles of adsorption and adsorption processes*, vol. 19, no. 2. John Wiley & Sons, Ltd, 1985.

[140] lee yuh Lang, “Chapter 9: Adsorption,” *National Cheng Kung University*, 2019. [Online]. Available: http://www.che.ncku.edu.tw/facultyweb/leeyl/94/Chapter 09 Adsorption.pdf. [Accessed: 25-Oct-2019].

[141] M. Soustelle, “Shapes of the Isotherms of Physical Adsorption Found Experimentally,” in *Thermodynamics of Surfaces and Capillary Systems, Volume 7*, vol. 34, no. 3, John Wiley & Sons, 2016, p. 163.

[142] M. Polanyi, “The Potential Theory of Adsorption,” *Science (80-.).*, vol. 141, no. 3585, pp. 1010–1013, Dec. 1963.

[143] Ralph T. Yang, *Gas Separation by Adsorption Processes*, vol. 1. London, United Kingdom: Elsevier, 1997.

[144] M. Ponce, L. Munguía, M. Esparza, I. Kornhauser, and F. Rojas, “On scrutinizing the classical polanyi adsorption potential theory for vapour uptake occurring in the mesopores of curved shapes,” *Adsorpt. Sci. Technol.*, vol. 29, no. 6, pp. 585–594, Jun. 2011.

[145] R. Ghosal and D. M. Smith, “Micropore Characterization using the Dubinin-Astakhov Equation to Analyze High Pressure CO2 (273 K) Adsorption Data,” Kluwer Academic Publishers, 1996.

[146] M. M. Dubinin, “The potential theory of adsorption of gases and vapors for

adsorbents with energetically nonuniform surfaces," *Chem. Rev.*, vol. 60, no. 2, pp. 235–241, 1960.

[147] M. M. Dubinin and V. A. Astakhov, "Description of Adsorption Equilibria of Vapors on Zeolites over Wide Ranges of Temperature and Pressure," *Adv. Chem.*, vol. 102, no. 44, pp. 69–85, Jun. 1971.

[148] E. Ozdemir, B. I. Morsi, and K. Schroeder, "CO2 adsorption capacity of argonne premium coals," *Fuel*, vol. 83, no. 7–8, pp. 1085–1094, May 2004.

[149] L. Cao and Y. Zhang, "Interpretation of Gibbs surface excess model for gas adsorption on heterogeneous coal particle," *Fuel*, vol. 214, no. June 2017, pp. 20–25, 2018.

[150] H. Cai, P. Li, Z. Ge, Y. Xian, and D. Lu, "A new method to determine varying adsorbed density based on Gibbs isotherm of supercritical gas adsorption," *Adsorpt. Sci. Technol.*, vol. 36, no. 9, pp. 1687–1699, 2018.

[151] J. Rouquerol, F. Rouquerol, P. Llewellyn, and R. Denoyel, "Surface excess amounts in high-pressure gas adsorption: Issues and benefits," *Colloids Surfaces A Physicochem. Eng. Asp.*, vol. 496, pp. 3–12, May 2016.

[152] S. Gumma and O. Talu, "Gibbs dividing surface and helium adsorption," *Adsorption*, vol. 9, no. 1, pp. 17–28, 2003.

[153] G. Richards, "Physical chemistry," *Nature*, vol. 272, no. 5648, pp. 101–102, 1978.

[154] S. Gumma and O. Talu, "Net adsorption: A thermodynamic framework for supercritical gas adsorption and storage in porous solids," *Langmuir*, vol. 26, no. 22, pp. 17013–17023, 2010.

[155] Z. Király and I. Dékány, "Interpretation of adsorption excess quantities: the absolute surface excess concentration," *Colloid Polym. Sci.*, vol. 268, no. 7, pp. 687–690, 1990.

[156] R. M. Bustin and C. R. Clarkson, “Geological controls on coalbed methane reservoir capacity and gas content,” *Int. J. Coal Geol.*, vol. 38, no. 1–2, pp. 3–26, Dec. 1998.

[157] C. Laxminarayana and P. J. Crosdale, “Role of coal type and rank on methane sorption characteristics of Bowen Basin, Australia coals,” *Int. J. Coal Geol.*, vol. 40, no. 4, pp. 309–325, Jul. 1999.

[158] G. Gürdal and M. N. Yalçin, “Gas adsorption capacity of Carboniferous coals in the Zonguldak basin (NW Turkey) and its controlling factors,” *Fuel*, vol. 79, no. 15, pp. 1913–1924, Dec. 2000.

[159] A. Busch, Y. Gensterblum, and B. M. Krooss, “Methane and CO2 sorption and desorption measurements on dry Argonne premium coals: Pure components and mixtures,” *Int. J. Coal Geol.*, vol. 55, no. 2–4, pp. 205–224, Aug. 2003.

[160] G. R. L. Chalmers and R. Marc Bustin, “On the effects of petrographic composition on coalbed methane sorption,” *Int. J. Coal Geol.*, vol. 69, no. 4, pp. 288–304, Mar. 2007.

[161] A. Hildenbrand, B. M. Krooss, A. Busch, and R. Gaschnitz, “Evolution of methane sorption capacity of coal seams as a function of burial history - A case study from the Campine Basin, NE Belgium,” *Int. J. Coal Geol.*, vol. 66, no. 3, pp. 179–203, Mar. 2006.

[162] S. Day, G. Duffy, R. Sakurovs, and S. Weir, “Effect of coal properties on CO2 sorption capacity under supercritical conditions,” *Int. J. Greenh. Gas Control*, vol. 2, no. 3, pp. 342–352, Jul. 2008.

[163] E. Ozdemir and K. Schroeder, “Effect of moisture on adsorption isotherms and adsorption capacities of CO2 on coals,” *Energy and Fuels*, vol. 23, no. 5, pp. 2821–2831, 2009.

[164] B. Nie *et al.*, “Sorption charateristics of methane among various rank coals:

impact of moisture," *Adsorption*, vol. 22, no. 3, pp. 315–325, Apr. 2016.

[165] D. Mohanty, S. Chattaraj, and A. K. Singh, "Influence of coal composition and maturity on methane storage capacity of coals of Raniganj Coalfield, India," *Int. J. Coal Geol.*, vol. 196, pp. 1–18, Aug. 2018.

[166] J. H. Levy, S. J. Day, and J. S. Killingley, "Methane capacities of Bowen Basin coals related to coal properties," *Fuel*, vol. 76, no. 9, pp. 813–819, Jul. 1997.

[167] H. Guo, Y. Cheng, L. Wang, S. Lu, and K. Jin, "Experimental study on the effect of moisture on low-rank coal adsorption characteristics," *J. Nat. Gas Sci. Eng.*, vol. 24, pp. 245–251, May 2015.

[168] R. Sander, Z. Pan, L. D. Connell, M. Camilleri, and D. Heryanto, "Experimental investigation of gas diffusion in coal - Comparison between crushed and intact core samples," *Soc. Pet. Eng. - SPE Asia Pacific Oil Gas Conf. Exhib. 2016*, pp. 1–14, 2016.

[169] S. Hokerek and O. Ozcelik, "Organic Facies Characteristics of the Miocene Soma Formation (Lower Lignite Succession-KM2), Soma Coal Basin, Western Turkey," in *Energy Procedia*, 2015, vol. 76, pp. 27–32.

[170] Ş. Şen, "A Petroleum Source Rock Assessment of the Middle Oligocene-Lower Miocene Coal Bearing Deltaic Sediments in NW Turkey," *Energy Sources, Part A Recover. Util. Environ. Eff.*, vol. 36, no. 8, pp. 843–850, Apr. 2014.

[171] A. Ürünveren, M. Altıner, Y. Kuvvetli, O. B. Ural, and S. Ural, "Prediction of Hardgrove Grindability Index of Afsin-Elbistan (Turkey) Low-grade Coals Based on Proximate Analysis and Ash Chemical Composition by Neural Networks," *Int. J. Coal Prep. Util.*, vol. 40, no. 10, pp. 701–711, Oct. 2020.

[172] M. Sudibandriyo, Z. Pan, J. E. Fitzgerald, R. L. Robinson, and K. A. M.

Gasem, “Adsorption of methane, nitrogen, carbon dioxide, and their binary mixtures on dry activated carbon at 318.2 K and pressures up to 13.6 MPa,” *Langmuir*, vol. 19, no. 13, pp. 5323–5331, Jun. 2003.

[173] J. Zhang, M. B. Clennell, K. Liu, M. Pervukhina, G. Chen, and D. N. Dewhurst, “Methane and Carbon Dioxide Adsorption on Illite,” *Energy and Fuels*, vol. 30, no. 12, pp. 10643–10652, Dec. 2016.

[174] M. Kunowsky, F. Suárez-García, and Á. Linares-Solano, “Adsorbent density impact on gas storage capacities,” *Microporous Mesoporous Mater.*, vol. 173, pp. 47–52, Jun. 2013.

[175] N. Siemons and A. Busch, “Measurement and interpretation of supercritical CO2 sorption on various coals,” *International Journal of Coal Geology*, vol. 69, no. 4. pp. 229–242, 01-Mar-2007.

[176] B. M. Krooss, F. Van Bergen, Y. Gensterblum, N. Siemons, H. J. M. Pagnier, and P. David, “High-pressure methane and carbon dioxide adsorption on dry and moisture-equilibrated Pennsylvanian coals,” *Int. J. Coal Geol.*, vol. 51, no. 2, pp. 69–92, Jul. 2002.

[177] S. Han, S. Sang, J. Liang, and J. Zhang, “Supercritical CO2 adsorption in a simulated deep coal reservoir environment, implications for geological storage of CO2 in deep coals in the southern Qinshui Basin, China,” *Energy Sci. Eng.*, vol. 7, no. 2, pp. 488–503, Apr. 2019.

[178] P. De Silva and P. Ranjith, “Understanding and application of CO2 adsorption capacity estimation models for coal types,” *Fuel*, vol. 121, pp. 250–259, Apr. 2014.

[179] J. S. Bae, S. K. Bhatia, J.-S. B. and, and S. K. Bhatia*, “High-Pressure Adsorption of Methane and Carbon Dioxide on Coal,” *Energy and Fuels*, vol. 20, no. 6, pp. 2599–2607, 2006.

[180] H. Liu *et al.*, “ Supercritical-CO 2 Adsorption Quantification and Modeling

for a Deep Coalbed Methane Reservoir in the Southern Qinshui Basin, China ," *ACS Omega*, vol. 4, no. 7, pp. 11685–11700, 2019.

[181] N. Ayawei, A. N. Ebelegi, and D. Wankasi, "Modelling and Interpretation of Adsorption Isotherms," *J. Chem.*, vol. 2017, pp. 1–11, 2017.

[182] K. V. Kumar, K. Porkodi, and F. Rocha, "Comparison of various error functions in predicting the optimum isotherm by linear and non-linear regression analysis for the sorption of basic red 9 by activated carbon," *J. Hazard. Mater.*, vol. 150, no. 1, pp. 158–165, 2008.

[183] Y. Cheng, H. Jiang, X. Zhang, J. Cui, C. Song, and X. Li, "Effects of coal rank on physicochemical properties of coal and on methane adsorption," *Int. J. Coal Sci. Technol.*, vol. 4, no. 2, pp. 129–146, 2017.

[184] S. Bachu Didier Bonijoly John Bradshaw Robert Burruss Niels Peter Christensen Sam Holloway, "Estimation of CO 2 Storage Capacity in Geological Media-Phase 2-Prepared by the Task Force on CO 2 Storage Capacity Estimation for the Technical Group (TG) of the Carbon Sequestration Leadership Forum (CSLF)," Melbourne, Sep. 2007.

[185] A. Goodman *et al.*, "U.S. DOE methodology for the development of geologic storage potential for carbon dioxide at the national and regional scale," *Int. J. Greenh. Gas Control*, vol. 5, pp. 952–965, 2011.

[186] S. Weniger, P. Weniger, and R. Littke, "Characterizing coal cleats from optical measurements for CBM evaluation," *Int. J. Coal Geol.*, vol. 154–155, pp. 176–192, 2016.

[187] B. Guo and A. Ghalambor, "Properties of Natural Gas," in *Natural Gas Engineering Handbook*, Elsevier, 2005, pp. 13–33.

[188] M. L. Mittal, "Estimates of Emissions from Coal Fired Thermal Power Plants in India," in *2012 International Emission Inventory Conference "Emission Inventories - Meeting the Challenges Posed by Emerging Global,*

National, Regional and Local Air Quality Issues," 2012, vol. 39, pp. 1–22.

[189] NIST, "Isothermal Properties for Carbon dioxide," *National Institute of Standards and Technology (NIST-USA).*, 23-Dec-2020. .

[190] A. Witkowski, M. Majkut, and S. Rulik, "Analysis of pipeline transportation systems for carbon dioxide sequestration," *Arch. Thermodyn.*, vol. 35, no. 1, pp. 117–140, 2014.

APPENDICES

A. Void volume estimation of the system

The helium gas was used to determine the void volume in the sample cell. Once the sample is loaded in the sample cell, and the leak test is over, all the valves were closed, then the following procedures are followed:

The expansion valve was opened, and the gas is expanded to the sample cell, continuing until the equilibrium is reached.

The gas law in equilibrium condition is:

$$P_{eq1} \cdot \left(V_{rf} + V_{sa} - V_{ske}\right) = Z_{eq1} \cdot n_{eq} \cdot R \cdot T \qquad 11.1$$

where P_{eq1} is the pressure in an equilibrium state, V_{sa} is the sample cell volume, V_{ske} is the sample skeletal volume, Z_{eq1} is the gas compressibility factor at pressure P_{eq1}, n_{eq} is the moles of gas in equilibrium condition. V_{sa} and V_{ske} were estimated by helium injection. The void volume is calculated as:

$$Void\ volume\ (V_{void}) = V_{sa} - V_{ske}$$

Therefore, substituting void volume in equation 11.1, we get:

$$P_{eq1} \cdot \left(V_{rf} + V_{void}\right) = Z_{eq1} \cdot n_{eq} \cdot R \cdot T\ .$$

The second gas injection is injected into the previously injected gas in the first injection, and the third and fourth follow the same pattern.

The mass balance equation can be expressed as:

$$n_{eq} = n_{inject} + n_{residual}$$

where $n_{residual}$ are moles of gas that have been already injected by the previous injection steps n_{inject} are the new injected number of moles and n_{eq} are the equilibrium number of moles for the new step.

The gas law corresponding to this number of moles are as follows:

$$P_2 \cdot \left(V_{rf} + V_{void}\right) = Z_2 \cdot n_{eq} \cdot R \cdot T$$

$$P_2 \cdot V_{rf} = Z_2 \cdot n_{inject} \cdot R \cdot T$$

$$P_{eq2} \cdot V_{void} = Z_{eq2} \cdot n_{residual} \cdot R \cdot T$$

where P_{eq1} & Z_{eq1} are the equilibrium pressure and gas compressibility from the previous step, respectively. The P_2 and Z_2 are the new pressure injection on the second step, whereas the P_{eq2} and Z_{eq2} are the second equilibrium value on the second step.

Therefore, for the second step, we recall that: $\boldsymbol{n_{eq} = n_{inject} + n_{residual}}$

$$\frac{P_2 \cdot V_{rf}}{Z_2} + \frac{P_{eq1} \cdot V_{void}}{Z_{eq1}}$$

Estimation of the void volume for the second step

$$V_{void} = \frac{\frac{P_2}{Z_2} - \frac{P_{eq2}}{Z_{eq2}}}{\frac{P_{eq2}}{Z_{eq2}} - \frac{P_{eq1}}{Z_{eq1}}} \cdot V_{rf} \qquad 11.2$$

For multiple *n* Injections, equation 11.2 becomes:

$$V_{void}(n) = \frac{\frac{P_n}{Z_n} - \frac{P_{eqn}}{Z_{eq2n}}}{\frac{P_{eqn}}{Z_{eqn}} - \frac{P_{eq(n-1)}}{Z_{eq(n-1)}}} \cdot V_{rf}$$

The void volume was determined at 40°C (273.15 K). For each pressure point, the void volume was determined.

The slope function in Microsoft Excel was used to make an average of the void volumes at every pressure point. Table 11.1 — Table 11.4 summarize the void volume estimation for all the coal samples. They show the details of each experiment's sample's weight and the void volume used in adsorption experiments.

1. Soma sample

Table 11.1. Void volume estimation for Soma samples

Experiment	**weight (g-daf)**	**P_{RF1} (bars)**	**P_{RF2} (bars)**	**V_{void} (cc)**	**Average V_{void} (cc)**
#1	37.93	2.3	1.4	45.70	45.85
		3.3	2	46.20	
		3.8	2.3	46.36	
		4.3	2.6	46.48	
		5.4	3.3	45.23	
		6.6	4	46.20	
#2	36.25	9.9	6.1	44.27	44.66
		14.2	11.1	44.06	
		24.8	19.5	44.84	
		34.2	28.5	45.01	
		44.6	38.4	44.51	
		55.8	49.1	44.50	
		63.8	58.1	45.01	
		75.8	69	44.34	
#3	37.9	3.9	2.4	44.43	45.36
		4.7	2.9	44.12	
		5	3.1	43.56	
		5.5	3.4	43.90	
		5.8	3.6	43.44	
		6.2	3.8	44.89	
		6.5	4	44.42	
		6.9	4.2	45.69	

1. Tunçbilek Sample

Table 11.2. Void volume estimation for Tunçbilek samples

Experiments	Weight (g-daf)	P_{RF1} (bars)	P_{RF2} (bars)	V_{void} (cc)	Average V_{void} (cc)
#1	22.03	7.3	4.2	52.46	52.53
		37.9	21.8	52.49	
		45.3	35.3	52.64	
		56.5	47.5	52.43	
		65.2	57.7	52.26	
		74.4	67.3	52.56	
		94.4	82.9	52.39	
#2	39.74	9.3	6	39.09	39.11
		16.3	12.8	36.58	
		21.4	18.4	38.07	
		28.6	25.1	37.12	
		34.8	31.4	38.35	
		47.3	41.7	38.64	
		54.5	49.9	39.87	
		61.1	57.2	37.97	
		73.9	68.1	37.82	
		80.7	76.3	38.13	
#3	40.8	10	6.5	38.27	39.15
		17.2	13.4	39.14	
		20.3	17.9	37.90	
		28.6	24.8	39.14	
		35	31.4	38.76	
		50.3	43.7	38.13	
		57.9	52.8	39.83	
		65.2	60.8	39.09	
		70.1	66.9	37.28	
		90.3	82	39.06	

1. Tekirdağ-Saray Sample

Table 11.3. Void volume estimation for Tekirdağ-Saray samples

Experiment	**weight (g-daf)**	**P_{RF1} (bars)**	**P_{RF2} (bars**	**V_{void} (cc)**	**Average V_{void} (cc)**
#1	21.036	63	35	56.85	56.13
		69.2	54.1	56.18	
		73	64.7	55.65	
		75.1	70.5	56.36	
		81.6	76.7	56.17	
#2	20	62.7	35	56.25	56.3
		70.1	54.4	57.51	
		74.5	65.6	56.47	
		76.3	71.5	57.82	
		82	77.3	57.59	
		85.6	81.9	57.16	
		90.3	86.5	58.71	
		93.3	90.4	52.85	
#3	18.6	56.2	31.4	56.13	56.4
		73.9	54.9	57.46	
		80.3	69.1	56.05	
		89.3	80.3	57.11	
		93.2	87.5	56.26	

1. Afşin-Elbistan sample

Table 11.4. Void volume estimation for Afşin-Elbistan samples

Experiment	weight (g-daf)	P_{RF1} (bars)	P_{RF2} (bars	V_{void} (cc)	Average V_{void} (cc)
#1	17.4	37.1	21.7	50.44	50.18
		45.6	35.7	50.25	
		53.7	46.2	50.76	
		64.2	56.7	50.76	
		74.3	67	50.37	
		80.2	74.7	50.76	
		91.5	84.5	50.76	
#2	16.9	24	14	50.76	50.48
		30.2	23.5	50.12	
		41.6	34.1	50.28	
		54.3	45.8	51.63	
		63	55.8	51.17	
		70.5	64.3	51.84	
#3	18.3	12	7.1	49.05	49.99
		17.3	13.1	49.75	
		25.6	20.4	50.62	
		39.5	31.6	50.13	
		42.3	37.8	51.58	
		56.2	48.6	50.01	
		63.4	57.1	52.67	

B. Reference and sample cells volume determination

A helium injection series determined the sample's empty volumes and reference cells from the reference cell to the sample cell. First, the sample cells were empty, and then we filled the sample cell with a cylindrical metal disk with a known volume. The expansion was carried out in steps from 10 up to 100 bars at 40 °C.

For an empty system, the equations were:

For Reference: $P_1 \cdot V_{rf} = Z_1 \cdot n_{inject} \cdot R \cdot T$

For the equilibrium step: $P_{eq}.\left(V_{rf} + V_{sa}\right) = Z_{eq} \cdot n_{eq} \cdot R \cdot T$

$n_{eq} = n_{inject}$

$$\frac{\left(V_{rf} + V_{sa}\right)}{V_{rf}} = \frac{P_1 \cdot Z_{eq}}{P_{eq} \cdot Z_1} \qquad 11.3$$

By plotting $P_1 \cdot Z_{eq}$ versus $P_{eq} \cdot Z_1$ we find a linear line with a slope m_1

We then fill the sample cell with a cylindrical disk of known volume. In this study, we used the disk volume (V_{disk}) of 16.071 cc.

The equation 11.3 becomes:

$$\frac{\left(V_{rf} + V_{sa} - V_{disk}\right)}{V_{rf}} = \frac{P_1 \cdot Z_{eq2}}{P_{eq2} \cdot Z_1}$$

By plotting $P_1 \cdot Z_{eq2}$ versus $P_{eq2} \cdot Z_1$ we find a linear line with a slope m_2

Therefore:

$$V_{sa} = V_{disk} \cdot \frac{-m_2}{m_1 - m_2}$$

$$V_{rf} = V_{sa} \cdot m_1$$

Table 11.5. Reference and sample cell calculations.

Pressure measurements for an empty system			**Pressure measurements with a disk in the sample cell**		
P_{RF} (bars)	P_{eq}(bars)	m_1	P_{RF}(bars)	P_{eq2} (bars)	m_2
13.1	6.4	0.489	20.6	11.3	0.549
19.8	9.7	0.490	29.3	16.2	0.553
25.8	12.7	0.492	35	19.4	0.554
33.5	16.5	0.493	43.4	23.8	0.548
45.1	22	0.488	52	28.4	0.546
54.3	26.5	0.488	57.2	31.4	0.549
64	31.2	0.487	64.8	35.6	0.549
73.9	35.9	0.486	75.1	41.2	0.549
87.1	42.3	0.486	85.3	46.6	0.546
94.5	45.8	0.485	93.2	51.1	0.548
$\mathrm{V_{RF}} = 71$ cc and $\mathrm{V_{sa}} = 75$ cc					

C. Adsorbed density calculation

The adsorbed density was estimated from equation 5.17. It is clear that when the free gas density approaches the value of adsorbed density, the excess adsorption will be zero. Therefore, the excess adsorption graph vs density of the free gas was used to estimate the density profile intercepts with excess adsorption equal to zero, as shown in Figure 11.1. shows the density profiles of the four coal samples. It shows that after some point, the function decreases linearly towards zero; therefore, by fitting the linear equation to the linear part, we can determine the point where the number of moles is zero and taken as adsorbed density.

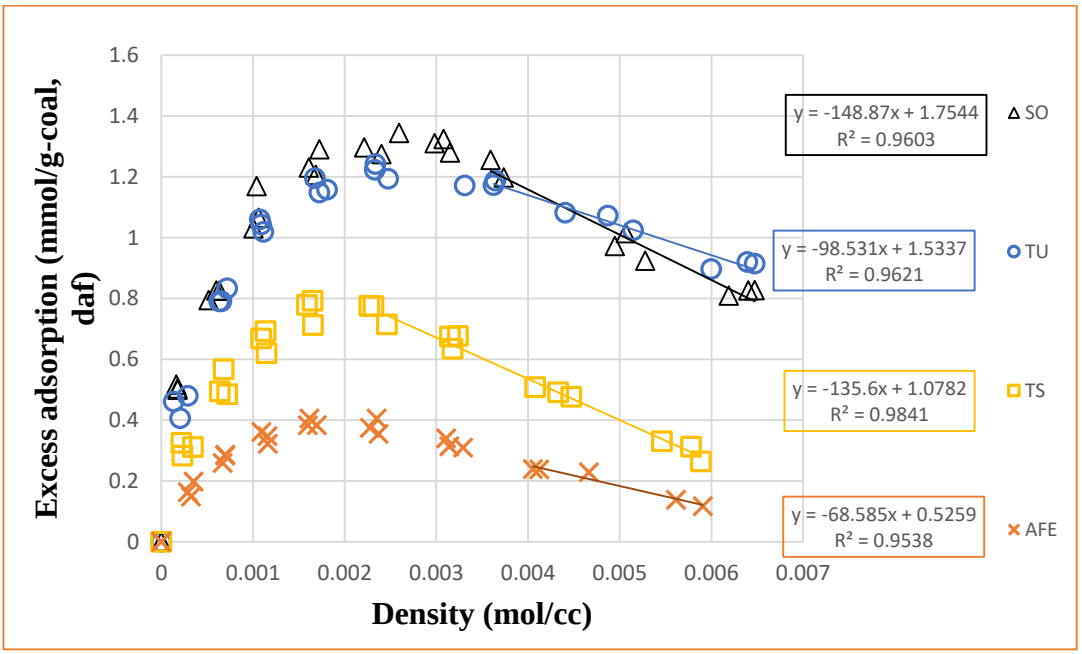

Figure 11.1. Adsorbed phase density estimation.

D. Carbon dioxide properties

Carbon dioxide is a chemical compound composed of one carbon bonded to two oxygen atoms. The most relevant properties to this study and phase diagram are given in Table 11.6 and Figure 11.2, respectively.

Table 11.6. Some properties of carbon dioxide [189]

Property	Value
Molecular weight	44 g/mol
Liquid density (at −20 °C, 19.7 bar)	1.032 g/cm3
Solid density	1.562 g/cm3
Gas density (at 15 °C, 1.013 bar)	0.002814 g/cm3
Compressibility factor (Z, at 15 °C, 1.013 bar)	0.9942
Specific volume (at 21°C, 1.013 bar)	547 cm3/g
Critical temperature (T_c)	31 °C
Critical pressure (P_c)	73.825 bar
Critical density (ρc)	0.464 g/cm3
Triple point temperature	−56.6 °C
Triple point pressure	5.185 bar

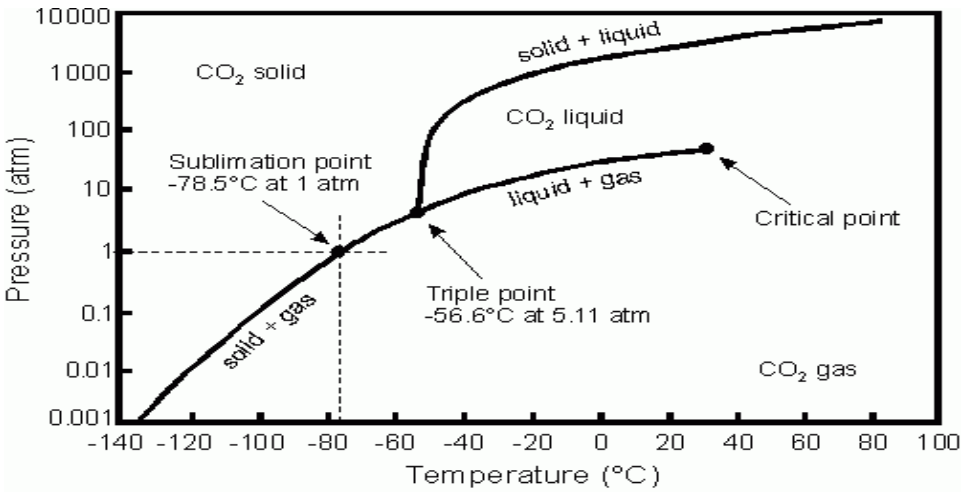

Figure 11.2. Phase diagram for CO_2 [190]

E. Compressibility factor and free gas density for CO_2

At each pressure point, the free gas density see Figure 11.3 was obtained from the National Institute of Standards and Technology (NIST-USA) [189].

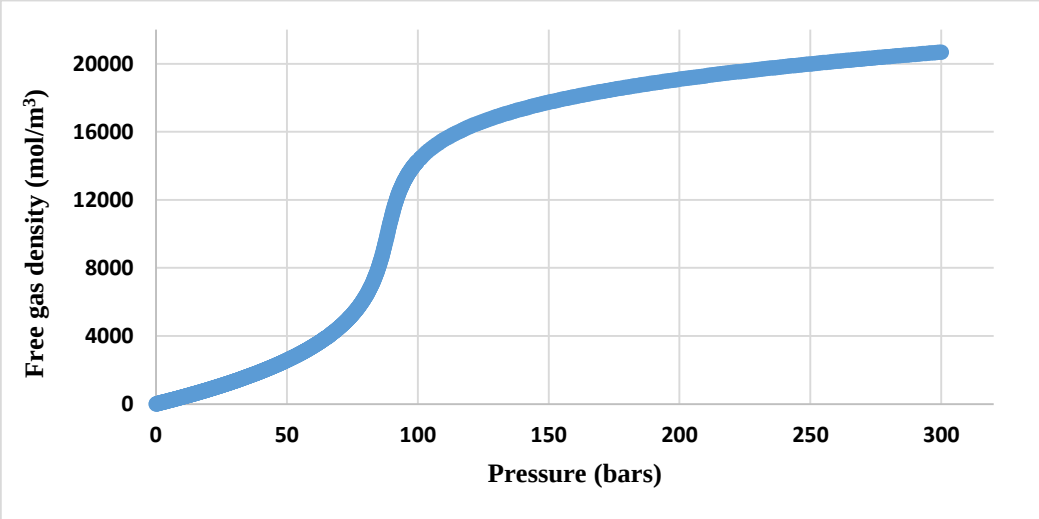

Figure 11.3. CO_2 density against pressure at 40 °C

The compressibility constant see Figure 11.4 was calculated also based on the values extracted from the NIST database [189].

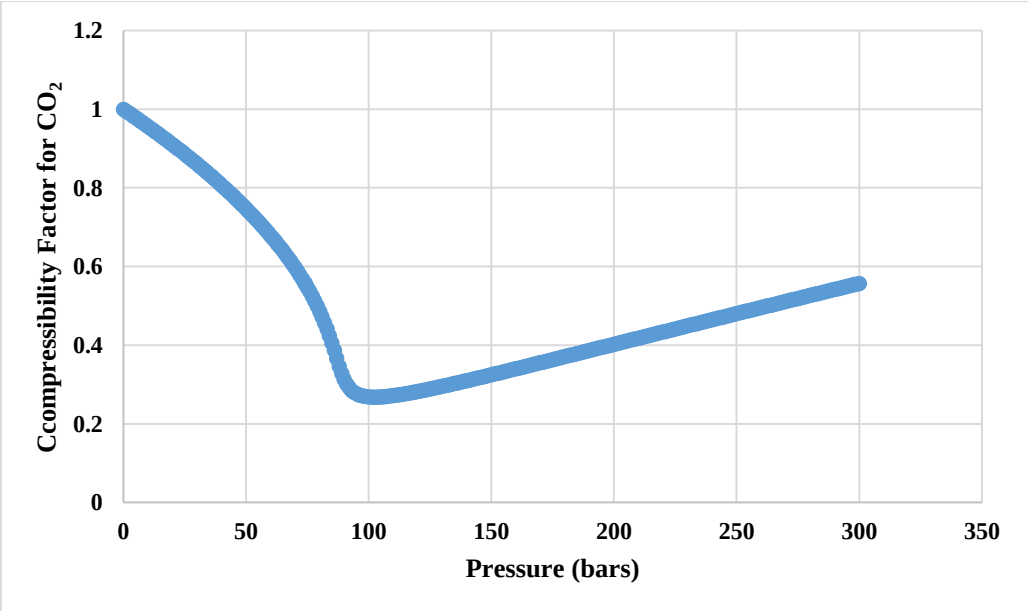

Figure 11.4. Gas compressibility factor (*Z*-factor) for CO_2.

F. Excess adsorption experimental data

All experiments were conducted at 40 °C (313.15 K)

1. Tunçbilek Coal Sample

Table 11.7. CO_2 adsorption experiment 1 Tunçbilek coal Sample

Pressure in the reference cell (bars)	Equilibrium pressure (bars)	Excess adsorption capacity (mmol/g)
0	0	0
15.8	7.3	0.48
23.8	15.9	0.79
33.4	25.6	1.02
47.1	38.4	1.16
55.3	48.7	1.19
65.2	59.1	1.17
74.6	69.3	1.08
82.7	78.7	0.9

Table 11.8. CO_2 adsorption experiment 2 Tunçbilek coal Sample

Pressure in the reference cell (bars)	Equilibrium pressure (bars)	Excess adsorption capacity (mmol/g)
0	0	0.00
11.6	3.5	0.46
25.1	15.3	0.79
32.6	24.9	1.06
43.1	36.2	1.20
51.9	46.6	1.22
68.5	62.6	1.19
77.7	74.3	1.02
82.1	80.6	0.91

Table 11.9. CO_2 adsorption experiment 3 Tunçbilek coal Sample

Pressure in the reference cell (bars)	Equilibrium pressure (bars)	Excess adsorption capacity (mmol/g)
0	0	0.00
13.5	5.2	0.41
28.3	17.3	0.83
31.4	25.1	1.04
43.7	37	1.15
52.1	46.7	1.24
68.4	62.4	1.17
76.3	72.6	1.07
82.1	80.3	0.92

2. Afşin-Elbistan coal Sample

Table 11.10. CO_2 adsorption experiment 1 for Afşin-Elbistan coal Sample

Pressure in the reference cell (bars)	Equilibrium pressure (bars)	Excess adsorption capacity (mmol/g)
0	0	0.00
13.1	7.3	0.16
23.6	16.8	0.28
31	25.2	0.35
41.5	35.1	0.40
53.9	46.9	0.41
62.4	56.8	0.35
77.5	71.2	0.26
82.6	79.1	0.21

Table 11.11. CO_2 adsorption experiment 2 for Afşin-Elbistan coal Sample

Pressure in the reference cell (bars)	Equilibrium pressure (bars)	Excess adsorption capacity (mmol/g)
0	0	0.00
14.3	8.1	0.15
22.1	16.2	0.26
33.5	26.6	0.32
40.3	34.8	0.38
54.4	47.2	0.35
65.3	58.9	0.31
71.4	67	0.24
81.2	76.9	0.14

Table 11.12. CO_2 adsorption experiment 3 for Afşin-Elbistan coal Sample

Pressure in the reference cell (bars)	Equilibrium pressure (bars)	Excess adsorption capacity (mmol/g)
0	0	0.00
15.7	8.8	0.20
22.5	16.8	0.28
33	26.5	0.35
42.9	36.5	0.38
51.5	45.8	0.37
63.5	57.2	0.31
71.3	66.4	0.24
82.9	78.3	0.12

3. Soma Coal Sample

Table 11.13. CO_2 adsorption experiment 1 for Soma coal Sample

Pressure in the reference cell (bars)	Equilibrium pressure (bars)	Excess adsorption capacity (mmol/g)
0	0	0.00
13.3	4.2	0.52
21	12.7	0.79
34	24.5	1.07
44.2	36.3	1.21
54.4	47.6	1.28
59.8	55.3	1.31
65.6	62.1	1.26
78.1	73.8	1.01
82.9	80.3	0.83

Table 11.14. CO_2 adsorption experiment 2 for Soma coal Sample

Pressure in the reference cell (bars)	Equilibrium pressure (bars)	Excess adsorption capacity (mmol/g)
0	0	0.00
13.3	4.5	0.50
23.9	14.6	0.83
32.6	24.1	1.17
45	37	1.29
57.5	50.3	1.34
59.8	56.5	1.32
66.6	63.5	1.20
79.2	75.1	0.92
81.4	79.5	0.81

Table 11.15. CO_2 adsorption experiment 3 for Soma coal Sample

Pressure in the reference cell (bars)	Equilibrium Pressure (bars)	Excess adsorption capacity (mmol/g)
0	0	0.00
13.6	4.5	0.50
25.2	15.3	0.83
30.3	23.4	1.03
43.2	35	1.23
50.9	44.9	1.30
63.5	57.3	1.28
78.4	73.1	0.97
83.5	80.8	0.73

4. Tekirdağ-Saray Coal Sample

Table 11.16. CO_2 adsorption experiment 1 for Tekirdağ-Saray coal Sample

Pressure in the reference cell (bars)	Equilibrium Pressure (bars)	Excess adsorption capacity (mmol/g)
0	0	0.00
12.1	5.6	0.33
25.4	16.4	0.57
33.7	26.1	0.69
42.9	35.7	0.79
53.5	46.4	0.77
63.9	57.3	0.67
76.1	69.8	0.48
81.6	77.7	0.31

Table 11.17. CO_2 adsorption experiment 2 for Tekirdağ-Saray coal Sample

Pressure in the reference cell (bars)	Equilibrium pressure (bars)	Excess adsorption capacity (mmol/g)
0	0	0.00
17	8.6	0.31
24.7	17.3	0.48
33.5	26.3	0.62
42.9	35.8	0.71
56.7	48.5	0.71
63.3	57.6	0.63
71.8	66.6	0.51
80.7	76.1	0.33

Table 11.18. CO_2 adsorption experiment 3 for Tekirdağ-Saray coal Sample

Pressure in the reference cell (bars)	Equilibrium pressure (bars)	Excess adsorption capacity (mmol/g)
0	0	0.00
12.1	5.8	0.28
23.8	15.5	0.49
32.9	25.1	0.67
41.8	34.6	0.78
53.1	45.7	0.78
65.7	58.3	0.68
74.3	68.7	0.49
82.5	78.2	0.26

G. Fitted parameters from adsorption models

Table 11.19. Fitted adsorption model parameters for Soma coal

	n_{max} (mmol/g)	ρ_L (mol/cc)	ρ_a (mol/cc)	k (cc/mol)	ARE (%)
Langmuir–modified	1.98	0.00056	0.0117	-	6.3
Langmuir–mod.+k	1.98	0.00056	0.0117	0	6.3
	n_{max} (mmol/g)	D	ρ_a (mol/cc)	k (cc/mol)	ARE (%)
D-R–modified	1.95	0.077	0.0113	-	4.9
D-R–modified+k	1.95	0.077	0.0113	0	4.9

Table 11.20. Fitted adsorption model parameters for Tunçbilek coal

	n_{max} (mmol/g)	ρ_L (mol/cc)	ρ_a (mol/cc)	k (cc/mol)	ARE (%)
Langmuir modified	1.98	0.00088	0.0135	-	3.8
Langmuir mod.+k	1.98	0.00088	0.0135	0	3.8
	n_{max} (mmol/g)	D	ρ_a (mol/cc)	k (cc/mol)	ARE (%)
D-R-modified	1.9	0.089	0.0126	-	3.7
D-R-modified+k	1.9	0.089	0.0126	0	3.7

Table 11.21. Fitted adsorption model parameters Tekirdağ-Saray for coal

	n_{max} (mmol/g)	ρ_L (mol/cc)	ρ_a (mol/cc)	k (cc/mol)	ARE (%)
Langmuir modified	1.43	0.0009	0.0075	-	5.96
Langmuir mod.+k	1.43	0.0009	0.0075	0	5.96
	n_{max} (mmol/g)	D	ρ_a (mol/cc)	k (cc/mol)	ARE (%)
D-R-modified	1.22	0.12	0.0075	-	5.92
D-R-modified+k	1.22	0.12	0.0075	0	5.92

Table 11.22. Fitted adsorption model parameters for Afşin-Elbistan sample

	n_{max} (mmol/g)	ρ_L (mol/cc)	ρ_a (mol/cc)	k (cc/mol)	ARE (%)
Langmuir modified	0.79	0.00106	0.00714	-	4.94
Langmuir mod.+k	0.79	0.00106	0.00714	0	4.94
	n_{max} (mmol/g)	D	ρ_a (mol/cc)	k (cc/mol)	ARE (%)
D-R-modified	0.63	0.127	0.00725	-	5.06
D-R-modified+k	0.63	0.127	0.00725	0	5.06

TEZ İZİN FORMU / THESIS PERMISSION FORM

PROGRAM / PROGRAM

Sürdürülebilir Çevre ve Enerji Sistemleri / Sustainable Environment and Energy Systems ☑

Siyaset Bilimi ve Uluslararası İlişkiler / Political Science and International Relations ☐

İngilizce Öğretmenliği / English Language Teaching ☐

Elektrik Elektronik Mühendisliği / Electrical and Electronics Engineering ☐

Bilgisayar Mühendisliği / Computer Engineering ☐

Makina Mühendisliği / Mechanical Engineering ☐

YAZARIN / AUTHOR

Soyadı / Surname : BUNANI KEZA

Adı / Name : BIENVENU CHRISTIAN

Programı / Program : SEES

TEZİN ADI / TITLE OF THE THESIS (**İngilizce** / English) : MEASUREMENTS OF CO_2 ADSORPTION CAPACITY ON SELECTED TURKISH COALS FOR CO_2 SEQUESTRATION PURPOSES

TEZİN TÜRÜ / DEGREE: **Yüksek Lisans** / Master ☑ **Doktora** / PhD ☐

1. **Tezin tamamı dünya çapında erişime açılacaktır. /** Release the entire work immediately for access worldwide. ☐

2. **Tez iki yıl süreyle erişime kapalı olacaktır.** / Secure the entire work for patent and/or proprietary purposes for a period of **two years**. * ☐

3. **Tez altı ay süreyle erişime kapalı olacaktır.** / Secure the entire work for period of **six months**. * ☑

Yazarın imzası / Author Signature Bunani **Tarih** / Date 15/03/2021

Tez Danışmanı / Thesis Advisor Full Name: Dr. AYKUT ARGÖNÜL

Tez Danışmanı İmzası / Thesis Advisor Signature: .....

Eş Danışmanı / Co-Advisor Full Name: Dr. DORUK ALP

Eş Danışmanı İmzası / Co-Advisor Signature: .....

Program Koordinatörü / Program Coordinator Full Name: Dr. CEREN INCE DEROGAR

Program Koordinatörü İmzası / Program Coordinator Signature: .....